Mechanisms of Drp1 recruitment to mitochondria

Thesis by

Raymond Liu

In Partial Fulfillment of the Requirements for the

Degree of

Doctor of Philosophy

California Institute of Technology

Pasadena, CA

2017

(Defended April 24, 2017)

Acknowledgements

I would like to thank my advisor, Professor David Chan, for his insightful comments, constant availability, Monday afternoon chats, and overall mentorship. His high standards and no-bullshit approach have shown me the true meaning of scientific rigor, and it has been a pleasure learning and working under his guidance. I would also like to thank the members of my committee, Professor Ray Deshaies, Professor Judy Campbell, and Professor Bill Dunphy, for their advice and support. It has been quite a delight for me gathering together the brightest scientists into one tiny room, just to discuss my work!

I am also grateful for the many past and present members of the Chan lab, including Dr. Hsiuchen Chen, for running the lab with a keen eye and keener smile; Dr. Anne Chomyn, for baking all those delicious birthday cakes; Prof. Prashant Mishra, for all the nerdy puzzles and adventures in discrete mathematics; Dr. Anh Pham, for all the temporary parking permits and consequent two months' worth of free parking; Dr. Anna Salazar, for the candied insects I have yet to eat; Dr. Elisabeth Yun Wang, for the In-n-out 6x6s; Dr. Anand Vaidya, for the philosophical musings and advice on greener living; Dr. Valentina Del Dotto for taking the lab out late into the night; Dr. Arbis Rojas, for the many words of encouragement; Dr. Huu Ngo, for keeping track of lab happy hour; Dr. Oliver Loson, for putting up with all the pranks; Dr. Chun-Shik Shin, for the insightful scientific discussions, Dr. Moon-Yong Cha, for being the most professional bay-mate; Dr. Rebecca Rojansky, for the "easy" hiking trips; Greg Varuzhanyan, for constantly schooling me in chess; Ruohan Wang, for the endless cheerfulness; and Shuxia Meng, for being one of the best lab managers I have worked with. They have made working in the lab a both a joy

and incredible learning experience. Dr. Nickie Chan was also nice to have around, for all the lunch, dinner, and weekend excursions.

I would like to thank Caltech Housing for introducing me to my colleague and friend, Phong Nguyen, with whom I have had the pleasure of enjoying many adventures with, including fun and enlightening gatherings with the ‘Costco’ group. Here I would like to sneak in a thank you to the prooofreader, who will likely be the only one to read through this whole thesis.

I owe a debt of gratitude to my previous mentor, Professor Susan Parkhurst, for everything she has taught me and for encouraging me to pursue this path. I would also like to thank Professor Phil Soriano for the Jelly Belly chats, and Professor Shoshana Levy for letting me undertake an undergraduate thesis project in her lab.

It would have been impossible for me to complete my graduate studies without the support of my family. I am forever in debt to my parents, my brother, and my friends, for their love and companionship. My accomplishments are their accomplishments, and I hope that I have made them proud.

And finally, I would like to express my deepest appreciation for my fiancée, Nadia Herrera, for her support, love, humor, insight, and passion for life. She brings out the best in me, and I cannot imagine a more amazing partner-in-crime to roll and fly with on this silly little journey.

Abstract

Dynamin-related protein 1 (Drp1) is a GTPase of the dynamin superfamily that catalyzes mitochondrial fission in the cell. Cytosolic Drp1 is recruited to mitochondria by receptors anchored to the outer mitochondrial membrane. Once there, Drp1 assembles into a complex around the mitochondrial circumference to drive division via a GTP-dependent constriction process. The four known receptors of Drp1 are Fis1, Mff, MiD51, and MiD49, but stable interactions between Drp1 and these proteins have not been established. In addition, though mounting evidence suggests these receptors have non-redundant roles in their interaction with Drp1, mechanistic details explaining these distinctions are lacking. Here we address these questions, and show that the Insert B domain of Drp1 inhibits its interaction with Mff. Removal of this domain stabilizes a complex of Drp1 and Mff in vitro. In addition, we show that Drp1 oligomerization is a requirement for Mff recruitment, but not for MiD51 or MiD49-mediated recruitment. Together the results suggest a model in which Drp1 recruitment to mitochondria is regulated by the oligomeric state of Drp1, such that Mff, MiD51, and MiD49 recruit different subpopulations of Drp1 from the cytosol.

With this model as a framework, we analyze the effect that a Drp1 R403C mutant, identified in several human patients presenting with encephalopathy and refractory epilepsy, has on mitochondrial morphology in cultured cells. We find that the loss of Drp1 oligomerization in these mutants impedes its ability to be recruited by Mff, leading to abnormal elongation of the mitochondrial population.

Published Content and Contributions

Liu, R., and Chan, D.C. (2015). The mitochondrial fission receptor Mff selectively recruits oligomerized Drp1. Mol Biol Cell. *26*, 4466-77. doi:10.1091/mbc.E15-08-0591.

R.L. participated in the conception of the project, performed the experiments, prepared the data, and participated in the writing of the manuscript.

Fahrner, J.A., Liu, R., Perry, M.S., Klein, J., and Chan, D.C. (2016). A novel de novo dominant negative mutation in DNM1L impairs mitochondrial fission and presents as childhood epileptic encephalopathy. Am J Med Genet A. *170*, 2002-11. doi:10.1002/ajmg.a.37721.

R.L. participated in the conception of the experiments, performed the experiments, analyzed the data, prepared figures 2, 3, and 4, and participated in the writing of the manuscript.

Table of Contents

List of Figures

Chapter 2

Chapter 3

Chapter 4

Chapter 1

Introduction

Discovery of mitochondrial dynamics

Mitochondria are organelles in the cell that perform a variety of duties required for proper cell function. They generate ATP through oxidative phosphorylation, regulate a number of metabolic pathways, synthesize fatty acids, heme and iron-sulfur clusters, store and release calcium ions, activate apoptosis, and mediate innate immune response signaling (Mitchell, 1961; Scheffler, 2002; Ajioka *et al.*, 2006; Wang and Youle, 2009; Hiltunen *et al.*, 2010; West *et al.*, 2011; Rizzuto *et al.*, 2012; Rouault, 2012). The number of individual mitochondria per mammalian cell is estimated to be anywhere from 10^2 to 10^3, with each containing their own genome with dedicated replication, transcription, and translation machinery (Sinclair and Stevens, 1966; Robin and Wong, 1988; Clayton, 1991; Taanman, 1999). Individually, the organelle is organized into a double membrane layer, with an outer membrane encasing an inner membrane layer, separated by an intermembrane space. The inner membrane, embedded with the electron transport chain, is organized into folds called cristae that involute from junctions into the central matrix compartment, creating a wrinkled appearance (Daems and Wisse, 1966; Mannella *et al.*, 1994). Early electron images of mitochondria show a static portrait of mitochondria as bean-shaped (Palade, 1953; Sjostrand, 1953). Advances in live-imaging microscopy and visualization tools introduced a more dynamic portrayal of mitochondria, revealing a highly mobile population of spaghetti-like tubules with varied lengths (Bereiter-Hahn and

Voth, 1994; Nunnari *et al.*, 1997). In cultured cells, such as mouse embryonic fibroblasts, individual tubules could be observed constantly moving and jiggling along invisible microtubule tracks, undergoing multiple fission events, in which a single tubule divides into two along the short or transverse axis, and fusion events, in which two tubules meet at end junctions to merge into one (Chen and Chan, 2004). These observations, and the discovery of developmentally essential factors controlling the process, launched the currently two decades worth of research in the field now called mitochondrial dynamics (Chan, 2006b, a).

Initial identification of essential factors for fission and fusion

Genetic studies in flies, yeast, and worms laid the early groundwork in understanding mitochondrial dynamics, identifying the factors required for the fission and fusion events. The first mitochondrial fusion protein discovered was fuzzy onions (Fzo), named for the fuzzy onion-like appearance of unfused mitochondria in the spermatids of *Drosophila fzo* mutants. Homologs in yeast (Fzo1p), mice, and humans (Mfn1 and Mfn2 for mitofusin 1 and mitofusin 2, respectively) were identified thereafter, with mutants harboring loss-of-function mutations in the genes of these proteins exhibiting fragmented mitochondria from reduction of mitochondrial fusion (Hermann *et al.*, 1998; Rapaport *et al.*, 1998; Santel and Fuller, 2001; Chen *et al.*, 2003; Eura *et al.*, 2003). These proteins, which came to be called mitofusins, localize to the outer mitochondrial membrane of mitochondria, and are essentiaal for the fusion of this outer layer (Hermann *et al.*, 1998; Rapaport *et al.*, 1998; Rojo *et al.*, 2002). Inner membrane fusion was found to be mediated by mitochondrial genome maintenance 1 (Mgm1p) in

yeast, and optic atrophy type 1 (Opa1) in mammals (Olichon *et al.*, 2002; Satoh *et al.*, 2003; Wong *et al.*, 2003; Meeusen *et al.*, 2006). In mammalian cells devoid of Opa1, outer membrane fusion, but not inner membrane fusion, is observed, suggesting complete full mitochondrial fusion proceeds in a sequential manner, first by mitofusin-mediated outer membrane fusion followed by Opa1-driven inner membrane fusion (Malka *et al.*, 2005; Song *et al.*, 2009).

Work in yeast and *C. elegans* identified the yeast DyNaMin-related 1 (Dnm1) protein and worm dynamin-related protein 1 (DRP-1) as the factor required for mitochondrial fission (Bleazard *et al.*, 1999; Labrousse *et al.*, 1999; Sesaki and Jensen, 1999). Mutations in the yeast Dnm1 and *C. elegans* DRP-1 were shown to block fission, resulting in highly elongated and networked mitochondria (Bleazard *et al.*, 1999; Sesaki and Jensen, 1999). Immuno-electron microscopy and live-imaging microscopy studies localized the proteins to puncta on mitochondria, and overexpression of the proteins resulted in fragmented mitochondria (Bleazard *et al.*, 1999; Labrousse *et al.*, 1999). Live-imaging studies with a green fluorescent protein (GFP) fusion of the mammalian homolog, dynamin-related protein 1 (Drp1), similarly showed a punctate localization to the mitochondria surface, and examination of dominant-negative Drp1 mutants revealed highly elongated mitochondria in cultured cells (Smirnova *et al.*, 1998; Smirnova *et al.*, 2001). Altogether, these studies of Drp1, mitofusins, and Opa1 established a "dual control" model of mitochondrial dynamics, in which the overall morphology of the mitochondrial population in a cell is determined by the opposing action of fission by Drp1 and fusion by Mfn1/2 and Opa1 (Detmer and Chan, 2007). Knockout mice studies clearly demonstrate that this balance is critical for organismal development, as loss of any

one of these major factors (Mfn1, Mfn2, Opa1, Drp1) leads to embryonic lethality (Chen *et al.*, 2003; Davies *et al.*, 2007; Ishihara *et al.*, 2009; Wakabayashi *et al.*, 2009). In addition, disease-causing variants of each of these factors have been described in humans (Chen and Chan, 2009).

Dynamins regulate mitochondrial fission and fusion

Mfn1, Mfn2, Opa1, and Drp1 belong to a family of large guanosine triphosphate hydrolases (GTPases) called dynamins, molecular machines that that are specialized for mediating membrane remodeling in the cell (Praefcke and McMahon, 2004). From a physical mechanics perspective, both mitochondrial fission and fusion require, at some point, fusion of two separate phospholipid bilayers. This carries a high energetic cost (Chernomordik and Kozlov, 2008; Lenz *et al.*, 2009). Dynamins, however, are well-suited for this challenge, by having several biochemical properties that help to solve this problem. Dynamin GTPase activity allows the coupling of nucleotide hydrolysis to membrane deformation, providing energy to lower the energetic cost of membrane fusion. The ability to bind lipids, and the ability to self-assemble into helical arrays, allow dynamins to induce curvature of its membrane substrate and modulate its tension, potentially lowering the energy barrier for fission and fusion (Morlot *et al.*, 2012; Antonny *et al.*, 2016). Though they have been identified to play specific roles in mitochondrial fission and fusion, the exact mechanism of how Mfn1, Mfn2, Opa1, and Drp1 carry out those roles is not well understood and is an active area of investigation. Since their biochemical properties likely form the basis behind the mechanism, many

studies have focused on understanding basic dynamin biochemistry (Antonny *et al.*, 2016).

Dynamin structure and biochemistry

Dynamin, the founding member of the dynamin protein family, was initially discovered in 1989 as a 100 kilodalton (kDa), microtubule-associated protein from mammalian brain lysates (Shpetner and Vallee, 1989). It was named "dynamin" from the Greek word "dynamis" for force or power, because of a dynamic microtubule sliding activity observed *in vitro* that was later found to be misattributed to the molecule. Cloning and sequencing of the gene eventually grouped it with a family of large GTP-binding and hydrolyzing proteins, alongside the mouse antiviral Mx proteins and the yeast vacuolar protein sorting factor, VPS1 (Obar *et al.*, 1990). Dynamin was shown to be homologous to the product of the *Drosophila shibire* (Japanese for "limbs going to sleep") gene, the mutants of which exhibit temperature-sensitive paralysis due to defects in endocytosis at neuronal synapses (Poodry and Edgar; Chen *et al.*, 1991; van der Bliek and Meyerowitz, 1991). Experiments showing the formation of dynamin collars at the neck of budding endocytic vesicles established its role in presynaptic vesicle formation, and images of its *in vitro* helical assembly around lipid tubules inspired the current model of dynamin as a self-assembling GTPase critical for vesicular membrane scission (Koenig and Ikeda, 1989; Hinshaw and Schmid, 1995; Takei *et al.*, 1995).

Elegant work by several groups has developed a basic picture of dynamin behavior. Dynamin can self-assemble into rings and helical spirals *in vitro* (Hinshaw and Schmid, 1995). When added to membrane templates such as liposomes, dynamin can

assemble into helical arrays that tubulate the membrane (Hinshaw and Schmid, 1995; Marks *et al.*, 2001). Addition of non-hydrolyzable GTP promotes and stabilizes the polymer on lipid tubules, and hydrolysis of GTP is required to disassemble and release dynamin from the membrane (Marks *et al.*, 2001). Hydrolysis of GTP also leads to constriction of the helical polymer, and is required for membrane scission during endocytosis (Marks *et al.*, 2001). Exactly how GTP hydrolysis and the resulting constriction lead to membrane scission, however, is unclear, and continues to be actively investigated (Antonny *et al.*, 2016).

Dynamin and its family members share a similar body plan, plus or minus a domain or two. At the 'head' or N-terminus of most dynamins sits the highly conserved GTPase domain (G domain), responsible for binding and hydrolyzing GTP (Faelber *et al.*, 2011; Ford *et al.*, 2011; Ferguson and De Camilli, 2012; Antonny *et al.*, 2016). This activity translates into a conformational rearrangement at the hinge-like 'neck' of dynamin, a short three-helical bundle signaling element (BSE) domain adjacent and continuous with the G domain (Chappie *et al.*, 2011; Faelber *et al.*, 2011; Ford *et al.*, 2011). The BSE connects the G domain to the main 'body' of dynamin, which consists of a cylinder-like, four-helical bundle stalk domain (Faelber *et al.*, 2011; Ford *et al.*, 2011; Reubold *et al.*, 2015). Classically referred to as the middle domain, the stalk domain mediates the hallmark oligomerization activity of dynamin. The opposite end of the stalk domain contains the least conserved region of dynamin, a domain that varies in size and function across the different dynamin family members (Strack and Cribbs, 2012). In most dynamins, this domain mediates its association with lipids, membrane surfaces, and interacting partners (Achiriloaie *et al.*, 1999; Lemmon, 2007).

The G domain of dynamin is unique in that it has a lower nucleotide binding affinity, and faster basal hydrolysis rate, than the G domains of other GTPases, such as those of the Ras family of small GTPases or G-protein coupled receptors (Song and Schmid, 2003). Not surprisingly, this property is more similar to that of ATP-driven motors such as kinesin, reflecting dynamin's role as a mechanoenzyme (Antonny *et al.*, 2016). Moreover, in contrast to the heterotypic associations seen with other GTPases, stimulation of GTP hydrolysis in dynamins is catalyzed by the homotypic association of via the G domain, similar to the bacterial tRNA modification GTPase MnmE protein or eukaryotic signal recognition particle SRP (Gasper *et al.*, 2009; Chappie *et al.*, 2010). One crystal structure model of the G domain bound to an unhydrolyzable GTP suggests that GTP binding results in a conformational switch at the BSE hinge region, relative to crystal structure models of the G domains in an apo or GDP-bound state (Niemann *et al.*, 2001; Chappie *et al.*, 2011). Together with cryo-electron microscopy (cryo-EM) reconstruction studies of dynamin assembled around a lipid tubule, the structures suggest an assembly model in which two GTP-bound G domains, from adjacent rungs of a dynamin spiral, reach across while in an extended BSE conformational state and dimerize with each other to catalyze GTP hydrolysis. Hydrolysis induces the BSE to return to the ground state, a movement that delivers a powerstroke that drives constriction of the dynamin polymer into a smaller diameter (Chappie *et al.*, 2011). Successive constrictions through this powerstroke mechanism is believed to squeeze the membrane tubule until membrane scission occurs.

The crystal structure of the stalk domain of the immunity-related myxovirus resistance protein 1 (MxA) provided the first mechanistic insight into how dynamin

forms its helical arrays (Arnheiter and Meier, 1990; Gao *et al.*, 2010). The structural model revealed a four-helical bundle that forms a stable interaction with another stalk through a symmetrical hydrophobic interface. This dimeric unit, typically depicted as a cross, interacts with an adjacent dimer to generate a tetrameric species. This occurs through a symmetrical hydrophobic interface near the BSE end of the stalk, and an asymmetric third interface, composed of poorly resolved loops located in two locations along the first helical span. Dynamin self-assembly is achieved by continued iteration at these two interfaces, at angles to achieve a helical pitch, to create the higher-order oligomeric rings and spirals observed in the electron microscopy studies previously mentioned. Mutations introduced into these interface residues in MxA, dynamin, and Drp1 result in stable dimers unable to form higher-order oligomers (Faelber *et al.*, 2011; Ford *et al.*, 2011; Gao *et al.*, 2011; Frohlich *et al.*, 2013). Supporting this model is the crystal structure of a dynamin tetramer that depicts resolved features of the loop interactions (Reubold *et al.*, 2015).

Mitochondrial fusion dynamins

The mitochondrial outer membrane dynamins, mitofusins Mfn1 and Mfn2, and the mitochondrial inner membrane fusion dynamin, Opa1, are unique in that they are tethered to their respective membranes (Rojo *et al.*, 2002; Griparic *et al.*, 2004). By analogy to the homologous bacterial dynamin-like protein (BDLP), the mitofusins are believed to be tethered to the outer membrane via a hydrophobic patch located at the variable region located at the tip of the dynamin stalk (Low and Lowe, 2006; Qi *et al.*, 2016; Cao *et al.*, 2017). Compared to the dynamin, BDLP is different in that its BSE

helices are longer and feature a much more acute angle at its junction with the stalk domain, creating an overall 'V' shape for the molecule (Low and Lowe, 2006). A cryo-EM reconstruction of BDLP, bound to the unhydrolyzable GTP analog GMPPNP and assembled around a lipid tubule, depicts a remarkably different conformation, with BDLP adopting a straightened linear configuration, such that the BSE and stalk helices are collinear (Low *et al.*, 2009). This suggests that the BDLP conformation is regulated by nucleotide binding and lipid association. Recent structures of mammalian mitofusin truncations, consisting of just the GTPase and BSE region of the molecule, bear a close resemblance to BDLP, suggesting a similar mechanism and overall structure might apply (Qi *et al.*, 2016; Cao *et al.*, 2017). Like other dynamins, the mitofusins also seem to be regulated by G domain-dimerization interactions, and are proposed to mediate the joining of opposing membranes to drive fusion. A tethering step, through an anti-parallel coiled-coil interaction between the C-terminal helices of two opposing mitofusins, might also feature in the fusion mechanism, as suggested by a crystal structure of the coiled-coil interaction (Koshiba *et al.*, 2004). How and whether higher-order oligomerizations might factor into the fusion process is not known.

Opa1 localizes to the mitochondrial intermembrane space, and is tethered to the inner membrane by a transmembrane domain located N-terminal to the GTPase domain (Olichon *et al.*, 2002). Between this transmembrane domain and the start of the dynamin-homologous half of the protein lies a relatively unstructured region, save for one or two predicted coiled-coil domains. This intermediary stretch contains two cleavage sites for protease-catalyzed release of Opa1 from the membrane into the intermembrane space. Cleavage results in a dual population of soluble 'short' form Opa1 in the intermembrane

space together with an uncleaved ‘long’ form tethered to the inner membrane (Ishihara *et al.*, 2006; Song *et al.*, 2007). It has been accepted that the long form is required for fusion of the inner membrane, but no agreement has been reached over the role of the short form (Song *et al.*, 2007; Anand *et al.*, 2014). *In vitro*, the behavior of short form Opa1 resembles that of dynamin in its ability to tubulate lipid templates, but other properties, such as its assembly mechanism and mode of higher-order oligomerization, might differ, as suggested by 2-D electron microscopy reconstructions of mgm1p that hint at trimeric interactions and our own unpublished observations that hint at a much weaker stalk-stalk interaction compared to dynamin or Drp1 (DeVay *et al.*, 2009; Ban *et al.*, 2010).

The mitochondrial fission dynamin, Drp1

The current working model of mitochondrial fission describes a coordinated series of mitochondrial constriction events beginning with an initial constriction mediated by circumscribing ER tubules, followed by the recruitment of the mitochondrial dynamin Drp1 to the mitochondrial surface to further the constriction and ultimately split the mitochondria (van der Bliek *et al.*, 2013). In mammalian cells, assistance from actin polymerization and an additional constriction step by dynamin have recently been implicated (Lee *et al.*, 2016).

The biochemical properties of Drp1 are remarkably similar to that of dynamin. It is able to oligomerize, tubulate lipid templates, and bind and hydrolyze GTP *in vitro* (Smirnova *et al.*, 2001; Mears *et al.*, 2011; Koirala *et al.*, 2013). Drp1 contains a GTPase domain, a BSE domain, a stalk domain, and in lieu of a PH domain, has so-called Insert B domain that has been shown to bind cardiolipin and is thought to mediate its interaction

with the mitochondrial outer membrane (Frohlich *et al.*, 2013; Wenger *et al.*, 2013; Bustillo-Zabalbeitia *et al.*, 2014). In the cell, the majority of Drp1 appears cytosolic, with a fraction observed to assemble as punctate foci on the surface of mitochondria (Smirnova *et al.*, 2001; Macdonald *et al.*, 2014). Genetic ablation of Drp1 results in elongated mitochondria, whereas overexpression results in fragmented mitochondria (Labrousse *et al.*, 1999; Ishihara *et al.*, 2009; Wakabayashi *et al.*, 2009). In mice, Drp1 is required for embryonic, brain, and heart development (Ishihara *et al.*, 2009; Wakabayashi *et al.*, 2009; Ashrafian *et al.*, 2010). A lethal point mutation in the stalk domain of Drp1 has been described in a human patient (Chang *et al.*, 2010).

Unlike the PH domain of dynamin, the Insert B domain of Drp1 is predicted to be largely unstructured, impeding efforts to crystallize the full-length protein (Frohlich *et al.*, 2013). The structure of Drp1, minus this domain, closely resembles that of dynamin, with the exceptions of an additional loop in the GTPase domain with unknown function, and a putative fourth interaction interface hypothesized to create a tetramer perpendicular to the oligomerization interface. This tetrameric unit is proposed to produce a double-beamed helical assembly instead of a single, spiraling row of polymers (Frohlich *et al.*, 2013). In addition to maintaining normal mitochondrial morphology, Drp1-mediated mitochondrial fission has also been demonstrated to be important for mitosis and apoptosis (Youle and Karbowski, 2005; Kashatus *et al.*, 2011). Regulation of Drp1 activity is primarily accomplished by phosphorylation at two different sites in the Insert B domain, though other post-translational modifications and modification sites exist (Chang and Blackstone, 2010).

Drp1 recruitment proteins

Drp1 primarily exists as a soluble dimer/tetramer equilibrium in the cytosol, and relies on outer mitochondrial membrane receptors to redirect it to the mitochondrial surface for membrane scission (Loson *et al.*, 2013; Macdonald *et al.*, 2014). In yeast, the only known receptors are mitochondrial fission protein 1 (Fis1), mitochondrial division protein 1 (Mdv1), and CCR4-associated factor 4 (Caf4) (Otera and Mihara, 2011). Fis1 is membrane-bound to the outer membrane, and forms a stable complex with one of the two cytosolic adaptors Mdv1 or Caf4 (Koirala *et al.*, 2010; Zhang *et al.*, 2012). A β-propeller domain in Mdv1 interacts with the Insert B domain of Dnm1 to recruit it to the mitochondrial surface (Bui *et al.*, 2012). The mammalian homolog of Fis1 was initially expected to be the receptor for Drp1 but later shown to have little to no role in mitochondrial fission in cultured cell under basal conditions (Otera *et al.*, 2010; Loson *et al.*, 2013). Instead, the major receptors appear to be the membrane-bound mitochondrial fission factor (Mff), mitochondrial dynamics protein of 51 kDa (MiD51), and mitochondrial dynamics protein of 49 kDa (MiD49) proteins (Otera *et al.*, 2010; Palmer *et al.*, 2011; Zhao *et al.*, 2011).

Mff is a C-tailed anchored protein discovered in 2008 as a mitochondrial and peroxisome-targeted protein required for recruiting Drp1 to mediate mitochondrial and peroxisomal fission, with homologs in mammals and flies but not yeast (Gandre-Babbe and van der Bliek, 2008). Like Drp1 depletion, Mff knockdown results in highly elongated mitochondria in mammalian cells (Gandre-Babbe and van der Bliek, 2008; Otera *et al.*, 2010). In contrast to Drp1 knockout mice, mouse knockouts of Mff are not embryonically lethal, suggesting other receptors exist that compensate for the loss of Mff

during development in these mutants (Chen *et al.*, 2015). These might be the MiD51 and MiD49 proteins, N-terminally anchored proteins discovered in 2011 as receptors for Drp1 in screens aimed at finding proteins that affected mitochondrial morphology (Palmer *et al.*, 2011; Zhao *et al.*, 2011). Predominantly found in higher eukaryotes, knockdown of the MiDs results in loss of mitochondrial fission, but paradoxically, over-expression also results in inhibition of fission, despite observable Drp1 recruitment. These findings of have produced two models of MiD function, one in which it functions as an inhibitor of mitochondrial fission and one as a promoting factor. Crystal structures of the soluble domains of MiD51 and MiD49 show that they belong to a family of nucleotidyl transferase proteins, but as of yet no enzymatic function has described for either of these proteins (Loson *et al.*, 2014; Richter *et al.*, 2014; Loson *et al.*, 2015). Simultaneous reduction of the MiD proteins and Mff, leads to additive increase in mitochondrial elongation, compared to of either alone, that almost recapitulates that seen in Drp1 knockout cells (Otera *et al.*, 2016; Loson *et al.*, 2013). This suggests that these receptors have non-redundant roles in mediating Drp1 recruitment, and together account for the majority of Drp1 recruitment activity.

Thesis outline

Drp1 recruitment to mitochondria is a necessary step for mitochondrial fission, and though the major receptors for Drp1 have been identified, many questions remain about the role of each receptor and overall mechanism of recruitment in mammalian cells. In yeast the model appears straightforward: Fis1, anchored to the outer mitochondrial membrane, complexes with soluble Mdv1 or Caf4, which in turn interacts with Dnm1 to

bring it to the mitochondrial surface. Mdv1 recruits Dnm1 through the insert B domain, and might also play a role as an effector protein in Dnm1 activation and assembly. The mammalian homolog of Fis1, however, appears to play a minor role in Drp1 recruitment under basal conditions, instead relinquishing this role to Mff and the MiD proteins. How Mff and MiD51 recruit Drp1 is unknown. In Chapter 2 of this thesis I examine the interaction between Drp1 and Mff to help understand the Drp1 recruitment process with respect to Mff. In Chapter 3, I examine how a point mutation of Drp1, recently discovered in patients presenting with encephalopathy and refractory epilepsy, affects its recruitment to mitochondria and mitochondrial morphology. In the concluding Chapter 4, I summarize my main findings, propose models of Mff and MiD function, and discuss future avenues of inquiry on the topic of Drp1 recruitment and regulation.

References

Achiriloaie, M., Barylko, B., and Albanesi, J.P. (1999). Essential Role of the Dynamin Pleckstrin Homology Domain in Receptor-Mediated Endocytosis. Molecular and Cellular Biology *19*, 1410-1415.

Ajioka, R.S., Phillips, J.D., and Kushner, J.P. (2006). Biosynthesis of heme in mammals. Biochimica et biophysica acta *1763*, 723-736.

Anand, R., Wai, T., Baker, M.J., Kladt, N., Schauss, A.C., Rugarli, E., and Langer, T. (2014). The i-AAA protease YME1L and OMA1 cleave OPA1 to balance mitochondrial fusion and fission. J Cell Biol *204*, 919-929.

Antonny, B., Burd, C., De Camilli, P., Chen, E., Daumke, O., Faelber, K., Ford, M., Frolov, V.A., Frost, A., Hinshaw, J.E., Kirchhausen, T., Kozlov, M.M., Lenz, M., Low, H.H., McMahon, H., Merrifield, C., Pollard, T.D., Robinson, P.J., Roux, A., and Schmid, S. (2016). Membrane fission by dynamin: what we know and what we need to know. The EMBO journal *35*, 2270-2284.

Arnheiter, H., and Meier, E. (1990). Mx proteins: antiviral proteins by chance or by necessity? The New biologist *2*, 851-857.

Ashrafian, H., Docherty, L., Leo, V., Towlson, C., Neilan, M., Steeples, V., Lygate, C.A., Hough, T., Townsend, S., Williams, D., Wells, S., Norris, D., Glyn-Jones, S., Land, J., Barbaric, I., Lalanne, Z., Denny, P., Szumska, D., Bhattacharya, S., Griffin, J.L., Hargreaves, I., Fernandez-Fuentes, N., Cheeseman, M., Watkins, H., and Dear, T.N. (2010). A Mutation in the Mitochondrial Fission Gene Dnm1l Leads to Cardiomyopathy. PLoS Genetics *6*.

Ban, T., Heymann, J.A., Song, Z., Hinshaw, J.E., and Chan, D.C. (2010). OPA1 disease alleles causing dominant optic atrophy have defects in cardiolipin-stimulated GTP hydrolysis and membrane tubulation. Human molecular genetics *19*, 2113-2122.

Bereiter-Hahn, J., and Voth, M. (1994). Dynamics of mitochondria in living cells: shape changes, dislocations, fusion, and fission of mitochondria. Microscopy research and technique *27*, 198-219.

Bleazard, W., McCaffery, J.M., King, E.J., Bale, S., Mozdy, A., Tieu, Q., Nunnari, J., and Shaw, J.M. (1999). The dynamin-related GTPase Dnm1 regulates mitochondrial fission in yeast. Nature cell biology *1*, 298-304.

Bui, H.T., Karren, M.A., Bhar, D., and Shaw, J.M. (2012). A novel motif in the yeast mitochondrial dynamin Dnm1 is essential for adaptor binding and membrane recruitment. The Journal of Cell Biology *199*, 613-622.

Bustillo-Zabalbeitia, I., Montessuit, S., Raemy, E., Basanez, G., Terrones, O., and Martinou, J.C. (2014). Specific interaction with cardiolipin triggers functional activation of Dynamin-Related Protein 1. PloS one *9*, e102738.

Cao, Y.L., Meng, S., Chen, Y., Feng, J.X., Gu, D.D., Yu, B., Li, Y.J., Yang, J.Y., Liao, S., Chan, D.C., and Gao, S. (2017). MFN1 structures reveal nucleotide-triggered dimerization critical for mitochondrial fusion. Nature *542*, 372-376.

Chan, D.C. (2006a). Mitochondria: dynamic organelles in disease, aging, and development. Cell *125*, 1241-1252.

Chan, D.C. (2006b). Mitochondrial fusion and fission in mammals. Annu Rev Cell Dev Biol *22*, 79-99.

Chang, C.R., and Blackstone, C. (2010). Dynamic regulation of mitochondrial fission through modification of the dynamin-related protein Drp1. Annals of the New York Academy of Sciences *1201*, 34-39.

Chang, C.R., Manlandro, C.M., Arnoult, D., Stadler, J., Posey, A.E., Hill, R.B., and Blackstone, C. (2010). A lethal de novo mutation in the middle domain of the dynamin-related GTPase Drp1 impairs higher order assembly and mitochondrial division. The Journal of biological chemistry *285*, 32494-32503.

Chappie, J.S., Acharya, S., Leonard, M., Schmid, S.L., and Dyda, F. (2010). G domain dimerization controls dynamin's assembly-stimulated GTPase activity. Nature *465*, 435-440.

Chappie, J.S., Mears, J.A., Fang, S., Leonard, M., Schmid, S.L., Milligan, R.A., Hinshaw, J.E., and Dyda, F. (2011). A pseudoatomic model of the dynamin polymer identifies a hydrolysis-dependent powerstroke. Cell *147*, 209-222.

Chen, H., and Chan, D.C. (2004). Mitochondrial dynamics in mammals. Curr Top Dev Biol *59*, 119-144.

Chen, H., and Chan, D.C. (2009). Mitochondrial dynamics–fusion, fission, movement, and mitophagy–in neurodegenerative diseases. Human molecular genetics *18*, R169-176.

Chen, H., Detmer, S.A., Ewald, A.J., Griffin, E.E., Fraser, S.E., and Chan, D.C. (2003). Mitofusins Mfn1 and Mfn2 coordinately regulate mitochondrial fusion and are essential for embryonic development. J Cell Biol *160*, 189-200.

Chen, H., Ren, S., Clish, C., Jain, M., Mootha, V., McCaffery, J.M., and Chan, D.C. (2015). Titration of mitochondrial fusion rescues Mff-deficient cardiomyopathy. J Cell Biol *211*, 795-805.

Chen, M.S., Obar, R.A., Schroeder, C.C., Austin, T.W., Poodry, C.A., Wadsworth, S.C., and Vallee, R.B. (1991). Multiple forms of dynamin are encoded by shibire, a Drosophila gene involved in endocytosis. Nature *351*, 583-586.

Chernomordik, L.V., and Kozlov, M.M. (2008). Mechanics of membrane fusion. Nat Struct Mol Biol *15*, 675-683.

Clayton, D.A. (1991). Replication and transcription of vertebrate mitochondrial DNA. Annual review of cell biology *7*, 453-478.

Daems, W.T., and Wisse, E. (1966). Shape and attachment of the cristae mitochondriales in mouse hepatic cell mitochondria. Journal of ultrastructure research *16*, 123-140.

Davies, V.J., Hollins, A.J., Piechota, M.J., Yip, W., Davies, J.R., White, K.E., Nicols, P.P., Boulton, M.E., and Votruba, M. (2007). Opa1 deficiency in a mouse model of autosomal dominant optic atrophy impairs mitochondrial morphology, optic nerve structure and visual function. Human molecular genetics *16*, 1307-1318.

Detmer, S.A., and Chan, D.C. (2007). Functions and dysfunctions of mitochondrial dynamics. Nature reviews. Molecular cell biology *8*, 870-879.

DeVay, R.M., Dominguez-Ramirez, L., Lackner, L.L., Hoppins, S., Stahlberg, H., and Nunnari, J. (2009). Coassembly of Mgm1 isoforms requires cardiolipin and mediates mitochondrial inner membrane fusion. J Cell Biol *186*, 793-803.

Eura, Y., Ishihara, N., Yokota, S., and Mihara, K. (2003). Two mitofusin proteins, mammalian homologues of FZO, with distinct functions are both required for mitochondrial fusion. Journal of biochemistry *134*, 333-344.

Faelber, K., Posor, Y., Gao, S., Held, M., Roske, Y., Schulze, D., Haucke, V., Noe, F., and Daumke, O. (2011). Crystal structure of nucleotide-free dynamin. Nature *477*, 556-560.

Ferguson, S.M., and De Camilli, P. (2012). Dynamin, a membrane-remodelling GTPase. Nature reviews. Molecular cell biology *13*, 75-88.

Ford, M.G., Jenni, S., and Nunnari, J. (2011). The crystal structure of dynamin. Nature *477*, 561-566.

Frohlich, C., Grabiger, S., Schwefel, D., Faelber, K., Rosenbaum, E., Mears, J., Rocks, O., and Daumke, O. (2013). Structural insights into oligomerization and mitochondrial remodelling of dynamin 1-like protein. The EMBO journal *32*, 1280-1292.

Gandre-Babbe, S., and van der Bliek, A.M. (2008). The novel tail-anchored membrane protein Mff controls mitochondrial and peroxisomal fission in mammalian cells. Molecular biology of the cell *19*, 2402-2412.

Gao, S., von der Malsburg, A., Dick, A., Faelber, K., Schroder, G.F., Haller, O., Kochs, G., and Daumke, O. (2011). Structure of myxovirus resistance protein a reveals intra- and intermolecular domain interactions required for the antiviral function. Immunity *35*, 514-525.

Gao, S., von der Malsburg, A., Paeschke, S., Behlke, J., Haller, O., Kochs, G., and Daumke, O. (2010). Structural basis of oligomerization in the stalk region of dynamin-like MxA. Nature *465*, 502-506.

Gasper, R., Meyer, S., Gotthardt, K., Sirajuddin, M., and Wittinghofer, A. (2009). It takes two to tango: regulation of G proteins by dimerization. Nature reviews. Molecular cell biology *10*, 423-429.

Griparic, L., van der Wel, N.N., Orozco, I.J., Peters, P.J., and van der Bliek, A.M. (2004). Loss of the intermembrane space protein Mgm1/OPA1 induces swelling and localized constrictions along the lengths of mitochondria. The Journal of biological chemistry *279*, 18792-18798.

Hermann, G.J., Thatcher, J.W., Mills, J.P., Hales, K.G., Fuller, M.T., Nunnari, J., and Shaw, J.M. (1998). Mitochondrial fusion in yeast requires the transmembrane GTPase Fzo1p. J Cell Biol *143*, 359-373.

Hiltunen, J.K., Autio, K.J., Schonauer, M.S., Kursu, V.A., Dieckmann, C.L., and Kastaniotis, A.J. (2010). Mitochondrial fatty acid synthesis and respiration. Biochimica et biophysica acta *1797*, 1195-1202.

Hinshaw, J.E., and Schmid, S.L. (1995). Dynamin self-assembles into rings suggesting a mechanism for coated vesicle budding. Nature *374*, 190-192.

Ishihara, N., Fujita, Y., Oka, T., and Mihara, K. (2006). Regulation of mitochondrial morphology through proteolytic cleavage of OPA1. The EMBO journal *25*, 2966-2977.

Ishihara, N., Nomura, M., Jofuku, A., Kato, H., Suzuki, S.O., Masuda, K., Otera, H., Nakanishi, Y., Nonaka, I., Goto, Y., Taguchi, N., Morinaga, H., Maeda, M., Takayanagi, R., Yokota, S., and Mihara, K. (2009). Mitochondrial fission factor Drp1 is essential for embryonic development and synapse formation in mice. Nature cell biology *11*, 958-966.

Kashatus, D.F., Lim, K.-H., Brady, D.C., Pershing, N.L.K., Cox, A.D., and Counter, C.M. (2011). RALA and RALBP1 regulate mitochondrial fission at mitosis. Nature cell biology *13*, 1108-1115.

Koenig, J.H., and Ikeda, K. (1989). Disappearance and reformation of synaptic vesicle membrane upon transmitter release observed under reversible blockage of membrane retrieval. J Neurosci *9*, 3844-3860.

Koirala, S., Bui, H.T., Schubert, H.L., Eckert, D.M., Hill, C.P., Kay, M.S., and Shaw, J.M. (2010). Molecular architecture of a dynamin adaptor: implications for assembly of mitochondrial fission complexes. J Cell Biol *191*, 1127-1139.

Koirala, S., Guo, Q., Kalia, R., Bui, H.T., Eckert, D.M., Frost, A., and Shaw, J.M. (2013). Interchangeable adaptors regulate mitochondrial dynamin assembly for membrane scission. Proceedings of the National Academy of Sciences *110*, E1342-E1351.

Koshiba, T., Detmer, S.A., Kaiser, J.T., Chen, H., McCaffery, J.M., and Chan, D.C. (2004). Structural basis of mitochondrial tethering by mitofusin complexes. Science (New York, N.Y.) *305*, 858-862.

Labrousse, A.M., Zappaterra, M.D., Rube, D.A., and van der Bliek, A.M. (1999). C. elegans dynamin-related protein DRP-1 controls severing of the mitochondrial outer membrane. Molecular cell *4*, 815-826.

Lee, J.E., Westrate, L.M., Wu, H., Page, C., and Voeltz, G.K. (2016). Multiple dynamin family members collaborate to drive mitochondrial division. Nature *540*, 139-143.

Lemmon, M.A. (2007). Pleckstrin Homology (PH) domains and phosphoinositides. Biochemical Society symposium, 81-93.

Lenz, M., Morlot, S., and Roux, A. (2009). Mechanical requirements for membrane fission: Common facts from various examples. FEBS letters *583*, 3839-3846.

Loson, O.C., Liu, R., Rome, M.E., Meng, S., Kaiser, J.T., Shan, S.O., and Chan, D.C. (2014). The Mitochondrial Fission Receptor MiD51 Requires ADP as a Cofactor. Structure *22*, 367-377.

Loson, O.C., Meng, S., Ngo, H., Liu, R., Kaiser, J.T., and Chan, D.C. (2015). Crystal structure and functional analysis of MiD49, a receptor for the mitochondrial fission protein Drp1. Protein science : a publication of the Protein Society *24*, 386-394.

Loson, O.C., Song, Z., Chen, H., and Chan, D.C. (2013). Fis1, Mff, MiD49, and MiD51 mediate Drp1 recruitment in mitochondrial fission. Molecular biology of the cell *24*, 659-667.

Low, H.H., and Lowe, J. (2006). A bacterial dynamin-like protein. Nature *444*, 766-769.

Low, H.H., Sachse, C., Amos, L.A., and Lowe, J. (2009). Structure of a bacterial dynamin-like protein lipid tube provides a mechanism for assembly and membrane curving. Cell *139*, 1342-1352.

Macdonald, P.J., Stepanyants, N., Mehrotra, N., Mears, J.A., Qi, X., Sesaki, H., and Ramachandran, R. (2014). A dimeric equilibrium intermediate nucleates Drp1 reassembly on mitochondrial membranes for fission. Molecular biology of the cell *25*, 1905-1915.

Malka, F., Guillery, O., Cifuentes-Diaz, C., Guillou, E., Belenguer, P., Lombes, A., and Rojo, M. (2005). Separate fusion of outer and inner mitochondrial membranes. EMBO Rep *6*, 853-859.

Mannella, C.A., Marko, M., Penczek, P., Barnard, D., and Frank, J. (1994). The internal compartmentation of rat-liver mitochondria: Tomographic study using the high-voltage transmission electron microscope. Microscopy research and technique *27*, 278-283.

Marks, B., Stowell, M.H.B., Vallis, Y., Mills, I.G., Gibson, A., Hopkins, C.R., and McMahon, H.T. (2001). GTPase activity of dynamin and resulting conformation change are essential for endocytosis. Nature *410*, 231-235.

Mears, J.A., Lackner, L.L., Fang, S., Ingerman, E., Nunnari, J., and Hinshaw, J.E. (2011). Conformational changes in Dnm1 support a contractile mechanism for mitochondrial fission. Nat Struct Mol Biol *18*, 20-26.

Meeusen, S., DeVay, R., Block, J., Cassidy-Stone, A., Wayson, S., McCaffery, J.M., and Nunnari, J. (2006). Mitochondrial inner-membrane fusion and crista maintenance requires the dynamin-related GTPase Mgm1. Cell *127*, 383-395.

Mitchell, P. (1961). Coupling of phosphorylation to electron and hydrogen transfer by a chemi-osmotic type of mechanism. Nature *191*, 144-148.

Morlot, S., Galli, V., Klein, M., Chiaruttini, N., Manzi, J., Humbert, F., Dinis, L., Lenz, M., Cappello, G., and Roux, A. (2012). Membrane shape at the edge of the dynamin helix sets location and duration of the fission reaction. Cell *151*, 619-629.

Niemann, H.H., Knetsch, M.L.W., Scherer, A., Manstein, D.J., and Kull, F.J. (2001). Crystal structure of a dynamin GTPase domain in both nucleotide-free and GDP-bound forms. The EMBO journal *20*, 5813-5821.

Nunnari, J., Marshall, W.F., Straight, A., Murray, A., Sedat, J.W., and Walter, P. (1997). Mitochondrial transmission during mating in Saccharomyces cerevisiae is determined by mitochondrial fusion and fission and the intramitochondrial segregation of mitochondrial DNA. Molecular biology of the cell *8*, 1233-1242.

Obar, R.A., Collins, C.A., Hammarback, J.A., Shpetner, H.S., and Vallee, R.B. (1990). Molecular cloning of the microtubule-associated mechanochemical enzyme dynamin reveals homology with a new family of GTP-binding proteins. Nature *347*, 256-261.

Olichon, A., Emorine, L.J., Descoins, E., Pelloquin, L., Brichese, L., Gas, N., Guillou, E., Delettre, C., Valette, A., Hamel, C.P., Ducommun, B., Lenaers, G., and Belenguer, P. (2002). The human dynamin-related protein OPA1 is anchored to the mitochondrial inner membrane facing the inter-membrane space. FEBS letters *523*, 171-176.

Otera, H., and Mihara, K. (2011). Discovery of the membrane receptor for mitochondrial fission GTPase Drp1. Small GTPases *2*, 167-172.

Otera, H., Wang, C., Cleland, M.M., Setoguchi, K., Yokota, S., Youle, R.J., and Mihara, K. (2010). Mff is an essential factor for mitochondrial recruitment of Drp1 during mitochondrial fission in mammalian cells. J Cell Biol *191*, 1141-1158.

Otera, H., Miyata, N., Kuge, O., and Mihara, K. (2016). Drp1-dependent mitochondrial fission via MiD49/51 is essential for apoptotic cristae remodeling. The Journal of Cell Biology *212*, 531-544.

Palade, G.E. (1953). An electron microscope study of the mitochondrial structure. J Histochem Cytochem *1*, 188-211.

Palmer, C.S., Osellame, L.D., Laine, D., Koutsopoulos, O.S., Frazier, A.E., and Ryan, M.T. (2011). MiD49 and MiD51, new components of the mitochondrial fission machinery. EMBO Rep *12*, 565-573.

Poodry, C.A., and Edgar, L. (1979). Reversible alteration in the neuromuscular junctions of Drosophila melanogaster bearing a temperature-sensitive mutation, shibire. J Cell Biol *81*, 520-527.

Praefcke, G.J.K., and McMahon, H.T. (2004). The dynamin superfamily: universal membrane tubulation and fission molecules? Nature reviews. Molecular cell biology *5*, 133-147.

Qi, Y., Yan, L., Yu, C., Guo, X., Zhou, X., Hu, X., Huang, X., Rao, Z., Lou, Z., and Hu, J. (2016). Structures of human mitofusin 1 provide insight into mitochondrial tethering. J Cell Biol *215*, 621-629.

Rapaport, D., Brunner, M., Neupert, W., and Westermann, B. (1998). Fzo1p is a mitochondrial outer membrane protein essential for the biogenesis of functional mitochondria in Saccharomyces cerevisiae. The Journal of biological chemistry *273*, 20150-20155.

Reubold, T.F., Faelber, K., Plattner, N., Posor, Y., Ketel, K., Curth, U., Schlegel, J., Anand, R., Manstein, D.J., Noe, F., Haucke, V., Daumke, O., and Eschenburg, S. (2015). Crystal structure of the dynamin tetramer. Nature *525*, 404-408.

Richter, V., Palmer, C.S., Osellame, L.D., Singh, A.P., Elgass, K., Stroud, D.A., Sesaki, H., Kvansakul, M., and Ryan, M.T. (2014). Structural and functional analysis of MiD51, a dynamin receptor required for mitochondrial fission. J Cell Biol *204*, 477-486.

Rizzuto, R., De Stefani, D., Raffaello, A., and Mammucari, C. (2012). Mitochondria as sensors and regulators of calcium signalling. Nature reviews. Molecular cell biology *13*, 566-578.

Robin, E.D., and Wong, R. (1988). Mitochondrial DNA molecules and virtual number of mitochondria per cell in mammalian cells. J Cell Physiol *136*, 507-513.

Rojo, M., Legros, F., Chateau, D., and Lombes, A. (2002). Membrane topology and mitochondrial targeting of mitofusins, ubiquitous mammalian homologs of the transmembrane GTPase Fzo. J Cell Sci *115*, 1663-1674.

Rouault, T.A. (2012). Biogenesis of iron-sulfur clusters in mammalian cells: new insights and relevance to human disease. Disease Models & Mechanisms *5*, 155-164.

Santel, A., and Fuller, M.T. (2001). Control of mitochondrial morphology by a human mitofusin. J Cell Sci *114*, 867-874.

Satoh, M., Hamamoto, T., Seo, N., Kagawa, Y., and Endo, H. (2003). Differential sublocalization of the dynamin-related protein OPA1 isoforms in mitochondria. Biochemical and biophysical research communications *300*, 482-493.

Scheffler, I.E. (2002). Metabolic Pathways Inside Mitochondria. In: Mitochondria: John Wiley & Sons, Inc., 246-272.

Sesaki, H., and Jensen, R.E. (1999). Division versus fusion: Dnm1p and Fzo1p antagonistically regulate mitochondrial shape. J Cell Biol *147*, 699-706.

Shpetner, H.S., and Vallee, R.B. (1989). Identification of dynamin, a novel mechanochemical enzyme that mediates interactions between microtubules. Cell *59*, 421-432.

Sinclair, J.H., and Stevens, B.J. (1966). Circular DNA filaments from mouse mitochondria. Proceedings of the National Academy of Sciences of the United States of America *56*, 508-514.

Sjostrand, F.S. (1953). Electron microscopy of mitochondria and cytoplasmic double membranes. Nature *171*, 30-32.

Smirnova, E., Griparic, L., Shurland, D.L., and van der Bliek, A.M. (2001). Dynamin-related protein Drp1 is required for mitochondrial division in mammalian cells. Molecular biology of the cell *12*, 2245-2256.

Smirnova, E., Shurland, D.L., Ryazantsev, S.N., and van der Bliek, A.M. (1998). A human dynamin-related protein controls the distribution of mitochondria. J Cell Biol *143*, 351-358.

Song, B.D., and Schmid, S.L. (2003). A molecular motor or a regulator? Dynamin's in a class of its own. Biochemistry *42*, 1369-1376.

Song, Z., Chen, H., Fiket, M., Alexander, C., and Chan, D.C. (2007). OPA1 processing controls mitochondrial fusion and is regulated by mRNA splicing, membrane potential, and Yme1L. J Cell Biol *178*, 749-755.

Song, Z., Ghochani, M., McCaffery, J.M., Frey, T.G., and Chan, D.C. (2009). Mitofusins and OPA1 Mediate Sequential Steps in Mitochondrial Membrane Fusion. Molecular biology of the cell *20*, 3525-3532.

Strack, S., and Cribbs, J.T. (2012). Allosteric modulation of Drp1 mechanoenzyme assembly and mitochondrial fission by the variable domain. The Journal of biological chemistry *287*, 10990-11001.

Taanman, J.W. (1999). The mitochondrial genome: structure, transcription, translation and replication. Biochimica et biophysica acta *1410*, 103-123.

Takei, K., McPherson, P.S., Schmid, S.L., and De Camilli, P. (1995). Tubular membrane invaginations coated by dynamin rings are induced by GTP-gamma S in nerve terminals. Nature *374*, 186-190.

van der Bliek, A.M., and Meyerowitz, E.M. (1991). Dynamin-like protein encoded by the Drosophila shibire gene associated with vesicular traffic. Nature *351*, 411-414.

van der Bliek, A.M., Shen, Q., and Kawajiri, S. (2013). Mechanisms of mitochondrial fission and fusion. Cold Spring Harbor perspectives in biology *5*.

Wakabayashi, J., Zhang, Z., Wakabayashi, N., Tamura, Y., Fukaya, M., Kensler, T.W., Iijima, M., and Sesaki, H. (2009). The dynamin-related GTPase Drp1 is required for embryonic and brain development in mice. J Cell Biol *186*, 805-816.

Wang, C., and Youle, R.J. (2009). The Role of Mitochondria in Apoptosis(). Annual review of genetics *43*, 95-118.

Wenger, J., Klinglmayr, E., Frohlich, C., Eibl, C., Gimeno, A., Hessenberger, M., Puehringer, S., Daumke, O., and Goettig, P. (2013). Functional mapping of human dynamin-1-like GTPase domain based on x-ray structure analyses. PloS one *8*, e71835.

West, A.P., Shadel, G.S., and Ghosh, S. (2011). Mitochondria in innate immune responses. Nat Rev Immunol *11*, 389-402.

Wong, E.D., Wagner, J.A., Scott, S.V., Okreglak, V., Holewinske, T.J., Cassidy-Stone, A., and Nunnari, J. (2003). The intramitochondrial dynamin-related GTPase, Mgm1p, is a component of a protein complex that mediates mitochondrial fusion. J Cell Biol *160*, 303-311.

Youle, R.J., and Karbowski, M. (2005). Mitochondrial fission in apoptosis. Nature reviews. Molecular cell biology *6*, 657-663.

Zhang, Y., Chan, N.C., Ngo, H.B., Gristick, H., and Chan, D.C. (2012). Crystal Structure of Mitochondrial Fission Complex Reveals Scaffolding Function for Mitochondrial Division 1 (Mdv1) Coiled Coil. The Journal of biological chemistry *287*, 9855-9861.

Zhao, J., Liu, T., Jin, S., Wang, X., Qu, M., Uhlen, P., Tomilin, N., Shupliakov, O., Lendahl, U., and Nister, M. (2011). Human MIEF1 recruits Drp1 to mitochondrial outer membranes and promotes mitochondrial fusion rather than fission. The EMBO journal *30*, 2762-2778.

Chapter 2

The mitochondrial fission receptor Mff selectively recruits oligomerized Drp1

Raymond Liu and David C. Chan

Division of Biology and Biological Engineering
California Institute of Technology
1200 East California Blvd
Pasadena, CA 91125.

This chapter was published in *Molecular Biology of the Cell*

ABSTRACT

Dynamin-related protein 1 (Drp1) is the GTP-hydrolyzing mechanoenzyme that catalyzes mitochondrial fission in the cell. Residing in the cytosol as dimers and tetramers, Drp1 is recruited by receptors on the mitochondrial outer membrane, where it further assembles into a helical ring that drives division via GTP-dependent constriction. The Drp1 receptor Mff is a major regulator of mitochondrial fission, and its overexpression results in increased fission. In contrast, the alternative Drp1 receptors MiD51 and MiD49 appear to recruit inactive forms of Drp1, because their overexpression inhibits fission. Using genetic and biochemical assays, we studied the interaction of Drp1 with Mff. We show the insert B region of Drp1 inhibits Mff-Drp1 interactions, such that recombinant Drp1 mutants lacking insert B form a stable complex with Mff. Mff cannot bind to assembly-deficient mutants of Drp1, suggesting that Mff selectively interacts with higher order complexes of Drp1. In contrast, the alternative Drp1 receptors MiD51 and MiD49 can recruit Drp1 dimers. Therefore, Drp1 recruitment by Mff versus MiD51 and MiD49 may result in different outcomes because they recruit different subpopulations of Drp1 from the cytosol.

INTRODUCTION

Mitochondria are dynamic organelles that continuously undergo regulated cycles of fission and fusion. These processes are essential for maintaining mitochondrial health and function, and have important roles in mitochondrial DNA stability and inheritance, respiratory capacity, apoptosis, and mitophagy (Westermann, 2010; Chan, 2012; Youle and van der Bliek, 2012). Fission is mediated by dynamin-related protein 1 (Drp1), a member of the dynamin superfamily of GTPases (Smirnova *et al.*, 2001). Like dynamin, Drp1 is a mechanoenzyme that has the capacity to self-assemble into oligomeric complexes that have enhanced GTP hydrolysis activity (Ferguson and De Camilli, 2012). In the cell, much of Drp1 resides in the cytosol but can be recruited to mitochondria via receptors anchored to the mitochondrial outer membrane (Loson *et al.*, 2013). Once recruited, Drp1 further assembles around the mitochondrial tubule to form an oligomeric ring that constricts and divides the mitochondrion in a GTP-dependent process (Ingerman *et al.*, 2005; Mears *et al.*, 2011). Mutation of Drp1 blocks mitochondrial fission, resulting in elongated mitochondrial networks due to unopposed mitochondrial fusion (Smirnova *et al.*, 2001). This cellular defect causes developmental lethality in mice and multi-system disease in humans (Waterham *et al.*, 2007; Ishihara *et al.*, 2009; Wakabayashi *et al.*, 2009).

Four receptors have been identified that recruit Drp1 to mitochondria: mitochondrial fission protein 1 (Fis1), mitochondrial fission factor (Mff), and mitochondrial dynamics proteins of 49 and 51 kDa (MiD49 and MiD51, respectively)

(Yoon *et al.*, 2003; Gandre-Babbe and van der Bliek, 2008; Palmer *et al.*, 2011; Zhao *et al.*, 2011). Fis1, the first identified candidate receptor, has a minor role in Drp1 recruitment (Otera *et al.*, 2010; Loson *et al.*, 2013), and recent results suggest instead a role in mitophagy (Shen *et al.*, 2014; Yamano *et al.*, 2014). There is good evidence that the latter three molecules are each capable of recruiting Drp1, as the loss of any of these receptors results in reduced Drp1 accumulation on mitochondria and increased mitochondrial tubule length (Palmer *et al.*, 2011; Loson *et al.*, 2013; Palmer *et al.*, 2013). Mff appears to be the primary receptor. Loss of Mff results in the greatest reduction of fission in mouse embryonic fibroblasts, while overexpression causes mitochondrial fragmentation consistent with increased fission rates (Otera *et al.*, 2010; Loson *et al.*, 2013). MiD51 and MiD49 both strongly recruit Drp1 and are associated with ER-mitochondria contact sites (Zhao *et al.*, 2011; Koirala *et al.*, 2013; Palmer *et al.*, 2013; Elgass *et al.*, 2015). However, in contrast to Mff, overexpression of MiD51 or MiD49 paradoxically results in mitochondrial elongation and inhibition of fission, presumably because they recruit an inactive form of Drp1 (Loson *et al.*, 2013; Palmer *et al.*, 2013).

An important issue is why Mff shows a different cellular behavior compared to MiD51 and MiD49. A route to addressing this issue is to examine the physical interaction between Drp1 and its receptors *in vitro*. However, such physical interactions have only been detected using cross-linking reagents, suggesting that the Drp1-receptor interactions are low affinity or transient (Otera *et al.*, 2010; Strack and Cribbs, 2012). In yeast, the interaction between Dnm1 (the yeast ortholog of Drp1) and its receptor, Mdv1, is much more stable and has been linked to the insert B domain, which associates with the B-

propeller domain of Mdv1 (Bui *et al.*, 2012). In mammals, the analogous insert B domain is a largely unstructured domain that is targeted for control by post-translational modifications and interacts with cardiolipin to associate Drp1 with lipid membranes (Chang and Blackstone, 2010; Frohlich *et al.*, 2013; Bustillo-Zabalbeitia *et al.*, 2014; Stepanyants *et al.*, 2015). Studies show that this domain is dispensable for Drp1 hydrolysis, membrane constriction, and mitochondrial recruitment (Strack and Cribbs, 2012; Francy *et al.*, 2015). These results imply that in mammals, the Drp1-receptor interaction is not mediated through the insert B domain.

In this study we examine the interaction between Drp1 and Mff to gain mechanistic insight into Drp1 recruitment. Using a yeast two-hybrid assay, we identify minimal interacting regions on both Mff and Drp1, with a short N-terminal fragment of Mff being sufficient to bind the Drp1 stalk domain. We find that removal of the insert B domain from Drp1 greatly enhances the Drp1-Mff interaction, resulting in a stable complex *in vitro* in the absence of cross-linkers. Using a mutational screen, we identify mutants of Drp1 that specifically abolish recruitment via Mff but not MiD51. Analysis of these mutants indicates that Drp1 oligomerization is required for Mff, but not MiD51 or MiD49, to physically associate with Drp1. Together the results suggest that the robust fission activity of Mff stems from its ability to selectively recruit oligomerized Drp1 to the mitochondrial surface.

RESULTS

The Mff N-terminal region and the Drp1 stalk form the core interaction unit

To interrogate the Drp1-Mff interaction, we first sought to determine the minimal region of Mff necessary for binding Drp1. By comparing the polypeptide sequence of Mff from the human, mouse, fish, frogc and fly orthologs, several notable features can be noted (Figure 2.S1A). At the N-terminus, there are two repeat motifs (R1 and R2) that are required for recruiting Drp1 (Otera *et al.*, 2010), as well as a third conserved motif (R3) that has no proposed function. Beyond R1-R3, there is a disordered region (Figure 2.S1B), followed by a conserved coiled-coil (CC) domain required for dimerization and a C-terminal transmembrane domain (TM). Previous assays examining the Drp1-Mff interaction have been hampered by the apparent transience or instability of the complex, and therefore its detection required stabilization by cross-linking agents (Gandre-Babbe and van der Bliek, 2008; Otera *et al.*, 2010; Strack and Cribbs, 2012). To detect this transient/unstable complex in the absence of cross-linkers, we developed a yeast two-hybrid interaction assay that allowed us to examine Drp1 recruitment by Mff. Initial attempts with an Mff bait truncated just N-terminal to the transmembrane segment (Figure 2.1A) resulted in auto-activation (Figure 2.S2A). We reasoned that the acidic coiled-coil domain might be responsible and deleted it to generate three MffΔCC baits based on splice variants 1, 3, 4 (RefSeq NP_083685.2, NP_001297626.1, and NP_001297628.1, respectively) reported previously (Gandre-Babbe and van der Bliek, 2008) (Figures 2.1A, 2.1B). Isoform 4 (Mff4ΔCC), the shortest construct, showed the most robust interaction, followed by isoform 3 (Mff3ΔCC) and then isoform 1

(Mff1ΔCC). To determine the minimal Mff region sufficient for recruiting Drp1, we made sequential C-terminal truncations of Mff and tested them against Drp1. Truncations that ended within the predicted disordered region retained binding, whereas truncations that deleted the R3 domain resulted in complete loss of recruitment (Figure 2.1C). Thus the N-terminal Mff region containing the three conserved R1-R3 motifs appeared sufficient for Drp1 binding. These results are consistent with experiments in cell culture indicating that R1 and R2 of Mff are essential for Drp1 recruitment (Otera *et al.*, 2010).

We similarly used the yeast two-hybrid assay to identify the Mff-interacting regions of Drp1. Structurally, Drp1 consists of 4 main domains: the GTPase domain, the bundle signaling element (BSE), the stalk region, and the insert B (IB) region (Figure 2.1D) (Schmid and Frolov, 2011; Ferguson and De Camilli, 2012; Frohlich *et al.*, 2013; Wenger *et al.*, 2013). We tested the ability of Mff to recruit Drp1 constructs containing deletions of one or more of these domains (Figure 2.1E). Deleting the GTPase domain (ΔG) reduced the interaction between Mff1ΔCC and Drp1, and Mff3ΔCC and Drp1, but did not appreciably affect recruitment by Mff4ΔCC or smaller constructs. This suggests that the GTPase domain promotes but is not required for Drp1 interaction with Mff. Drp1 constructs lacking the insert B domain (ΔIB), on the other hand, enhanced the interaction between Drp1 and Mff. The formerly weak recruitment by Mff isoforms 1 and 3 were now more robust, and new additional interactions between Drp1 and Mff fragments 1-100, 1-61, and 1-50 (weakly) were now detected. These data suggest that the insert B domain is dispensable for the Drp1-Mff interaction and is in fact inhibitory. Removing the GTPase, BSE, and insert B domains (to generate the stalk alone) did not greatly alter

Drp1 interaction with Mff relative to Drp1ΔIB alone. The interaction data therefore suggest that the minimal regions required for the Drp1-Mff interaction are the Mff R1+R2 motifs and the Drp1 stalk domain.

Removing insert B from Drp1 stabilizes the Drp1-Mff interaction *in vitro*

The results from our two-hybrid analysis strongly suggest that the insert B region inhibits the interaction of Drp1 with Mff. Since previous efforts to demonstrate binding between Drp1 and Mff *in vitro* required cross-linking (Otera *et al.*, 2010; Strack and Cribbs, 2012; Frohlich *et al.*, 2013), we wondered whether removing the insert B region might stabilize the Drp1-Mff complex. To test this idea, we constructed a GST fusion protein containing the N-terminal 61 residues of Mff (the minimal binding fragment) and assayed its ability to bind full-length Drp1 or Drp1ΔIB in a GST pull-down assay (Figure 2.2A). Whereas full-length Drp1 weakly co-immunoprecipitated, Drp1ΔIB showed efficient co-association with Mff, suggesting substantial stabilization of binding. The insert B domain of Drp1 therefore inhibits formation of a stable Drp1-Mff interaction.

We further tested whether the Mff truncations examined in the yeast two-hybrid assay could similarly interact with Drp1 and Drp1ΔIB in the assay. Consistent with previous reports, we found poor binding between full-length Drp1 and the Mff constructs, even though such constructs show interaction in the two-hybrid assay (Figure 2.2B, top half). In contrast, Drp1ΔIB showed robust association with Mff (1-61) and Mff (1-50), and less binding to longer constructs (Figure 2.2B, bottom half). The larger number of interactions detected with the two-hybrid assay is consistent with the idea that the two-

hybrid can detect weak or transient interactions (Van Criekinge and Beyaert, 1999) that are missed by biochemical assays. The pull-down results suggest that the strongest interacting pair is between Drp1ΔIB and Mff (1-61). To test the stability of this interaction, we mixed Mff (1-61)-GST with Drp1ΔIB and analyzed the mixture on an analytical size-exclusion column to test for a complex (Figure 2.2C). Compared to Drp1ΔIB or Mff (1-61)-GST alone samples (Figure 2.2C, left panel), the mixture showed a distinct peak migrating at a higher molecular weight, concomitant with a decrease in the peaks corresponding to individual Drp1ΔIB and Mff (1-61)-GST (Figure 2.2C, middle and third panels). To determine the identity of this size-shifted species, we collected and analyzed the fractions from the SEC runs and found that fractions corresponding to the new peak contained both Drp1ΔIB and Mff (1-61)-GST (Figure 2.2D), suggesting that Drp1ΔIB and Mff (1-61)-GST are co-migrating as a complex.

Identification of Drp1 mutants that have selective loss of Mff versus MiD51 binding

The identification of the stalk region of Drp1 as the Mff-interaction domain provided us with a smaller target for determining the interacting residues on Drp1. We previously utilized a mutation screening strategy to identify a Drp1-interacting loop on MiD51 (Loson *et al.*, 2014). Similarly, we tested a series of Drp1 mutants for interactions with Mff in our yeast two-hybrid assay. The screening considerations were as follows: (1) We limited our mutations to surface-exposed residues of Drp1 with low homology to dynamin 2, as reasoned by the lack of an Mff interaction with dynamin 2 in our yeast two-hybrid assay (Figure 2.S2C); (2) Two Mff constructs of various binding efficiency (Figure 2.1A) were used as baits to provide additional sensitivity for the screen; (3)

Because previous studies indicated that the yeast two-hybrid assay provides a readout of Drp1 oligomerization (Naylor *et al.*, 2006; Chang *et al.*, 2010), we included a Drp1 bait to obtain information about the oligomerization activity of the Drp1 mutants; (4) Because Mff-specific mutants were desired, MiD51 was included as a bait to screen against Drp1 mutants that also affected MiD51 binding.

We assayed 42 Drp1 mutants (Figure 2.3A, Table S1) for binding to the Mff, Drp1, and MiD51 baits. Several interesting patterns emerged from the screen. All mutants that affected Drp1 oligomerization, as interpreted by loss of interaction with the Drp1 bait, also abolished binding to Mff (Figure 2.3A: Mutants 8, 9, 15, 18, 20). In contrast, some of these mutants retained MiD51 binding (Mutants 9, 15). Loss of Drp1 oligomerization therefore correlates tightly with loss of Mff binding but not MiD51 binding. In addition, we recovered several Drp1 mutants that failed to bind Mff, but retained binding to both Drp1 and MiD51. We chose six for further study (Mutants 10, 13, 16, 17, 22, 28) and introduced them into a Drp1ΔIB background to test whether removing the insert B domain could rescue the loss of binding (Figure 2.3B). In three of six mutants we found recovery of interaction with Mff, consistent with the notion that the insert B domain is inhibitory to the interaction. This secondary screen left us with three mutants that we interpret as bona fide Mff-binding mutants for further characterization (Figure 2.3C). We tested the three mutants in our *in vitro* interaction assays to validate the results of the yeast two-hybrid assay. Whereas wild-type Drp1ΔIB binds robustly to Mff (1-61), all three mutants (in the context of Drp1ΔIB) failed to co-precipitate with Mff (1-61) by GST pull-down (Figure 2.4A). Furthermore, by SEC analysis, these mutants

showed loss of complex formation with Mff (1-61) (Figure 2.4B). Together the data suggests that these mutants are indeed defective in Mff binding.

Drp1 mutants are defective for fission, mitochondrial recruitment and are specific to Mff versus MiD51 and MiD49

To assess the physiological function of these mutants, we expressed them in *Drp1*-null mouse embryonic fibroblasts (MEFs). Due to loss of mitochondrial fission, *Drp1*-null MEFs have highly elongated and interconnected mitochondria. Re-expression of wild-type Drp1 restores mitochondrial fission, resulting in shorter mitochondrial tubules (Figure 2.5A). In contrast, expression of the three Drp1 mutants defective in Mff binding did not shorten the mitochondrial network, indicating that they are nonfunctional for fission (Figure 2.5A). To understand this defect, we assessed whether localization of the Drp1 mutants to mitochondria was impaired. Because the strong cytosolic signal of over-expressed Drp1 obscured this analysis, we briefly permeabilized the cells with digitonin to remove soluble Drp1 before immunostaining. This treatment artifactually resulted in mitochondrial fragmentation but greatly improved the visualization of Drp1 complexes on the mitochondria (Figure 2.5B). In wild-type cells, there is a substantial amount of endogenous Drp1 localized to mitochondria. In *Mff*-null cells, there is little Drp1 on mitochondria, consistent with its role as the major Drp1 recruiter (Otera *et al.*, 2010; Loson *et al.*, 2013). When wild-type Drp1 is expressed in *Drp1*-null cells, there is robust recruitment of Drp1 on the mitochondria (Figure 2.5B, magnification insets). In contrast, the three Mff-binding mutants show a major loss of Drp1 puncta on

mitochondria (Figure 2.5B, magnification insets). Mutant 17 appears to form aggregates in the cell, but the majority of these aggregates did not co-localize with mitochondria.

To determine whether these mutants are selectively defective for Mff binding, we tested their recruitment by ectopically targeted Mff, MiD51 and MiD49. FLAG-tagged versions of the three Drp1 receptors were targeted to lysosomes by fusion to lysosomal-associated membrane protein 1 (LAMP1). These constructs were expressed in *Drp1*-null cells, and localization of wild-type Drp1 versus mutant Drp1 was assessed (Figure 2.6). When wild-type Drp1 was expressed, it was robustly recruited to FLAG-positive puncta in the Mff-, MiD51-, and MiD49-expressing cell lines (Figure 2.6A). When the three Drp1 mutants were expressed, they strongly localized to FLAG-positive puncta in the lysosome-targeted MiD51 and MiD49 cell lines, but not in the lysosome-targeted Mff cell line (Figures 2.6B, C and D). Together the data suggest that mutants 10, 16, and 17 specifically disrupt the interaction of Drp1 with Mff, but not MiD49 or MiD51, and that the major reduction of Drp1 puncta on mitochondria observed (Figure 2.5B) can be attributed specifically to loss of Mff-mediated recruitment.

Oligomerization-dependent recruitment of Drp1 by Mff

In our two-hybrid screen for Drp1 mutants defective for Mff binding, we explicitly screened against mutants that had defects in oligomerization and ultimately recovered three mutants that fulfilled our criteria. However, the results from the screen suggested that Drp1 oligomerization is tightly associated with its ability to bind Mff, as every Drp1 mutant defective in oligomerization is also deficient in Mff binding. We

therefore wondered if the identified mutants (10, 16, 17) might have a moderate oligomerization defect that was not detectable in the yeast two-hybrid assay. This concern was increased by the observation that the mutated residues are located adjacent to known oligomerization loops for Drp1 and dynamin (Figure 2.3C) (Frohlich *et al.*, 2013; Reubold *et al.*, 2015). For these reasons, we considered the possibility that the yeast two-hybrid screen may not have provided a sufficiently stringent filter against oligomerization mutants. We therefore performed two independent tests of oligomerization activity to assess the behavior of the mutants against that of wild-type and a known mutant termed 4A (the four residues 401GPRP404 mutated to AAAA) that forms dimers but cannot form tetramers or higher order oligomers (Frohlich *et al.*, 2013). In a GTPγS-stimulated assembly assay, about 50% of Drp1 sediments when incubated in 50 mM NaCl (Figure 2.7A). In contrast, the 4A mutant is almost completely deficient in assembly and remains highly soluble. Mutants 16 and 17 sedimented substantially less than wild-type Drp1, but more than the dimeric 4A mutant. Mutant 10 did not show a clear sedimentation defect. Under low salt conditions that promote oligomerization, SEC analysis of the mutants show that mutants 10, 16, and 17 all migrate substantially more slowly than wild-type, indicating a defect in forming higher order oligomers (Figure 2.7B). Mutant 17 migrated similarly to the 4A mutant, whereas mutants 10 and 16 showed a somewhat less pronounced defect. Together the results suggest that all three mutants can form dimers but are inefficient at further oligomerization, although the defects are not as strong as the canonical 4A oligomerization mutant.

If Drp1 oligomerization is necessary for Mff binding, then our model predicts that the 4A mutant would be unable to bind Mff. To test this we examined the mutant in the yeast two-hybrid assay (Figure 2.7C), the GST pull-down assay (Figure 2.7D), and the complex formation assay (Figure 2.7E). Consistent with our model, we find that the 4A mutant shows strong defects in Mff association in all assays. Importantly, the two-hybrid assay shows that 4A has normal binding to MiD51.

DISCUSSION

Mff is likely to be the major Drp1 receptor. Cells lacking Mff, compared to the other receptors (Fis1, MiD51, MiD49), show the most highly elongated mitochondria (Otera *et al.*, 2010; Loson *et al.*, 2013). However, the lack of a stable interaction between the two proteins *in vitro* has been puzzling. Here we show that recombinant Drp1 lacking the insert B region, unlike full-length Drp1, forms a stable complex with the N-terminal region of Mff. This observation indicates that insert B inhibits Drp1 binding to Mff. In contrast to the mammalian situation, insert B in yeast Dnm1 has been shown to promote binding to the Mdv1/Fis1 receptor complex (Bui *et al.*, 2012). It is tempting to speculate that the mammalian Drp1 insert B domain may regulate mitochondrial fission by dampening Drp1-Mff interactions until signals to activate fission are present. To understand this issue, it will be important to determine how the inhibitory effect of insert B on Mff binding is modulated. Because insert B has been shown to interact with cardiolipin (Bustillo-Zabalbeitia *et al.*, 2014; Macdonald *et al.*, 2014; Ugarte-Uribe *et al.*, 2014; Stepanyants *et al.*, 2015), the possible role of lipids in regulating Drp1-Mff interactions should be tested. In addition, it is interesting to note that insert B contains residues are targeted for phosphorylation and sumoylation (Figueroa-Romero *et al.*, 2009; Chang and Blackstone, 2010). Phosphorylation of serine-616 in human Drp1 (corresponding to serine-579 in mouse Drp1) activates its fission activity (Taguchi *et al.*, 2007; Kashatus *et al.*, 2011). This serine residue resides in insert B, but phosphomimetic mutants of this residue do not increase the binding of full-length Drp1 to Mff *in vitro* (Figure 2.S3).

Our analysis of Drp1 mutants that are deficient for Mff binding suggests that the oligomerization state of Drp1 is closely linked to its interaction with Mff. In the cytosol, Drp1 exists in a dimer/tetramer/high-order equilibrium, with data supporting either tetramers and dimers as the predominant species (Zhu *et al.*, 2004; Koirala *et al.*, 2013; Macdonald *et al.*, 2014). Our mutational screen shows that Mff is unable to stably associate with Drp1 that is oligomerization-defective. Importantly, our mutations do not disrupt the Drp1 monomer:monomer interaction surface (termed "interface 2") in the stalk region that is important for formation of the cross-like stalk dimer (Ferguson and De Camilli, 2012; Frohlich *et al.*, 2013). Like the 4A mutant, mutants 10, 16, and 17 are all capable of forming dimers, but are defective in formation of higher order states. Therefore, it appears that the Drp1 oligomeric state recruited by Mff is a tetramer or higher. In contrast, MiD51 and MiD49 do not show this strong requirement for Drp1 oligomerization.

Two general models can explain why Mff strongly prefers a higher order state of Drp1. For simplicity in presenting the models, we will assume that Mff binds to a Drp1 tetramer, although the bound form may be a larger assembly. In the first model, the Mff-binding site is generated only when two Drp1 dimers form a tetramer. The cross-like Drp1 dimers come together through apposition of their stalk domains, forming a new surface that is now directly recognized by the N-terminal region of Mff. In the second model, the Mff binding surface exists in the Drp1 dimer, but formation of the Drp1 dimer:dimer complex is required for stability. In both cases, the functional result is that only the oligomerized form of Drp1 is recruited, while Drp1 dimers are left in the

cytosol. Both models are consistent with the observation that the Mff-binding unit consists of the Drp1 stalk, which contains the interfaces supporting Drp1 tetramerization (Frohlich *et al.*, 2013; Francy *et al.*, 2015; Reubold *et al.*, 2015). Because Mff has a coiled coil domain, it is also possible that Mff dimerization may facilitate formation of additional Drp1-Drp1 interactions. In yeast, Mdv1 functions to nucleate Dnm1 assembly (Lackner *et al.*, 2009).

In binding only to higher order Drp1 oligomers, Mff differs strikingly from MiD51 and MiD49. Our studies show that the latter proteins are still able to bind Drp1 mutants that can only form dimers. In this regard, the Drp1-MiD interaction resembles that of yeast Dnm1-Mdv1, which is not affected by oligomerization-defective mutations in Dnm1 (Ingerman *et al.*, 2005; Bhar *et al.*, 2006). These results underscore a major difference between Mff- and MiD-mediated recruitment, and may explain their distinct cellular effects. In cells, over-expressed Mff results in increased fission (Otera *et al.*, 2010). In contrast, over-expressed MiD51 or MiD49 results in high accumulation of Drp1 on mitochondria, but the net effect is reduced fission and mitochondrial elongation because the recruited Drp1 is inactive (Loson *et al.*, 2013; Palmer *et al.*, 2013). We speculate that by selectively recruiting the subpopulation of Drp1 that is oligomeric, Mff might be recruiting an active pool of Drp1 that is fission-competent. In contrast, the MiDs appear to recruit an inactive Drp1 population, including dimers, that requires an additional trigger before fission induction (Figure 2.7F).

MATERIALS AND METHODS

Cloning for protein expression

Mouse Drp1 isoform b (699 amino acids), Drp1ΔIB (1-513 fused to 603-699), Drp1ΔIB 4A (401GPRP404 mutated to AAAA), Drp1 mutants 10, 16 and 17 (mutations described in Table S1) were cloned into the NdeI and BamHI sites of a modified pET21b+ vector containing a downstream PreScission Protease cleavage site (Novagen). Mouse Mff isoform 4ΔCC, Mff (1-50), Mff (1-61), Mff (1-102), and Mff (1-146) were cloned into the NdeI and BamHI sites of a modified pET28a(+) vector containing a downstream PreScission Protease cleavage site and GST tag (Novagen). The parental vector, which produces a tagged GST, was used to express the T7-GST negative control used in GST pull-down assays. OPA1 (262-1015, Isoform 8), used as a negative control in GST pull-down assays, was cloned into a modified pET28a(+) vector with an upstream PreScission Protease site. Mutants were generated by overlap PCR mutagenesis and verified by sequencing.

Protein expression and purification

Recombinant protein was expressed in Rosetta (DE3) BL21 *E. coli* (Novagen). Transformed bacteria were grown in 1 liter of terrific broth containing 25 μg/mL chloramphenicol and either 100 μg/mL ampicillin (pET21 vectors) or 50 μg/mL kanamycin (pET28 vectors) at 37°C to an OD_{600} of 1.5, shifted to 16°C and induced with 0.5 mM isopropyl β-D-1-thiogalactopyranoside for overnight expression, typically 18 hours. Cells were harvested and pellets were stored at -20°C. For His_6-tagged proteins, cell pellets were thawed and resuspended in buffer containing 25 mM 4-(2-

hydroxyethyl)-1-piperazineethanesulfonic acid (HEPES) pH 7.8, 500 mM NaCl, 10% glycerol, 5 mM β-mercaptoethanol (β-Me) (His Lysis Buffer) plus 5 mM Imidazole and 1X HALT protease inhibitors (Thermo-Pierce, Rockford, IL), lysed by sonication, and cleared by centrifugation at 43,000 x g, for 30 minutes at 4°C. Supernatant was applied to 1 mL bed volume of washed Talon beads (Clontech) for 3 hours, washed with His Lysis buffer plus 20 mM Imidazole, and exchanged into buffer containing 20 mM HEPES, pH 7.5, 300 mM NaCl, 10% glycerol, and 2 mM β-Me for overnight cleavage (typically 20 hours) with 60 units of PreScission Protease (GE Healthcare). Following cleavage, glutathione sepharose 4B beads (GE Healthcare) were added to remove the PreScission Protease and elutions were loaded onto a HiLoad Superdex 200 16/60 column (GE Healthcare) driven by an AKTA Purifier (Amersham) and pre-equilibrated with buffer containing 20 mM HEPES pH 7.5, 300 mM NaCl, 5% glycerol, and 5 mM β-Me for size-exclusion chromatography purification. Peak fractions were collected and concentrated in Amicon-Ultra 15 concentrators, 50 MWCO (Millipore). Proteins were flash frozen and stored at -80°C. For Mff-GST proteins, the lysis, coupling to glutathione sepharose beads, and washes were performed in buffer containing 20 mM HEPES, pH 7.5, 300 mM NaCl, 10% glycerol, and 5 mM β-Me. GST fusion proteins were eluted with 10 mM reduced glutathione (Sigma) in buffer containing 20 mM HEPES, pH 7.5, 150 mM NaCl, 10% glycerol, and 5 mM β-Me, desalted with Zeba desalting columns, 7 MWCO (Life Technologies) pre-equilibrated with buffer without glutathione, flash frozen, and stored at -80°C. For the Drp1-Mff co-migration SEC assays, Mff (1-61)-GST was additionally purified by size exclusion chromatography as above, with peak fractions collected and

concentrated in Amicon Ultra 15 concentrators, 30 MWCO, before freezing and storage at -80°C.

Yeast Two-Hybrid Assay

The Drp1 constructs in Figure 2.1E consist of the following truncations and fusions: FL, full-length Drp1, amino acids (aa) 1-699; ΔG, Drp1 minus the GTPase domain, aa309-667; ΔIB, Drp1 minus the insert B domain, aa1-508 fused to aa605-699 with a GGGSGGS linker; Stalk, Drp1 minus the GTPase, BSE and insert B domains, aa329-508 fused to aa605-662 with a GGGSGGS linker; Insert B domain, aa493-605; G+BSE domain, aa1-328 fused to 674-699 with a KHGTDSRV linker (Chappie *et al.*, 2010). Mouse Dynamin 2, Drp1 isoform b, Drp1ΔIB 4A, Drp1 truncations and mutants in Figure 2.1E and Table 2.S1, MiD51 (47-463), MffΔTM (Δ272-291), MffΔCC (Δ235-291), and Mff truncations in Figure 2.1C, were cloned (into either the pGAD-C1 or pGBDU-C1 vectors) and transformed into PJ69-4α and PJ69-4a yeast strains, respectively. Transformants were selected with leucine- and uracil-deficient plates, respectively, and haploid combinations for interaction testing were mated by spotting on YPD plus adenine plates. Diploids were selected by replica-plating onto leucine- and uracil-deficient plates (labeled as +Adenine in the figures) and interactions were assayed following replica-plating on leucine-, uracil- and adenine-deficient plates (labeled as -Adenine in the figures). Growth on adenine-deficient plates indicates a positive interaction, and interaction tests were performed at least three times. Mutants were generated by overlap PCR mutagenesis and verified by sequencing. Residues for the mutational screen were selected from the set of accessible surface area residues as

determined by the "Surface Residues" function in Pymol, using a solvent radius of 2.5 angstroms applied to the structure of Drp1 (PDB file 4BEJ).

GST pull-downs assays

Each GST-fusion and target protein pair was incubated with washed glutathione sepharose beads in buffer containing 20 mM HEPES, pH 7.5, 150 mM NaCl, 10% glycerol, 0.1% Triton X-100, 2 mM $MgCl_2$, and 5 mM β-mercaptoethanol, at room temperature for 1 hour. The beads were washed twice with buffer and the bound fraction was analyzed by SDS-PAGE followed by Coomassie staining. For target proteins, 10% of the input amount is shown.

Cell lines and cell culture

All cell lines were cultured in DMEM containing 10% fetal bovine serum, 100 I.U./ml streptomycin and 100 µg/ml penicillin. *Mff*-null cell lines were previously published (Loson *et al.*, 2013). *Drp1*-null cell lines were a generous gift from Katsuyoshi Mihara (Kyushu University, Fukuoka, Japan). *Drp1*-null cells lines stably expressing Drp1 and Drp1 mutants were generated by retroviral transduction of pQCXIP (Clontech) vectors with Kozak-Drp1 cloned into the BamHI/EcoRI sites, and maintained in 0.5 µg/mL puromycin.

To generate the LAMP1 constructs, the Kozak sequence and FLAG-tag-Strep-tagII was fused to the rat Lamp1 sequence to generate a Kozak-LAMP1-FLAG construct, which was then fused to the N-terminus of Mff, MiD51, and MiD49. LAMP1-FLAG-Mff

Isoform 4 ΔTM (Δ272-291), LAMP1-FLAG-MiD51(134-463), and LAMP1-FLAG-MiD49 (124-454) were cloned into the XhoI/HpaI sites of pMSCVhyg (Clontech), retrovirally transduced into *Drp1*-null cell lines expressing Drp1 or Drp1 mutants, and maintained with 0.5 μg/mL puromycin and 100 μg/mL hygromycin.

Immunofluorescence and imaging

For immunostaining, antibodies to Drp1 (mouse anti-Dlp1, BD Biosciences, San Diego, CA), Tom20 (rabbit anti-Tom20, Santa Cruz Biotechnology, Santa Cruz, CA) and FLAG (rabbit anti-FLAG, Sigma-Aldrich, St. Louis, MO) were used. Cells were grown in LabTek chambered glass slides (Nunc, Rochester, NY) for fixed-cell imaging. Cells were fixed in pre-warmed 4% formaldehyde for 10 minutes at 37°C, permeabilized in 0.1% Triton X-100, and incubated with antibodies in 5% fetal calf serum. For cytosol clearing of soluble Drp1, cells were permeabilized with 0.005% digitonin in buffer containing 20 mM HEPES, pH 7.3, 110 mM potassium acetate, 2 mM magnesium acetate, 0.5 mM ethylene glycol tetraacetic acid (EGTA), 220 mM mannitol, 70 mM sucrose, and 2 mM fresh dithiothreitol for 90 seconds at room temperature, then fixed and immunostained as above. Scoring of mitochondrial morphology was performed blind to genotype in triplicates of 100 cells. Imaging was performed with a Plan-Apochromat 63x/1.4 oil objective on a Zeiss LSM 710 confocal microscope driven by Zen 2009 software (Carl Zeiss, Jena, Germany). Images were cropped, globally adjusted for contrast and brightness, and median filtered using ImageJ (National Institutes of Health, Bethesda, MD).

Size exclusion chromatography

For the analysis of Drp1-Mff complex formation, 80 µg Drp1ΔIB/mutants and 80 µg Mff (1-61)-GST were incubated separately or together in 100 µL of 20 mM HEPES, pH 7.5, 150 mM NaCl, 10% glycerol, 2 mM $MgCl_2$, and 5 mM β-Me for 1 hour at room temperature, filtered through a 0.1µm Durapore filter column (EMD Millipore), and loaded onto a Shodex KW804 column (Wyatt Technology, Goleta, CA) driven by a Varian HPLC (Varian Inc, Palo Alto, CA) at 0.5 mL/min. Fractions were collected manually at 1 minute intervals. For analysis of oligomerization, 12.5 µM Drp1 was incubated in the above buffer at 100 mM NaCl prior to loading onto the column.

Pelleting assay

15 µM Drp1 or mutants were incubated in buffer containing 20 mM HEPES, pH 7.5, 50 mM NaCl, 2 mM $MgCl_2$, 5mM β-Me, and 1mM GTPγS for 30 minutes at room temperature, then centrifuged at 100,000 x *g* with a TLA100.3 rotor in a Beckman Optima MAX Ultracentrifuge for 20 minutes at 22°C. Supernatants were removed, and the pellet was resuspended in an equal volume of buffer. Equal amounts of supernatant and pellets were analyzed by SDS-PAGE followed by Coomassie staining.

Sequence alignments and analysis

Sequence alignments were performed with MultAlin (Corpet, 1988) and formatted with ESPript (Robert and Gouet, 2014). Disorder prediction was performed with DisMeta (Huang *et al.*, 2014).

ACKNOWLEDGEMENTS

R.L. was supported by a National Science Foundation Graduate Research Fellowship Program award (1144469). We are grateful to Katsuyoshi Mihara (Kyushu University, Fukuoka, Japan) for the *Drp1*-null MEFs. This work was supported by NIH RO1 grant GM110039.

FIGURE LEGENDS

Figure 2.1. The N-terminal region of Mff binds the Drp1 stalk domain.

(A) Diagram of three Mff isoforms (top three lines) and key Mff constructs (bottom four lines) used in this study. (B) Interaction of Mff isoforms 1, 3 and 4 with Drp1 in the two-hybrid assay. Mouse Mff isoforms 1, 3, and 4 with the coiled-coil domain deleted (ΔCC) were expressed from the pGBDU vector as GAL4 DNA-binding domain (BD) fusion proteins and tested against Drp1 expressed from the pGAD vector as GAL4 activation domain (AD) fusion proteins. For all two-hybrid assays in this study, growth on adenine-deficient plates indicates an interaction. The AD only and BD only samples are negative controls. (C) Deletion analysis of Mff. Mff fragments beginning from amino acid 1 to the number indicated above each column were expressed as BD-fusion proteins and tested against Drp1 expressed as AD fusion proteins. Mff (1-110) is uninformative due to auto-activation (Adenine-deficient plate shows growth with AD only). (D) Ribbon diagram of Drp1 structure, from PDB file 4BEJ. The major domains of Drp1 are highlighted. (E) Domain analysis of Drp1. Mff truncations were expressed as BD fusion proteins and tested against Drp1 truncations expressed as AD fusion proteins. FL: full-length Drp1, ΔG: Drp1 minus the GTPase domain, ΔIB: Drp1 minus the insert B domain, Stalk: Drp1 minus the GTPase, bundle signaling element (BSE) and insert B domains, G+BSE domain: GTPase plus the BSE domain. The associated diploid selection plates are shown in Supplementary Figure 2.S2.

Figure 2.2. Mff61 and Drp1ΔIB form a stable complex.

(A) GST pull-down assays for purified recombinant Drp1 (full-length), Drp1ΔIB, or OPA1 versus purified recombinant Mff61-GST (Mff fragment 1-61 fused C-terminally to GST) or T7-GST (T7tag-fused to GST). Shown are Coomassie-stained bands of either the input protein (lanes 1-3) or eluates from the pull-downs (lanes 4-9) following separation by SDS-PAGE. In lanes 4-9, the bottom row shows the isolated GST fusion proteins. The top row depicts the co-immunoprecipitated proteins. (B) GST pull-down assays for purified recombinant full-length Drp1 (upper half) or Drp1ΔIB (bottom half) versus purified recombinant Mff truncations. Shown are Coomassie-stained bands of the input Drp1ΔIB or full-length Drp1 proteins (lane 1) and eluates from the pull-downs (lanes 2-7) following separation by SDS-PAGE. The Drp1ΔIB or Drp1 FL row depicts the respective proteins pulled down by the GST fusion proteins in the lower row. (C) Size-exclusion chromatography (SEC) analyses of Drp1ΔIB and Mff61-GST. Left panel: UV absorbance profiles of elutions from a SEC run of either purified recombinant Mff61-GST alone (in red) or purified recombinant Drp1ΔIB alone (in blue). Middle panel: UV absorbance profile of elutions from a SEC run of Mff61-GST and Drp1ΔIB pre-incubated together for an hour before loading, overlaid on top of the profiles from the left panel. Arrowheads depict a loss of Mff61-GST and Drp1ΔIB UV signal in the mixed sample. The arrow depicts the formation of a new peak eluting at an earlier time, indicating the formation of higher molecular weight species. Right panel: Magnification of the middle panel to highlight the size-shifted species of the new peak (underneath the bracket) from the Mff61-GST+Drp1ΔIB run. (D) SDS-PAGE analysis of fractions collected from the SEC runs in (C). Fractions from the times indicated at the top were collected from the

SEC runs in (C), resolved by SDS-PAGE and Coomassie-stained. The top panel depicts the Drp1ΔIB bands from the Drp1ΔIB only run, the middle panel depicts the Drp1ΔIB and Mff61-GST bands (arrows) from the combined run, and the bottom panel depicts the Mff61-GST bands from the Mff61-GST only run. The brackets highlight the presence of both Drp1ΔIB and Mff61-GST in the combined run not present in the individual runs, indicating a Drp1-Mff complex.

Figure 2.3. Identification of Drp1 mutants that fail to bind Mff.

(A) Screen of Drp1 mutants by the yeast two-hybrid assay. Full-length Drp1 and Drp1 mutants 1 to 42 (see Table S1) were expressed as AD fusion proteins and tested against Mff104 (Mff fragment 1-104), Mff isoform 4 with its coiled-coil domain deleted (Mff4ΔCC), full-length Drp1, and MiD51 expressed as BD fusions. The adenine-deficient plates are shown. The associated diploid selection plates are shown in Supplementary Figure 2.S2. Brackets indicate Drp1 mutants that did not interact with Mff, black asterisks denote Drp1 mutants that did not interact with Drp1 (indicating loss of oligomerization ability), and red asterisks denote the subset of Mff-binding deficient mutants that were selected for further characterization. (B) Secondary screen for Drp1 mutants. The indicated Drp1 mutants were screened against full-length Drp1, Mff104, Mff4ΔCC, and Mff146 (Mff fragment 1-146). The Drp1 mutants were constructed in full-length Drp1 (FL) and Drp1ΔIB. The adenine-deficient plates are shown. The associated diploid selection plate are shown in Supplementary Figure 2.S2. Mutants highlighted in red from the Drp1ΔIB assay were selected for further characterization. (C)

Location of mutations 10, 16, and 17 indicated on the structure of Drp1 (PDB file 4BEJ). Loops implicated in higher order assembly of Drp1 are marked.

Figure 2.4. Drp1 mutants display loss of interaction with Mff *in vitro*.

(A) GST pull-down assays for purified recombinant Drp1 variants against purified recombinant Mff61-GST or T7-GST. Shown are Coomassie-stained bands of either the input protein (10% input lanes) or eluates from the pull-downs (GST pull-down lanes) following separation by SDS-PAGE. The top row (lanes 5-12) depicts the Drp1 proteins pulled down by the GST fusion proteins in the bottom row. (B) Size-exclusion chromatography analyses of Mff61-GST with Drp1ΔIB and Drp1ΔIB mutants. For Drp1ΔIB and each mutant, two SEC runs were performed, one with Mff61-GST and one without. Depicted are overlays of the UV absorbance profiles from the two separate runs. The brackets highlight the elution time during which the Drp1-Mff complex appears in the Drp1ΔIB (wild-type) + Mff61-GST run. This complex is absent in runs with the Drp1 mutants. In the upper left panel, the arrowhead highlights the reduction in Drp1 signal from the combined run, relative to the original peak position in the Drp1ΔIB alone runs (dotted). The corresponding signals in the mutant samples do not show a decrease.

Figure 2.5. Drp1 mutants lack fission activity and are not recruited to mitochondria.

(A) Fission activity upon expression in *Drp1*-null MEFs. Wild-type MEFs, *Drp1*-null MEFs, and *Drp1*-null MEFs expressing wild-type Drp1, Drp1 Mutant 10, Drp1 Mutant 16, or Mutant 17 were immunostained against Tom20 to visualize their mitochondrial morphology and scored into 3 categories: fragmented, short tubular, or elongated with

swelled mitochondria. Quantitation was done in triplicate, with 100 cells scored per experiment. Error bars, SEM. (B) Analysis of Drp1 recruitment to mitochondria. The cell lines indicated were briefly permeabilized with digitonin to clear cytosolic Drp1 before fixation. Mitochondria were fragmented in the process, but Drp1 puncta remained on mitochondria for visualization by immunostaining with an antibody against Drp1 (Drp1, green). Mitochondria were visualized by immunostaining against the outer membrane protein Tom20 (Mito, red). Cells were imaged and images were processed under identical settings to properly assess changes in Drp1 levels from cell to cell. The Drp1 signal, mitochondrial signal, and merged signals are shown. Squares to the right are magnifications of the boxed region in the main image.

Figure 2.6. Drp1 mutants are recruited by MiD51 and MiD49, but not Mff.

(A-D) FLAG-tagged Mff isoform 4, MiD51Δ, and MiD49 were targeted to lysosomes by fusion with the lysosomal-associated membrane protein 1 (LAMP1) protein in *Drp1*-null cells expressing wild-type (A) or mutant Drp1 (B-D). These cells were fixed and immunostained against Drp1 (green) and FLAG (red) for assessment of co-localization. The boxes regions are magnified.

Figure 2.7. Drp1 oligomerization is required for binding to Mff.

(A) Sedimentation analysis of Drp1 assembly. Purified recombinant full-length Drp1, mutants 10, 16, 17 and the oligomerization mutant 4A were incubated with GTPγS in 50 mM salt for 30 minutes. Assembled Drp1 was pelleted by sedimentation at 100,000x g. Equivalent volumes of the supernatant (S) and pellet (P) were loaded and resolved by

SDS-PAGE. Numbers below show the percentages in the supernatant and pellet, based on densitometry measurements. (B) Size-exclusion chromatography analysis of full-length Drp1 and mutants. Purified recombinant full-length Drp1, mutants 10, 16, 17, and the oligomerization mutant 4A were analyzed by size-exclusion chromatography under medium salt conditions (100 mM NaCl) to assess their ability to form higher order oligomers. 4A (red) is known to run as a dimer. Protein eluting before this peak is considered to represent higher order oligomers. (C) Analysis of the 4A mutant by the yeast two-hybrid assay. Drp1, Mff104, and MiD51 were expressed as BD fusion proteins and tested against Drp1, Mutants 10, 16, and 17, and the oligomerization mutant 4A expressed as AD fusion proteins. (D) Analysis of the 4A mutant by GST pull-down. Shown are Coomassie-stained bands of either the input protein (10% input lanes) or eluates from the pull-downs (GST pull-down, lanes 4-9) following separation by SDS-PAGE. The top row depicts the Drp1 protein pulled down by the GST fusion proteins in the bottom row. (E) Analysis of the 4A mutant by size-exclusion chromatography (SEC). Depicted are overlays from SEC runs of the 4A mutant with and without Mff61-GST. The brackets highlight the absence of a Drp1-Mff complex at the expected elution time (compare to Figure 2.4B). (F) Model of differential recruitment of Drp1 by Mff versus MiD51 and MiD49. Drp1 exists in the cytosol as a pool of dimers (cross) and tetramers (two adjacent crosses). Whereas MiD51 and MiD49 (MiDs, left) can recruit Drp1 dimers, Mff (right) requires oligomerization of Drp1 dimers. The Drp1 recruited by MiD51 and MiD49 remains inactive unless additional cellular signals are triggered. For simplicity, Mff is depicted as recruiting tetramers, but it is possible that the recruited form of Drp1 is in a higher assembly state.

FIGURES

Figure 2.1

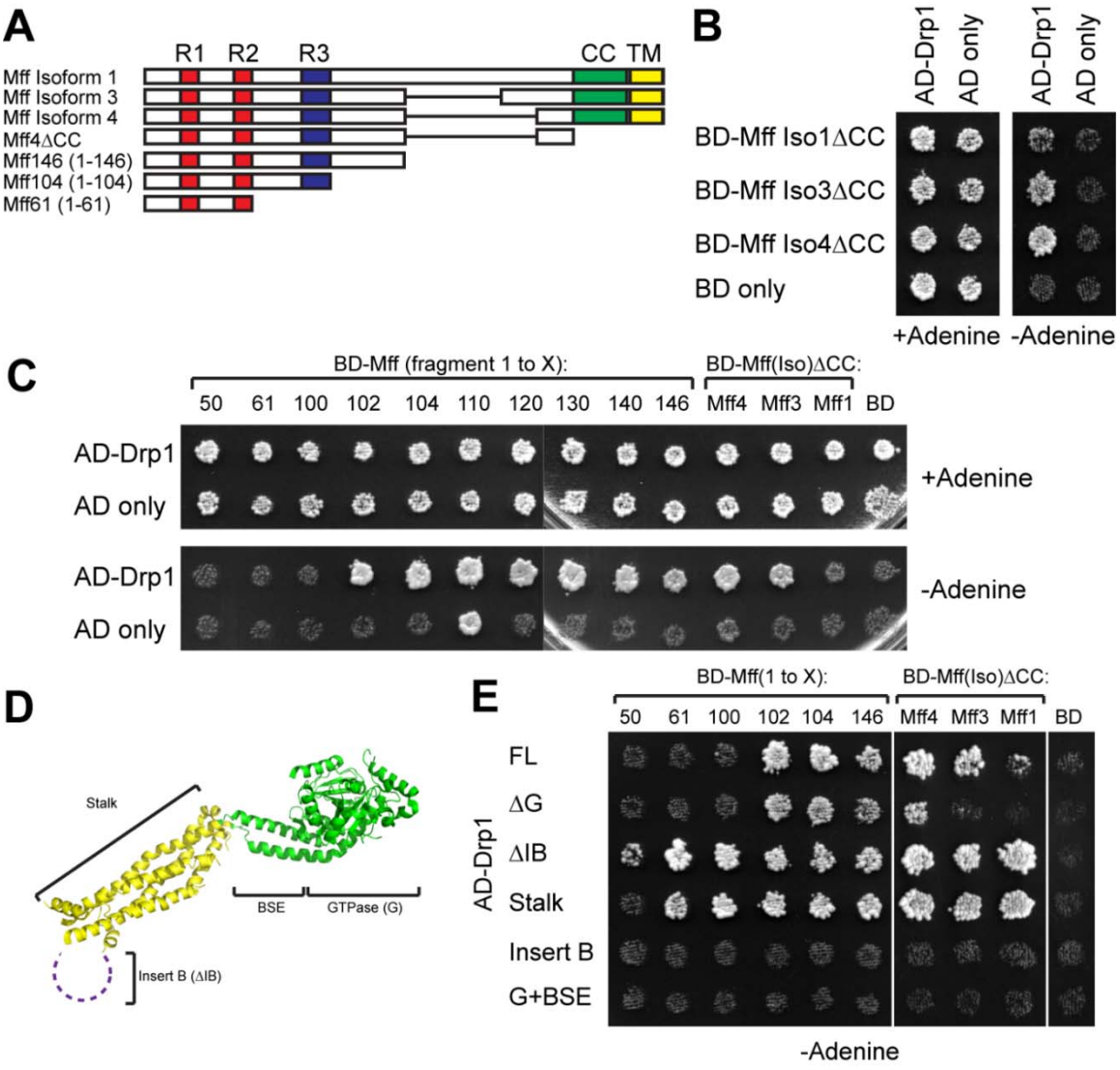

Figure 2.2

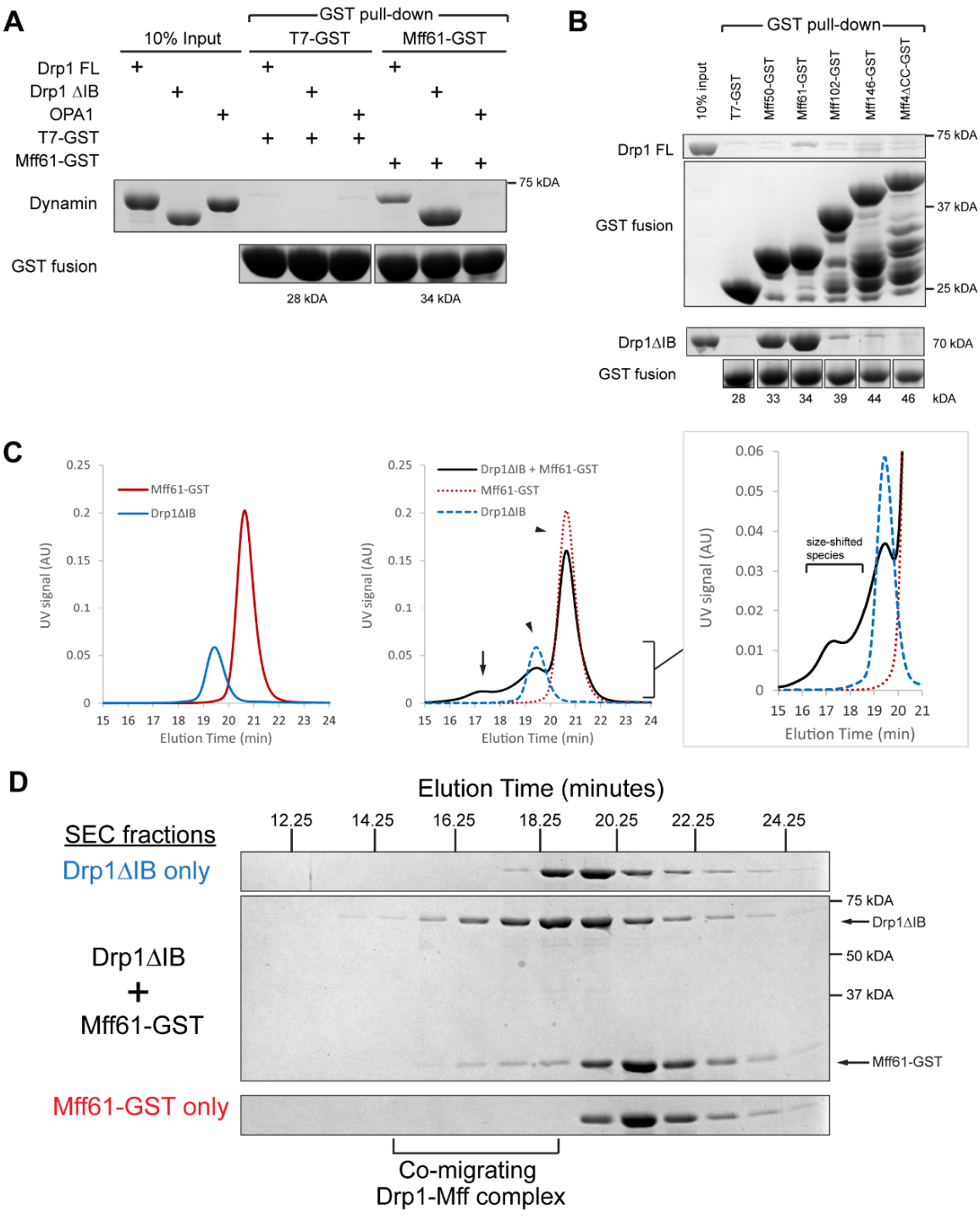
A
GST pull-down
10% Input
T7-GST
Mff61-GST
Drp1 FL
Drp1 ΔIB
OPA1
T7-GST
Mff61-GST
Dynamin
75 kDA
GST fusion
28 kDA
34 kDA
B
GST pull-down
10% input
T7-GST
Mff50-GST
Mff61-GST
Mff102-GST
Mff146-GST
Mff4ΔCC-GST
Drp1 FL
75 kDA
GST fusion
37 kDA
25 kDA
Drp1ΔIB
70 kDA
GST fusion
28 33 34 39 44 46 kDA
C
Mff61-GST
Drp1ΔIB
UV signal (AU)
Elution Time (min)
Drp1ΔIB + Mff61-GST
Mff61-GST
Drp1ΔIB
size-shifted species
D
Elution Time (minutes)
12.25 14.25 16.25 18.25 20.25 22.25 24.25
SEC fractions
Drp1ΔIB only
Drp1ΔIB
+
Mff61-GST
Mff61-GST only
75 kDA
Drp1ΔIB
50 kDA
37 kDA
Mff61-GST
Co-migrating
Drp1-Mff complex

Figure 2.3

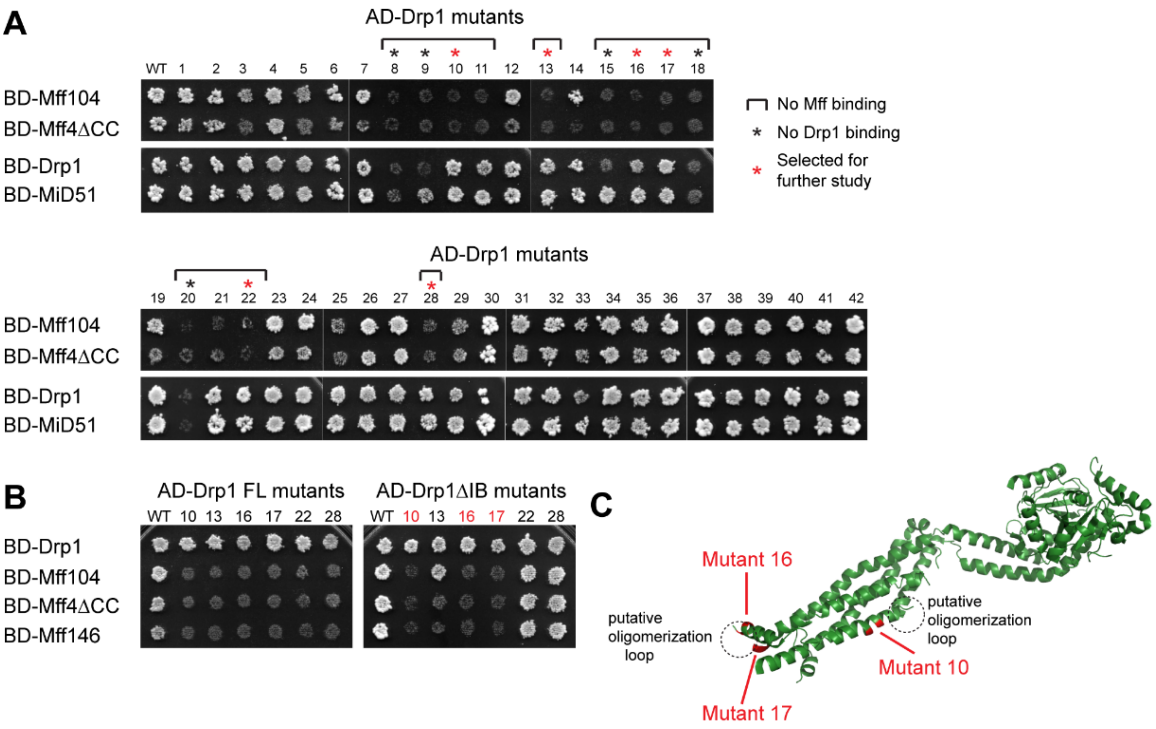
A
AD-Drp1 mutants
WT 1 2 3 4 5 6 7 8 9 10 11 12 13 14 15 16 17 18
BD-Mff104
BD-Mff4ΔCC
BD-Drp1
BD-MiD51
No Mff binding
No Drp1 binding
Selected for further study
AD-Drp1 mutants
19 20 21 22 23 24 25 26 27 28 29 30 31 32 33 34 35 36 37 38 39 40 41 42
BD-Mff104
BD-Mff4ΔCC
BD-Drp1
BD-MiD51
B
AD-Drp1 FL mutants
AD-Drp1ΔIB mutants
WT 10 13 16 17 22 28
WT 10 13 16 17 22 28
BD-Drp1
BD-Mff104
BD-Mff4ΔCC
BD-Mff146
C
Mutant 16
putative oligomerization loop
putative oligomerization loop
Mutant 10
Mutant 17

Figure 2.4

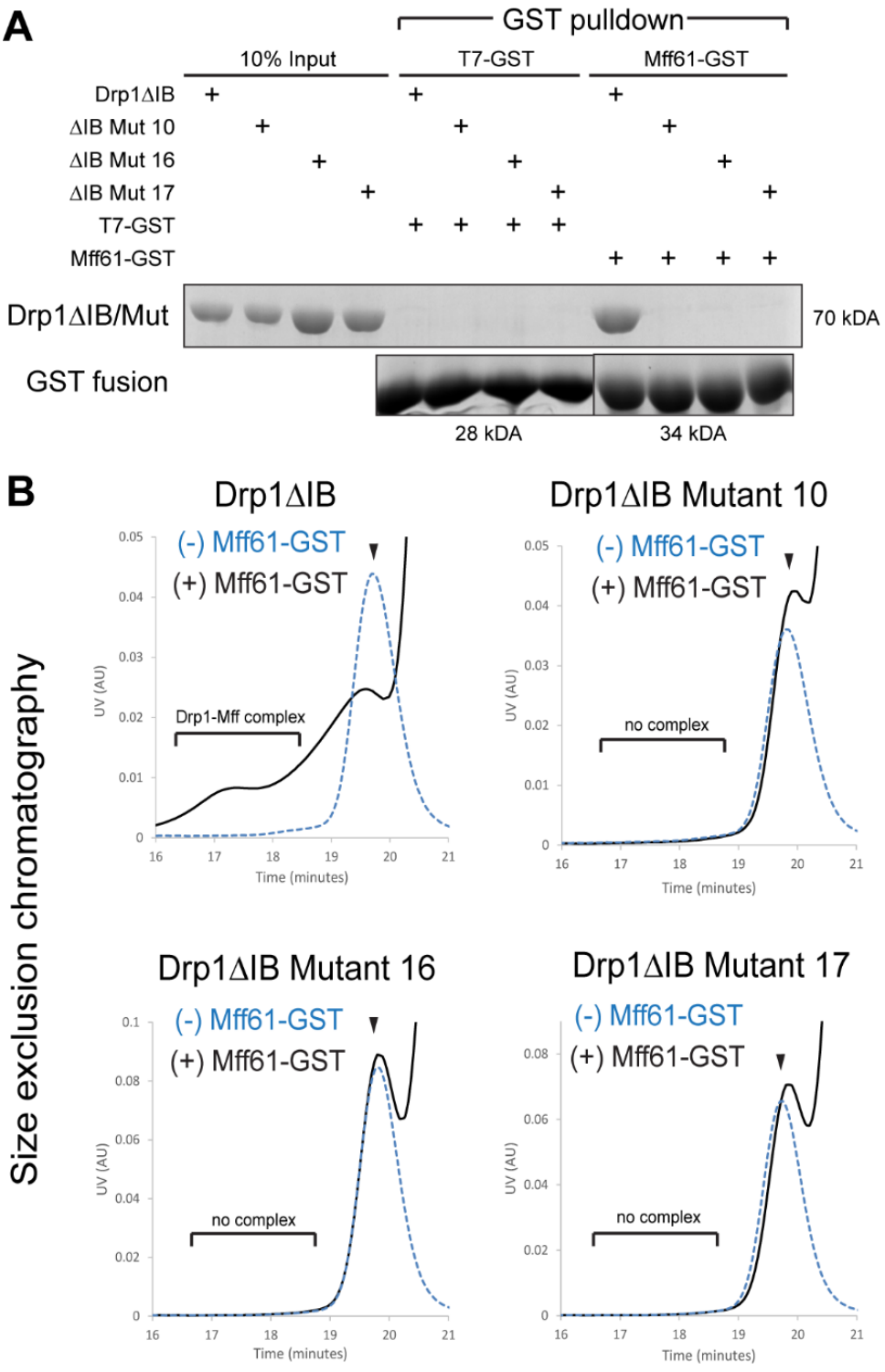
A
GST pulldown
10% Input
T7-GST
Mff61-GST
Drp1ΔIB
ΔIB Mut 10
ΔIB Mut 16
ΔIB Mut 17
T7-GST
Mff61-GST
Drp1ΔIB/Mut
70 kDA
GST fusion
28 kDA
34 kDA
B
Size exclusion chromatography
Drp1ΔIB
(-) Mff61-GST
(+) Mff61-GST
Drp1-Mff complex
UV (AU)
Time (minutes)
Drp1ΔIB Mutant 10
no complex
Drp1ΔIB Mutant 16
Drp1ΔIB Mutant 17

Figure 2.5

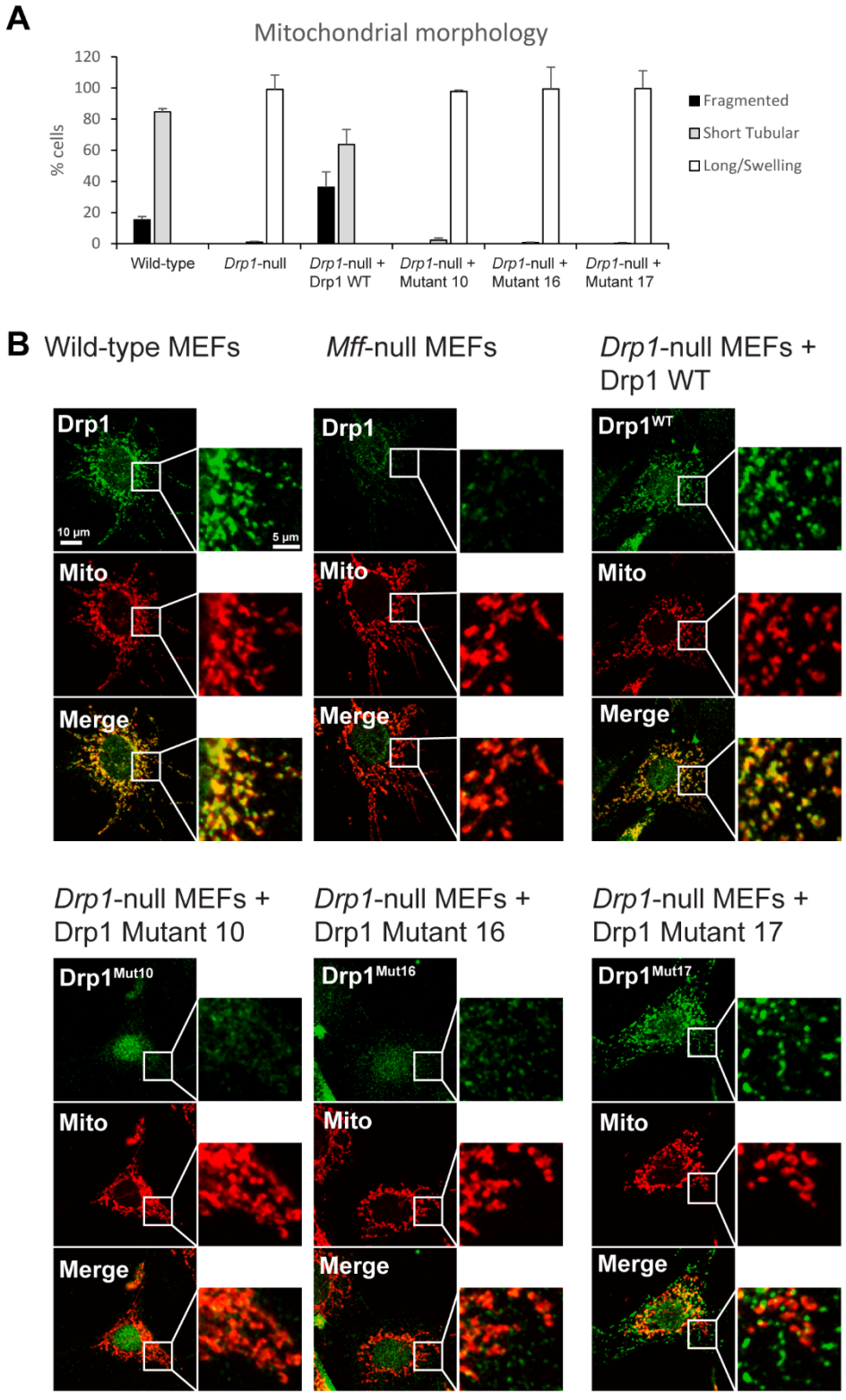
A
Mitochondrial morphology
% cells
120
100
80
60
40
20
0
Wild-type
Drp1-null
Drp1-null + Drp1 WT
Drp1-null + Mutant 10
Drp1-null + Mutant 16
Drp1-null + Mutant 17
Fragmented
Short Tubular
Long/Swelling
B
Wild-type MEFs
Mff-null MEFs
Drp1-null MEFs + Drp1 WT
Drp1-null MEFs + Drp1 Mutant 10
Drp1-null MEFs + Drp1 Mutant 16
Drp1-null MEFs + Drp1 Mutant 17
Drp1
Drp1WT
Drp1Mut10
Drp1Mut16
Drp1Mut17
Mito
Merge
10 µm
5 µm

Figure 2.6

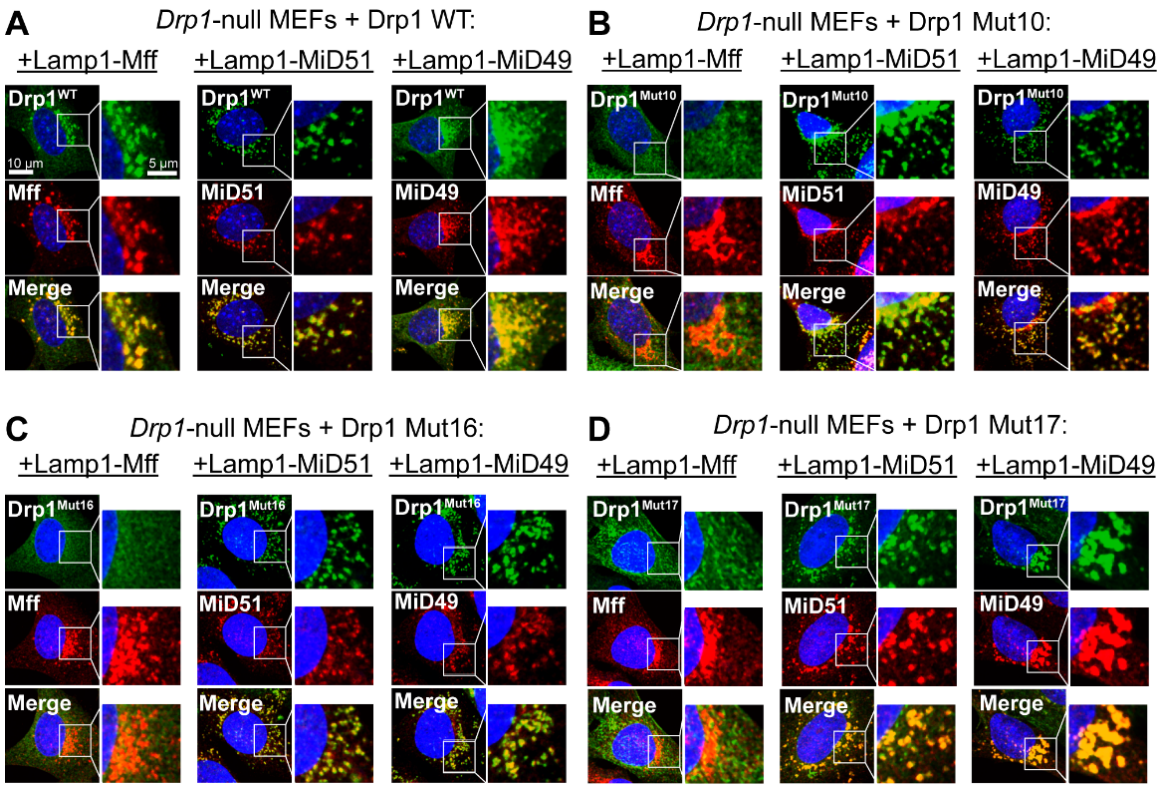
A
Drp1-null MEFs + Drp1 WT:
+Lamp1-Mff
+Lamp1-MiD51
+Lamp1-MiD49
Drp1WT
10 μm
5 μm
Mff
MiD51
MiD49
Merge
B
Drp1-null MEFs + Drp1 Mut10:
+Lamp1-Mff
+Lamp1-MiD51
+Lamp1-MiD49
Drp1Mut10
Mff
MiD51
MiD49
Merge
C
Drp1-null MEFs + Drp1 Mut16:
+Lamp1-Mff
+Lamp1-MiD51
+Lamp1-MiD49
Drp1Mut16
Mff
MiD51
MiD49
Merge
D
Drp1-null MEFs + Drp1 Mut17:
+Lamp1-Mff
+Lamp1-MiD51
+Lamp1-MiD49
Drp1Mut17
Mff
MiD51
MiD49
Merge

Figure 2.7

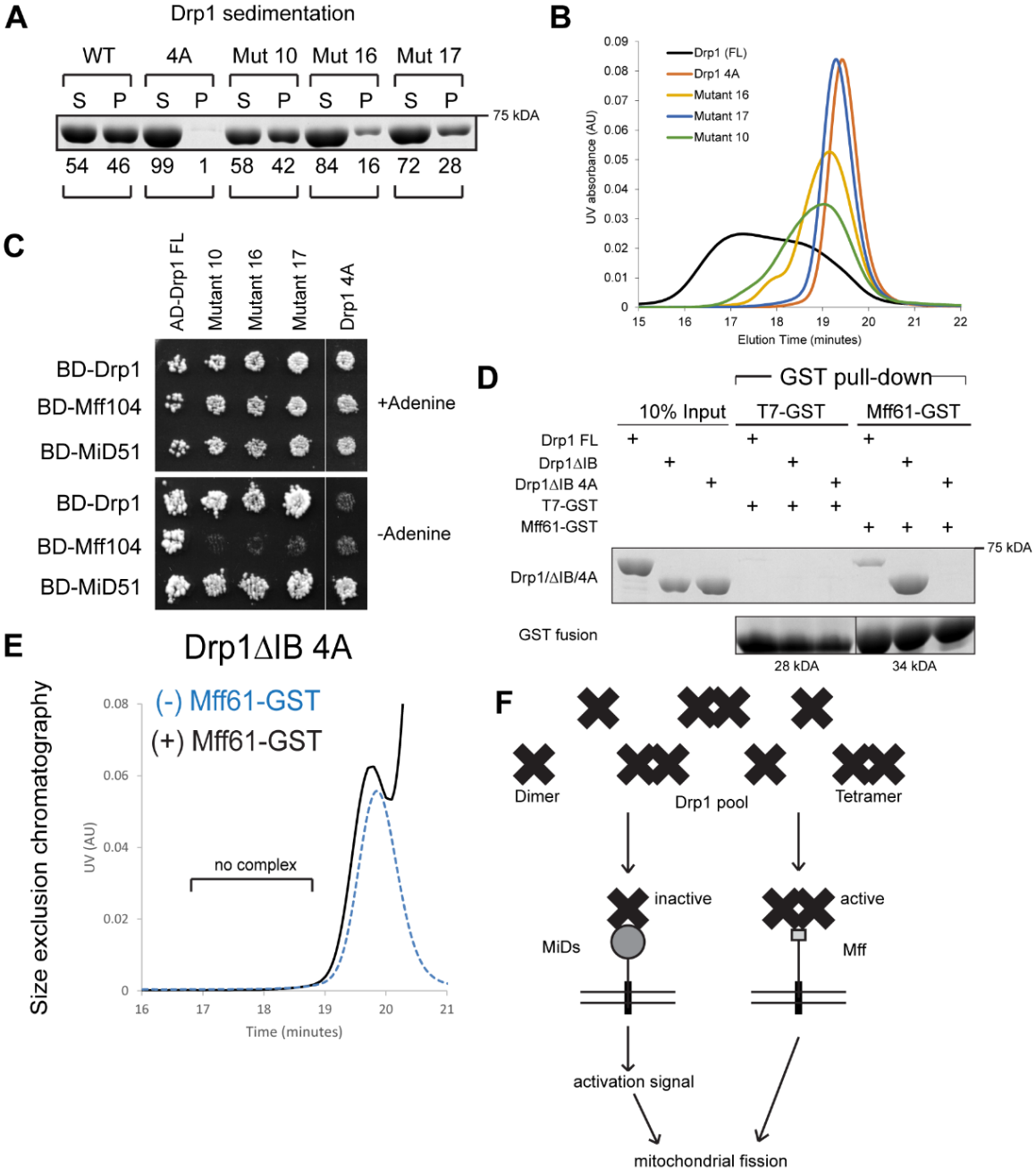
A
Drp1 sedimentation
WT
4A
Mut 10
Mut 16
Mut 17
S P S P S P S P S P
75 kDA
54 46 99 1 58 42 84 16 72 28
B
Drp1 (FL)
Drp1 4A
Mutant 16
Mutant 17
Mutant 10
UV absorbance (AU)
Elution Time (minutes)
C
AD-Drp1 FL
Mutant 10
Mutant 16
Mutant 17
Drp1 4A
BD-Drp1
BD-Mff104
BD-MiD51
+Adenine
-Adenine
D
GST pull-down
10% Input
T7-GST
Mff61-GST
Drp1 FL
Drp1ΔIB
Drp1ΔIB 4A
T7-GST
Mff61-GST
75 kDA
Drp1/ΔIB/4A
GST fusion
28 kDA
34 kDA
E
Drp1ΔIB 4A
(-) Mff61-GST
(+) Mff61-GST
no complex
Size exclusion chromatography
UV (AU)
Time (minutes)
F
Dimer
Drp1 pool
Tetramer
inactive
active
MiDs
Mff
activation signal
mitochondrial fission

SUPPLEMENTAL FIGURE LEGENDS

Figure 2.S1. Mff sequence analysis**.**

(A) Multiple sequence alignment of Mff orthologs from human, mouse, fly, frog, and fish. Conserved residues are boxed in blue. Residues with 100% identity are highlighted in red with white text, and residues conserved in 70% of sequences are in red text. Notable regions included: Repeat 1 (R1) and Repeat 2 (R2) as previously identified (Gandre-Babbe and van der Bliek, 2008), an additional conserved region (R3), the coiled-coil domain (CC) and the transmembrane segment (TM). The Mff sequences used in this alignment are (RefSeq): Homo sapiens mitochondrial fission factor isoform b (NP_001263991.1), Mus musculus mitochondrial fission factor isoform 1, NP_083685.2, Danio rerio mitochondrial fission factor homolog A, (NP_001018402.2), Xenopus laevis mitochondrial fission factor homolog B, (NP_001085443.1), and Drosophila melanogaster transport and golgi organization 11, isoform A (NP_726111.1). Alignments were performed with MultAlin (Corpet, 1988) and formatted with ESPript (Robert and Gouet, 2014).

(B) Disordered regions in Mff. DisMeta, the Disorder Prediction MetaServer (Huang et al., 2014), was used to predict disordered regions in mouse Mff isoform 1. The consensus among 8 different predictors is plotted against each residue. A consensus above 50% of these predictors (dotted line) is indicative of disorder. The diagram of mouse Mff isoform 1 is aligned with the plot.

Figure 2.S2. Yeast two-hybrid assay controls.

(A) Auto-activation of Mff lacking the transmembrane region. Mouse Mff isoforms 1, 3, and 4 with the transmembrane domain deleted (ΔTM) were expressed from the pGBDU vector as BD fusion proteins and tested against Drp1 expressed from the pGAD vector as AD fusion proteins. Growth on adenine-deficient plates, but not against AD or BD only, indicates an interaction. The growth of the Mff constructs against AD only on adenine-deficient plates (white asterisks) indicates auto-activation, making results with these constructs uninformative. (B) Diploid selection growths for the adenine-deficient plates in Figure 2.1E. (C) Lack of interaction between dynamin 2 and Mff. Mouse Dynamin 2, Drp1, MiD51, and Mff isoform 4 with the transmembrane domain deleted (Mff4ΔCC) were expressed as BD fusion proteins and tested against Dynamin 2 expressed as an AD fusion protein. Dynamin 2 interacted with itself, but did not interact with Drp1, MiD51, or Mff4ΔCC. (D) Diploid selection plates for the adenine-deficient plates in Figure 2.3A. (E) Diploid selection plates for the adenine-deficient plates in Figure 2.3B.

Figure 2.S3. Phosphomimetic Drp1 does not interact with Mff61.

(A) GST pull-down assays for purified recombinant Drp1ΔIB, Drp1 (full-length), Drp1 S579D (full-length), and Drp1 S579E (full-length) versus purified recombinant Mff61-GST (Mff fragment 1-61 fused C-terminally to GST) or T7-GST (T7tag-fused to GST). Shown are Coomassie-stained bands of either the input protein (lanes 1-4) or eluates from the pull-downs (lanes 5-12) following separation by SDS-PAGE. In lanes 5-12, the bottom row shows the isolated GST fusion proteins. The top row depicts the co-immunoprecipitated proteins.

SUPPLEMENTAL TABLE AND FIGURES

Figure 2.S1

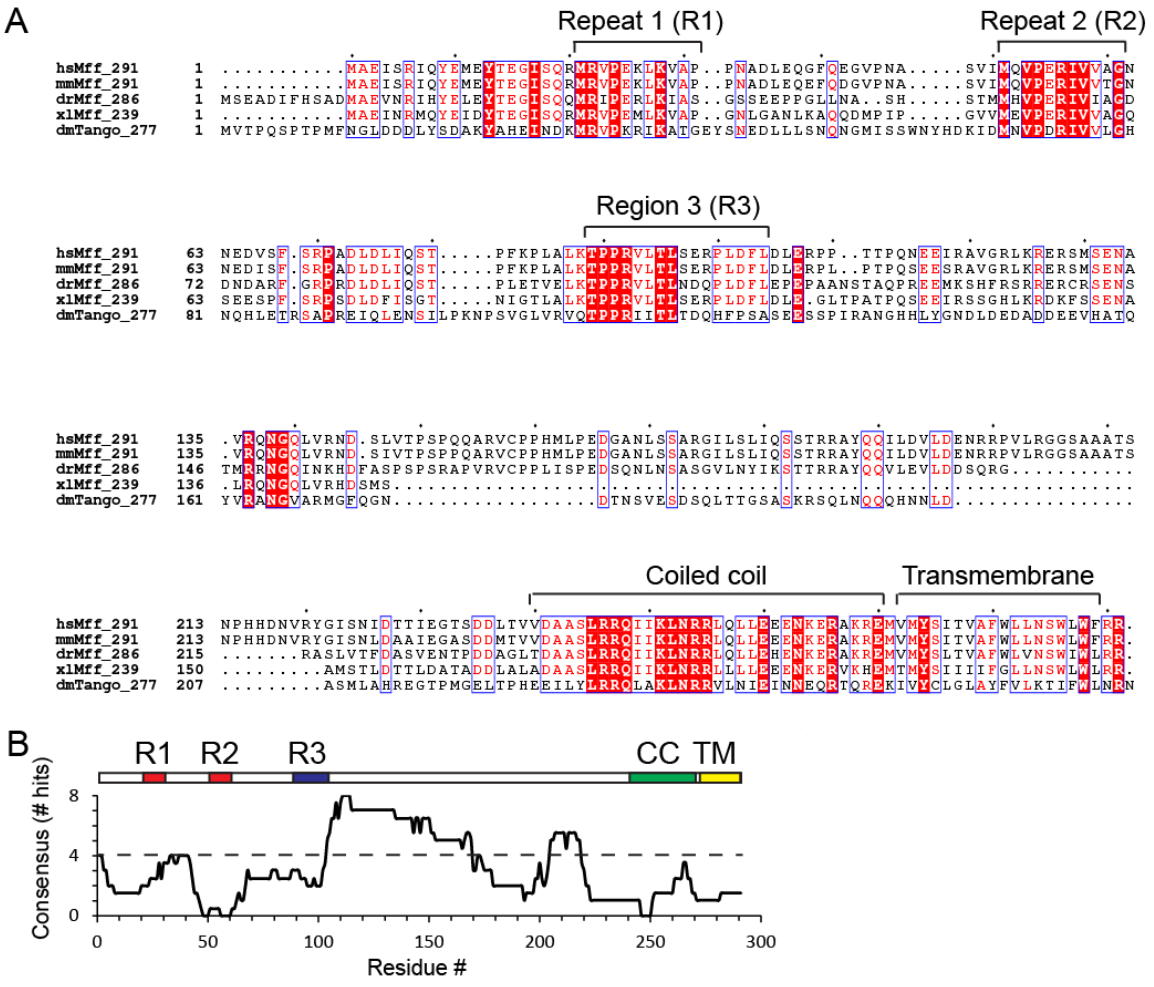

Figure 2.S2

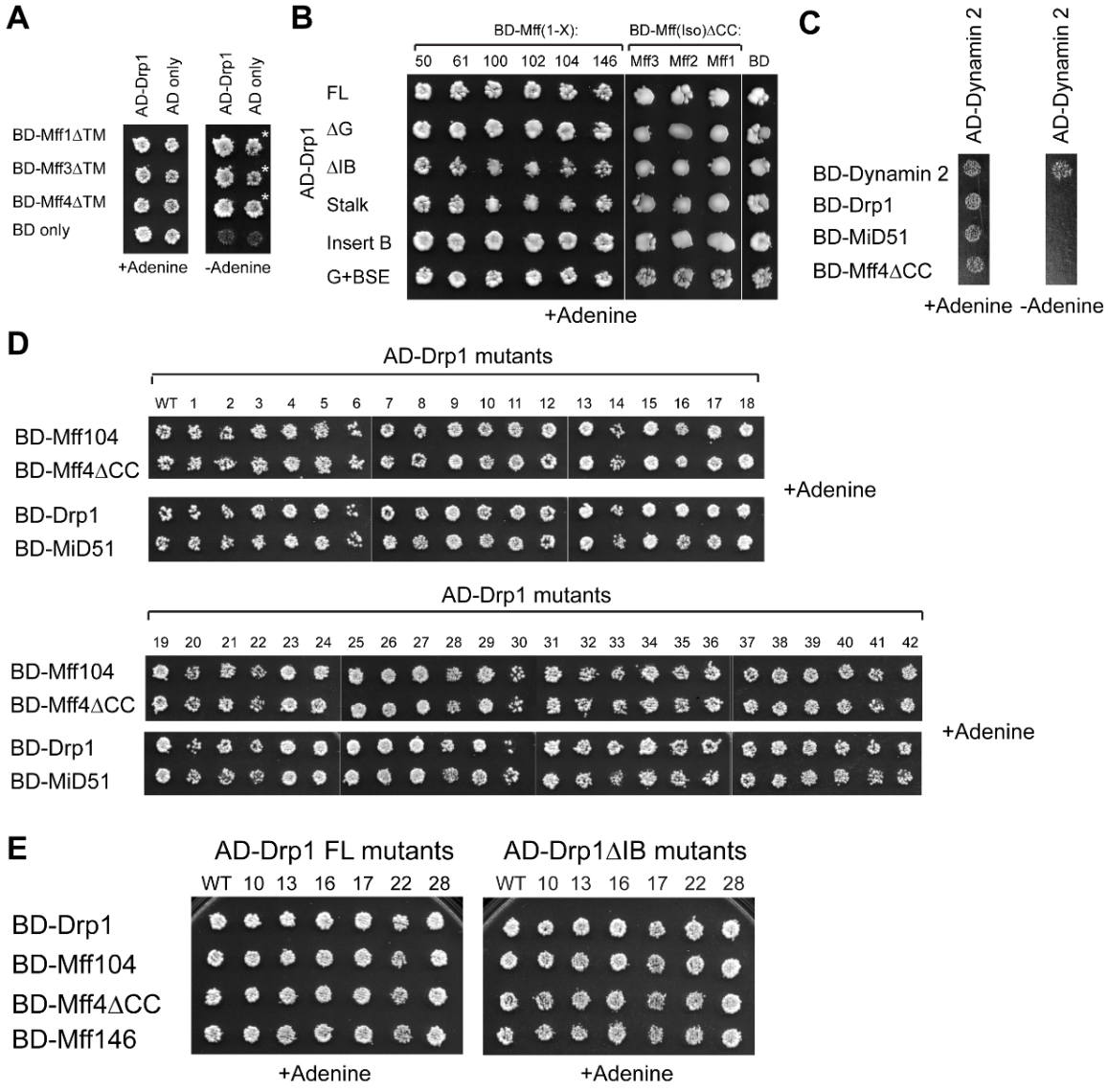
A
AD-Drp1
AD only
AD-Drp1
AD only
BD-Mff1ΔTM
BD-Mff3ΔTM
BD-Mff4ΔTM
BD only
+Adenine
-Adenine
B
BD-Mff(1-X):
BD-Mff(Iso)ΔCC:
50 61 100 102 104 146 Mff3 Mff2 Mff1 BD
AD-Drp1
FL
ΔG
ΔIB
Stalk
Insert B
G+BSE
+Adenine
C
AD-Dynamin 2
AD-Dynamin 2
BD-Dynamin 2
BD-Drp1
BD-MiD51
BD-Mff4ΔCC
+Adenine -Adenine
D
AD-Drp1 mutants
WT 1 2 3 4 5 6 7 8 9 10 11 12 13 14 15 16 17 18
BD-Mff104
BD-Mff4ΔCC
BD-Drp1
BD-MiD51
+Adenine
AD-Drp1 mutants
19 20 21 22 23 24 25 26 27 28 29 30 31 32 33 34 35 36 37 38 39 40 41 42
BD-Mff104
BD-Mff4ΔCC
BD-Drp1
BD-MiD51
+Adenine
E
AD-Drp1 FL mutants
WT 10 13 16 17 22 28
AD-Drp1ΔIB mutants
WT 10 13 16 17 22 28
BD-Drp1
BD-Mff104
BD-Mff4ΔCC
BD-Mff146
+Adenine
+Adenine

Figure 2.S3

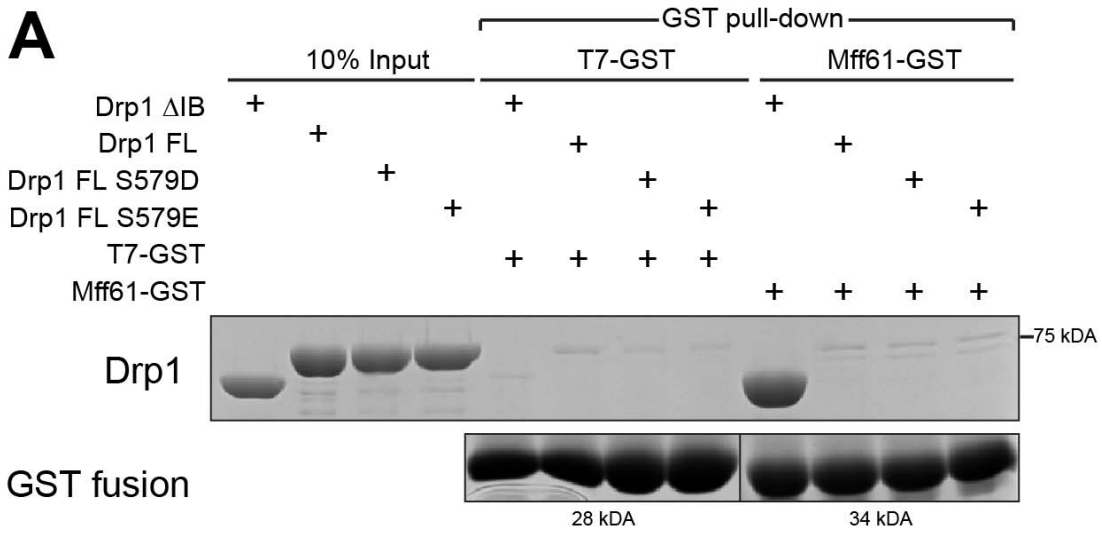
A
GST pull-down
10% Input
T7-GST
Mff61-GST
Drp1 ΔIB
Drp1 FL
Drp1 FL S579D
Drp1 FL S579E
T7-GST
Mff61-GST
Drp1
75 kDA
GST fusion
28 kDA
34 kDA

Table 2.S1

Table S1. **Drp1 mutants used in yeast two-hybrid screen**

Mutant	Point mutations	Mutant	Point mutations
1	Q314A, Y315A, Q316A, S317A, L318A	22	E437A, Q440A, R441A
2	L319A, N320A, S321A, Y322A	23	Q444A, N448A, Y449A
3	G323A, P325A, V326A, D327A	24	H445A, C446A, S447A
4	S330A, T332A	25	Q452A, E453A, L455A, R456A
5	Q335A, L336A, T338A	26	K459A, H461A, D462A
6	K339A, T342A, N346A	27	D462A, V465A, E466A
7	T351S, A 352D, K353G, Y354Q	28	K474A, L476A, P477A, V478A
8	S358A, E359A, L360A	29	E481A, M482A, H484A, N485A
9	R365A, C367A, H371A	30	K497A, P499A
10	Y368A, E372A	31	D503A, A504R
11	G375A, T377A, S380A	32	E611A, R612A, K615A
12	R376A, E379A	33	L613A, S616A, Y617A
13	V381A, D382A, P383A, L384A	34	R622A, K623A, N624A, Q626A
14	G385D, G386E	35	D627A, S628A, K631A
15	I390A, T394A, R397A	36	H635A, F636A, N639A, H640A
16	N398A, T400A	37	K642A, D643A, T644A, Q646A
17	L406A, F407A, V408A, P409A	38	S647A, E648A, V650A, G651A
18	F413A, E414A, L415A, L416A	39	K655A, S656A, S657A, L658A, L659A
19	R419A, R423A, E425A	40	D660A, D661A, T664A
20	E426A, P427A, L429A, R430A	41	E667A, D668A, M669A
21	E433A, L434A, H436A	42	K674A, E675A, D678A

REFERENCES

Bhar, D., Karren, M.A., Babst, M., and Shaw, J.M. (2006). Dimeric Dnm1-G385D interacts with Mdv1 on mitochondria and can be stimulated to assemble into fission complexes containing Mdv1 and Fis1. The Journal of biological chemistry *281*, 17312-17320.

Bui, H.T., Karren, M.A., Bhar, D., and Shaw, J.M. (2012). A novel motif in the yeast mitochondrial dynamin Dnm1 is essential for adaptor binding and membrane recruitment. The Journal of cell biology *199*, 613-622.

Bustillo-Zabalbeitia, I., Montessuit, S., Raemy, E., Basanez, G., Terrones, O., and Martinou, J.C. (2014). Specific interaction with cardiolipin triggers functional activation of Dynamin-Related Protein 1. PloS one *9*, e102738.

Chan, D.C. (2012). Fusion and fission: interlinked processes critical for mitochondrial health. Annual review of genetics *46*, 265-287.

Chang, C.R., and Blackstone, C. (2010). Dynamic regulation of mitochondrial fission through modification of the dynamin-related protein Drp1. Annals of the New York Academy of Sciences *1201*, 34-39.

Chang, C.R., Manlandro, C.M., Arnoult, D., Stadler, J., Posey, A.E., Hill, R.B., and Blackstone, C. (2010). A lethal de novo mutation in the middle domain of the dynamin-related GTPase Drp1 impairs higher order assembly and mitochondrial division. The Journal of biological chemistry *285*, 32494-32503.

Chappie, J.S., Acharya, S., Leonard, M., Schmid, S.L., and Dyda, F. (2010). G domain dimerization controls dynamin's assembly-stimulated GTPase activity. Nature *465*, 435-440.

Corpet, F. (1988). Multiple sequence alignment with hierarchical clustering. Nucleic acids research *16*, 10881-10890.

Elgass, K.D., Smith, E.A., LeGros, M.A., Larabell, C.A., and Ryan, M.T. (2015). Analysis of ER-mitochondria contacts using correlative fluorescence microscopy and soft X-ray tomography of mammalian cells. Journal of cell science *128*, 2795-2804.

Ferguson, S.M., and De Camilli, P. (2012). Dynamin, a membrane-remodelling GTPase. Nature reviews. Molecular cell biology *13*, 75-88.

Figueroa-Romero, C., Iniguez-Lluhi, J.A., Stadler, J., Chang, C.R., Arnoult, D., Keller, P.J., Hong, Y., Blackstone, C., and Feldman, E.L. (2009). SUMOylation of the mitochondrial fission protein Drp1 occurs at multiple nonconsensus sites within the B

domain and is linked to its activity cycle. FASEB journal : official publication of the Federation of American Societies for Experimental Biology *23*, 3917-3927.

Francy, C.A., Alvarez, F.J., Zhou, L., Ramachandran, R., and Mears, J.A. (2015). The mechanoenzymatic core of dynamin-related protein 1 comprises the minimal machinery required for membrane constriction. The Journal of biological chemistry *290*, 11692-11703.

Frohlich, C., Grabiger, S., Schwefel, D., Faelber, K., Rosenbaum, E., Mears, J., Rocks, O., and Daumke, O. (2013). Structural insights into oligomerization and mitochondrial remodelling of dynamin 1-like protein. The EMBO journal *32*, 1280-1292.

Gandre-Babbe, S., and van der Bliek, A.M. (2008). The novel tail-anchored membrane protein Mff controls mitochondrial and peroxisomal fission in mammalian cells. Molecular biology of the cell *19*, 2402-2412.

Huang, Y.J., Acton, T.B., and Montelione, G.T. (2014). DisMeta: a meta server for construct design and optimization. Methods in molecular biology *1091*, 3-16.

Ingerman, E., Perkins, E.M., Marino, M., Mears, J.A., McCaffery, J.M., Hinshaw, J.E., and Nunnari, J. (2005). Dnm1 forms spirals that are structurally tailored to fit mitochondria. The Journal of cell biology *170*, 1021-1027.

Ishihara, N., Nomura, M., Jofuku, A., Kato, H., Suzuki, S.O., Masuda, K., Otera, H., Nakanishi, Y., Nonaka, I., Goto, Y., Taguchi, N., Morinaga, H., Maeda, M., Takayanagi, R., Yokota, S., and Mihara, K. (2009). Mitochondrial fission factor Drp1 is essential for embryonic development and synapse formation in mice. Nature cell biology *11*, 958-966.

Kashatus, D.F., Lim, K.H., Brady, D.C., Pershing, N.L., Cox, A.D., and Counter, C.M. (2011). RALA and RALBP1 regulate mitochondrial fission at mitosis. Nature cell biology *13*, 1108-1115.

Koirala, S., Guo, Q., Kalia, R., Bui, H.T., Eckert, D.M., Frost, A., and Shaw, J.M. (2013). Interchangeable adaptors regulate mitochondrial dynamin assembly for membrane scission. Proceedings of the National Academy of Sciences of the United States of America *110*, E1342-1351.

Lackner, L.L., Horner, J.S., and Nunnari, J. (2009). Mechanistic analysis of a dynamin effector. Science *325*, 874-877.

Loson, O.C., Liu, R., Rome, M.E., Meng, S., Kaiser, J.T., Shan, S.O., and Chan, D.C. (2014). The Mitochondrial Fission Receptor MiD51 Requires ADP as a Cofactor. Structure *22*, 367-377.

Loson, O.C., Song, Z., Chen, H., and Chan, D.C. (2013). Fis1, Mff, MiD49, and MiD51 mediate Drp1 recruitment in mitochondrial fission. Molecular biology of the cell *24*, 659-667.

Macdonald, P.J., Stepanyants, N., Mehrotra, N., Mears, J.A., Qi, X., Sesaki, H., and Ramachandran, R. (2014). A dimeric equilibrium intermediate nucleates Drp1 reassembly on mitochondrial membranes for fission. Molecular biology of the cell *25*, 1905-1915.

Mears, J.A., Lackner, L.L., Fang, S., Ingerman, E., Nunnari, J., and Hinshaw, J.E. (2011). Conformational changes in Dnm1 support a contractile mechanism for mitochondrial fission. Nature structural & molecular biology *18*, 20-26.

Naylor, K., Ingerman, E., Okreglak, V., Marino, M., Hinshaw, J.E., and Nunnari, J. (2006). Mdv1 interacts with assembled dnm1 to promote mitochondrial division. The Journal of biological chemistry *281*, 2177-2183.

Otera, H., Wang, C., Cleland, M.M., Setoguchi, K., Yokota, S., Youle, R.J., and Mihara, K. (2010). Mff is an essential factor for mitochondrial recruitment of Drp1 during mitochondrial fission in mammalian cells. The Journal of cell biology *191*, 1141-1158.

Palmer, C.S., Elgass, K.D., Parton, R.G., Osellame, L.D., Stojanovski, D., and Ryan, M.T. (2013). Adaptor proteins MiD49 and MiD51 can act independently of Mff and Fis1 in Drp1 recruitment and are specific for mitochondrial fission. The Journal of biological chemistry *288*, 27584-27593.

Palmer, C.S., Osellame, L.D., Laine, D., Koutsopoulos, O.S., Frazier, A.E., and Ryan, M.T. (2011). MiD49 and MiD51, new components of the mitochondrial fission machinery. EMBO reports *12*, 565-573.

Reubold, T.F., Faelber, K., Plattner, N., Posor, Y., Ketel, K., Curth, U., Schlegel, J., Anand, R., Manstein, D.J., Noe, F., Haucke, V., Daumke, O., and Eschenburg, S. (2015). Crystal structure of the dynamin tetramer. Nature *525*, 404-408.

Robert, X., and Gouet, P. (2014). Deciphering key features in protein structures with the new ENDscript server. Nucleic acids research *42*, W320-324.

Schmid, S.L., and Frolov, V.A. (2011). Dynamin: functional design of a membrane fission catalyst. Annual review of cell and developmental biology *27*, 79-105.

Shen, Q., Yamano, K., Head, B.P., Kawajiri, S., Cheung, J.T., Wang, C., Cho, J.H., Hattori, N., Youle, R.J., and van der Bliek, A.M. (2014). Mutations in Fis1 disrupt orderly disposal of defective mitochondria. Molecular biology of the cell *25*, 145-159.

Smirnova, E., Griparic, L., Shurland, D.L., and van der Bliek, A.M. (2001). Dynamin-related protein Drp1 is required for mitochondrial division in mammalian cells. Molecular biology of the cell *12*, 2245-2256.

Stepanyants, N., Macdonald, P.J., Francy, C.A., Mears, J.A., Qi, X., and Ramachandran, R. (2015). Cardiolipin's propensity for phase transition and its reorganization by dynamin-related protein 1 form a basis for mitochondrial membrane fission. Molecular biology of the cell.

Strack, S., and Cribbs, J.T. (2012). Allosteric modulation of Drp1 mechanoenzyme assembly and mitochondrial fission by the variable domain. The Journal of biological chemistry *287*, 10990-11001.

Taguchi, N., Ishihara, N., Jofuku, A., Oka, T., and Mihara, K. (2007). Mitotic phosphorylation of dynamin-related GTPase Drp1 participates in mitochondrial fission. The Journal of biological chemistry *282*, 11521-11529.

Ugarte-Uribe, B., Muller, H.M., Otsuki, M., Nickel, W., and Garcia-Saez, A.J. (2014). Dynamin-related protein 1 (Drp1) promotes structural intermediates of membrane division. The Journal of biological chemistry *289*, 30645-30656.

Van Criekinge, W., and Beyaert, R. (1999). Yeast Two-Hybrid: State of the Art. Biological procedures online *2*, 1-38.

Wakabayashi, J., Zhang, Z., Wakabayashi, N., Tamura, Y., Fukaya, M., Kensler, T.W., Iijima, M., and Sesaki, H. (2009). The dynamin-related GTPase Drp1 is required for embryonic and brain development in mice. The Journal of cell biology *186*, 805-816.

Waterham, H.R., Koster, J., van Roermund, C.W., Mooyer, P.A., Wanders, R.J., and Leonard, J.V. (2007). A lethal defect of mitochondrial and peroxisomal fission. The New England journal of medicine *356*, 1736-1741.

Wenger, J., Klinglmayr, E., Frohlich, C., Eibl, C., Gimeno, A., Hessenberger, M., Puehringer, S., Daumke, O., and Goettig, P. (2013). Functional mapping of human dynamin-1-like GTPase domain based on x-ray structure analyses. PloS one *8*, e71835.

Westermann, B. (2010). Mitochondrial fusion and fission in cell life and death. Nature reviews. Molecular cell biology *11*, 872-884.

Yamano, K., Fogel, A.I., Wang, C., van der Bliek, A.M., and Youle, R.J. (2014). Mitochondrial Rab GAPs govern autophagosome biogenesis during mitophagy. eLife *3*, e01612.

Yoon, Y., Krueger, E.W., Oswald, B.J., and McNiven, M.A. (2003). The mitochondrial protein hFis1 regulates mitochondrial fission in mammalian cells through an interaction with the dynamin-like protein DLP1. Molecular and cellular biology *23*, 5409-5420.

Youle, R.J., and van der Bliek, A.M. (2012). Mitochondrial fission, fusion, and stress. Science *337*, 1062-1065.

Zhao, J., Liu, T., Jin, S., Wang, X., Qu, M., Uhlen, P., Tomilin, N., Shupliakov, O., Lendahl, U., and Nister, M. (2011). Human MIEF1 recruits Drp1 to mitochondrial outer membranes and promotes mitochondrial fusion rather than fission. The EMBO journal *30*, 2762-2778.

Zhu, P.P., Patterson, A., Stadler, J., Seeburg, D.P., Sheng, M., and Blackstone, C. (2004). Intra- and intermolecular domain interactions of the C-terminal GTPase effector domain of the multimeric dynamin-like GTPase Drp1. The Journal of biological chemistry *279*, 35967-35974.

Chapter 3

A novel *de novo* dominant negative mutation in *DNM1L* impairs mitochondrial fission and presents as childhood epileptic encephalopathy

Jill A. Fahrner,[1,*] Raymond Liu,[2] M. Scott Perry,[3] Jessica Klein,[4,5] David C. Chan[2,**]

[1]McKusick-Nathans Institute of Genetic Medicine
Department of Pediatrics
Johns Hopkins University School of Medicine
Baltimore, Maryland 21287, USA

[2]California Institute of Technology
Division of Biology and Biological Engineering
Pasadena, CA 91125, USA

[3]Comprehensive Epilepsy Program
Jane and John Justin Neuroscience Center
Cook Children's Medical Center
Fort Worth, TX 76104, USA

[4]Division of Pediatric Neurology
Department of Neurology
Johns Hopkins University School of Medicine
Baltimore, Maryland 21287, USA

[5]Department of Pediatrics, Medical University of South Carolina, Charleston, SC 29425, USA

This chapter, to which I contributed writing and Figures 3.2, 3.3, 3.4, was published in *American Journal of Medical Genetics Part A*

ABSTRACT

DNM1L encodes dynamin-related protein (DLP1/DRP1), a key component of the mitochondrial fission machinery that is essential to proper functioning of the mammalian brain. Two previously reported probands with *de novo* missense mutations in *DNM1L* presented in the first year of life with severe encephalopathy and refractory epilepsy, one with death in the first 2 months of life. We report identical novel missense mutations in *DNM1L* in two unrelated probands who experienced essentially normal development for several years before presenting with refractory focal status epilepticus leading to subsequent neurological disability. We expand the phenotype of *DNM1L*-related mitochondrial fission defects, reveal common unique clinical characteristics and imaging findings, and compare the cellular impact of this novel mutation to the previously reported A395D lethal variant. We demonstrate that our R403C mutation generates a dominant-negative variant that reduces the oligomerization, mitochondrial fission activity, and mitochondrial recruitment of DRP1, but to a lesser extent compared to A395D. These observations suggest a common pathogenic mechanism for *DNM1L* mutations and are consistent with the less severe phenotype seen in individuals with R403C.

INTRODUCTION

Mitochondria are essential for proper cellular function. Classically, "mitochondrial disease" implies a primary defect in a nuclear- or mitochondrial-encoded gene, whose disrupted protein product precludes adequate oxidative phosphorylation, and thus energy production in cells.[1] Mitochondrial disease can present with a variety of disparate phenotypic features affecting multiple organ systems and may include developmental delay and regression, which can worsen with intercurrent illness, as well as myopathy, seizures, and other findings.[1] Recently, with the advent of clinical whole exome sequencing, the list of conditions associated with mitochondrial dysfunction has greatly expanded and the term mitochondrial disease has been used more broadly. One group of conditions that has emerged involves disrupted mitochondrial dynamics.[2]

Mitochondrial dynamics, consisting of fusion and fission, is an important regulator of mitochondrial function. Dynamin-related protein 1 (DRP1), or dynamin-like protein 1 (DLP1), encoded by *DNML1*,[3] is the central molecular player that mediates mitochondrial fission. It is produced in the cytosol but can be recruited to the mitochondrial surface by receptors located on the outer membrane. There are currently four known DRP1 receptors: FIS1, MFF, MID49, and MID51.[4] MFF appears to be the major DRP1 receptor, because removal of MFF causes the greatest defect in mitochondrial fission.[5,6] Once recruited to mitochondria, DRP1 assembles into an oligomeric ring that drives constriction and scission of the mitochondrial tubule.[7,8] DRP1 has also been shown to be important for peroxisomal division.[9]

DRP1 belongs to the GTP-hydrolyzing dynamin superfamily of mechanoenzymes whose activity is regulated by self-assembly via a stalk domain with multiple interacting regions (classically referred to as the middle domain).[10,11] DRP1 initially forms dimers that are stabilized by stalk-stalk interactions. Via a separate set of stalk-stalk interactions, these dimers then build higher order assemblies that form rings wrapping around the mitochondrial tubule. These rings are thought to constrict the diameter of the mitochondrial tubule and facilitate close lipid membrane interactions that are needed for scission.[7,8] DRP1 self-assembly is also important because it stimulates GTP hydrolysis, which is necessary for scission. Finally, self-assembly facilitates DRP1 recruitment to the mitochondrial surface, because the major DRP1 receptor, MFF, only binds stably to oligomerized DRP1.[12]

As a key component of mitochondrial fission, DRP1 is essential for proper mitochondrial function and furthermore, is critically important in the proper functioning of the mammalian brain and for survival in general. Constitutive homozygous *Dnm1l* knockout mice die during embryogenesis, and conditional *Dnm1l* ablation in mouse brain leads to developmental defects, both of which are associated with impaired mitochondrial fission.[13,14] In humans, two probands with distinct *de novo* missense mutations in *DNM1L* have been reported in the literature. One presented in the first days of life with severe neonatal encephalopathy, microcephaly, abnormal brain development in the form of dysmyelination and altered gyral pattern, and optic atrophy. She died at 37 days of age after attaining no developmental milestones.[15] She was found to have a *de novo* missense mutation in the middle domain of DRP1 (p.A395D), resulting in abnormal mitochondrial

and peroxisomal fission. The second proband presented at 6 months of age with global developmental delay, developed refractory epilepsy at one year of age with multiple subsequent episodes of status epilepticus, and remains profoundly globally developmentally delayed. He harbored a *de novo* missense change in the middle domain of DRP1 (p.G362D), again causing abnormal mitochondrial fission.[16] In addition, two abstracts have reported additional individuals with *DNM1L* variants or mutations. The first reported two siblings with an autosomal recessive disorder due to compound heterozygous truncating mutations, both of whom died within the first month of life (Yoon et al., 2014, Neuromuscular disorders, abstract), and the second reported two unrelated individuals with distinct *de novo* missense changes in *DNM1L* and global developmental delay (L. Roback et al., 2015, American Society of Human Genetics, abstract).

Here, we report identical, novel, *de novo,* heterozygous missense mutations in *DNM1L* [c.1207C>T (p.R403C)] in two unrelated individuals who share a remarkably similar phenotype that is delayed in onset compared to the previously reported cases. Despite the later onset, the course remains quite devastating. Both young boys had undergone a period of essentially normal development but then presented acutely in childhood with status epilepticus after minor metabolic insults and had variably progressive, yet remarkably similar courses involving refractory epilepsy, encephalopathy, developmental regression, myoclonus, and characteristic MRI findings. Through functional studies, we demonstrate that this mutation impacts a critical amino acid residue within the middle domain of DRP1 and exhibits a dominant negative effect

involving decreased recruitment of DRP1 to mitochondria, decreased DRP1 oligomerization, and impaired mitochondrial fission, though not as marked as the previously reported A395D lethal variant. Based on these investigations, the R403C mutation appears to be less severe and better tolerated at the phenotypic and cellular level, expanding the clinical presentation of disease associated with *DNM1L*-related mitochondrial fission defects.

MATERIALS AND METHODS

Appropriate informed consent was obtained from human subjects.

Exome Sequencing and Variant Filtering

Clinical exome sequencing, including variant filtering, was performed by Baylor Miraca Genetics laboratories.

Cloning

Isoform b of mouse dynamin-like protein 1 isoform b (699 amino acids, NCBI NP_001021118.1) was used. DRP1 mutants A395D and R403C were generated by overlapping PCR mutagenesis and verified by sequencing.

Cell lines and cell culture

Cell lines were cultured in DMEM containing 10% fetal bovine serum, 100 I.U./ml streptomycin and 100 µg/ml penicillin. *Drp1*-null mouse cell lines were a generous gift from Katsuyoshi Mihara (Kyushu University, Fukuoka, Japan). *Mff*-null mouse cell lines were as previously described.[5] Wild-type and *Drp1*-null MEF cell lines stably expressing mouse DRP1 and DRP1 mutants were generated by retroviral transduction of pQCXIP-based (Clontech, Mountain View, CA) vectors with *DRP1* cloned into the BamHI/EcoRI sites with a Kozak sequence. Transduced cells were selected in 0.5 µg/mL puromycin.

Immunostaining and imaging

Antibodies to DRP1 (mouse anti-DLP1, BD Biosciences, San Diego, CA) and TOM20 (rabbit anti-TOM20, Santa Cruz Biotechnology, Santa Cruz, CA) were used for immunostaining. Cells were grown in LabTek chambered glass slides (Nunc, Rochester, NY), then fixed in pre-warmed 4% formaldehyde for 10 minutes at 37°C, permeabilized in 0.1% Triton X-100, and incubated with antibodies in 5% fetal calf serum. For cytosol clearing of soluble DRP1, cells were permeabilized with 0.005% digitonin in buffer containing 20 mM HEPES, pH 7.3, 110 mM potassium acetate, 2 mM magnesium acetate, 0.5 mM ethylene glycol tetraacetic acid (EGTA), 220 mM mannitol, 70 mM sucrose, and 2 mM fresh dithiothreitol for 90 seconds at room temperature, then fixed and immunostained as above. Scoring of mitochondrial morphology was performed blind to genotype in triplicates of 100 cells. Imaging was performed with a Plan-Apochromat 63x/1.4 oil objective on a Zeiss LSM 710 confocal microscope driven by Zen 2009 software (Carl Zeiss, Jena, Germany). Images were cropped, globally adjusted for contrast and brightness, and median filtered using ImageJ (National Institutes of Health, Bethesda, MD).

Yeast Two-Hybrid Assay

DRP1 and DRP1 mutants were cloned into either the pGAD-C1 or pGBDU-C1 vectors and transformed into PJ69-4α and PJ69-4a yeast strains, respectively. Transformants were selected with leucine- and uracil-deficient plates, respectively, and haploid combinations for interaction testing were mated by spotting on YPD plus adenine plates, at 30°C. Diploids were selected by replica-plating onto leucine- and uracil-deficient

plates (labeled as +Adenine) at room temperature, and interactions were assayed following replica-plating on leucine-, uracil- and adenine-deficient plates (labeled as -Adenine), at room temperature. Growth on adenine-deficient plates indicates a positive interaction, and interaction tests were performed at least three times.

RESULTS

Exome sequencing reveals identical *de novo* missense *DNM1L* mutations in two unrelated, previously healthy children with sudden-onset epileptic encephalopathy

Proband 1 was a previously healthy 4 year old male who presented with partial status epilepticus characterized by right hemibody clonus and impaired consciousness two weeks following his Diptheria, Tetanus, and Pertussis (DTaP) booster. The family denied any other illness or trauma in the weeks prior to presentation. Video electroencephalogram on admission revealed diffuse slowing with left central spikes time locked to right hand clonus, and magnetic resonance imaging (MRI) demonstrated curvilinear diffusion changes in the left thalamus (Figure 3.1A, arrow). MR angiogram was normal. He failed aggressive treatment with multiple antiepileptic drugs, ultimately being placed in pharmacologic coma with pentobarbital titrated to burst suppression for 5 days. Following resolution of his status epilepticus he had expressive and receptive dysphasia, difficulty ambulating without maximum assistance, and decline in cognitive level to that of a toddler. Although his seizures improved on a regimen of phenytoin, levetiracetam, lacosamide, and clonazepam, he was readmitted 6 months after initial discharge with epilepsia partialis continua, which resolved over several days.

His evaluation was extensive and included normal electrolytes, lactate, pyruvate, plasma amino acids, urine organic acids, acylcarnitine profile, very long chain fatty acids and ammonia. Cerebrospinal fluid cell count, protein, glucose, culture, HSV PCR and encephalitis panels were normal. Autoimmune testing for anti-NMDA, anti-GAD, anti-

thyroglobulin and ANA was negative. Enzyme testing of palmitoyl-protein thioesterase 1 and tripeptidyl peptidase 1 was normal. Mutation analysis for MELAS (MIM# 540000) and DNA sequencing of *POLG* (MIM#174763) were negative. Muscle biopsy was normal. Whole exome sequencing revealed a heterozygous *de novo* variant of unknown significance in *DNM1L* [c.1207C>T (p.R403C)].

At 8 years of age, seizures continue to occur on average 1-3 times per month without subsequent hospitalizations. He can ambulate short distances without assistance, but requires a wheelchair for longer distance. He has slow processing, inattention, cognitive delay, and intermittent aggressive behavior. He is able to speak, but has dysphasia. Follow-up MRI demonstrates mild diffuse cerebral atrophy, which is marked in the bilateral hippocampi (Figure 3.1B, C).

Proband 2 was a previously healthy typically developing 5 year old male, except for mild expressive speech delay and dysarthria, who presented suddenly with focal status epilepticus and encephalopathy after minor head trauma involving a collision with another child without loss of consciousness and in the setting of a normal head CT. He had had a viral illness the week prior to presentation, during which he reportedly experienced increased clumsiness and subtle changes in behavior. Prior to that, he had tolerated routine childhood illnesses well. Initial electroencephalogram showed diffuse cerebral disturbance with widespread epileptiform activity maximal over the right fronto-temporal region, correlating with his clinical presentation of status epilepticus involving the left side of his body. His status epilepticus was refractory to multiple therapies,

requiring several anti-epileptic medications, steroids, pharmacologic coma with pentobarbital, intravenous immune globulin (IVIg), ketogenic diet, and plasmapheresis prior to resolution. He experienced significant developmental regression and developed sustained myoclonus. He briefly recovered some function, including walking and speaking a few words initially. However, a few months later he presented again in refractory status epilepticus and has not recovered as well. Currently, at age 7, he has profound global developmental delay and remains hypertonic, hyperreflexic with myoclonus, tracheostomy and G-tube dependent, and wheelchair bound.

Initial magnetic resonance imaging revealed a non-specific T2 hyperintensity in the right thalamus (Figure 3.1D, arrow) with follow up imaging showing similar T2 hyperintensities in the right putamen and right frontal lobe (data not shown). Serial magnetic resonance imaging also revealed progressive global cerebral volume loss, particularly involving the right posterior putamen and bilateral hippocampi, with left greater than the right (Figures 3.1E,F). Magnetic resonance angiogram was normal. Magnetic resonance spectroscopy revealed decreased N-acetyl aspartate consistent with neuroaxonal loss or dysfunction, as well as elevated lactate, which can be seen in status epilepticus and in disorders involving mitochondrial dysfunction. An elevated glutamate/glutamine (Glx) peak was also observed, the significance of which is unclear, though it may be related to seizure activity. EEGs during his two hospital admissions continued to show intermittent focal status epilepticus mainly over the right hemisphere, sometimes associated with clinical seizure activity and sometimes subclinically. His EEG

progressed to showing bilateral background slowing with rhythmic slowing over the right hemisphere, consistent with a diffuse encephalopathy and focal seizure disorder.

Extensive neurologic, infectious, rheumatologic, and biochemical genetics evaluations were mostly negative. Notably, lactate and amino acids in plasma and in cerebrospinal fluid were normal, as were analysis of very long chain fatty acids and two separate analyses of urine organic acids. He was found on SNP array to harbor an interstitial duplication on Xp21.3p21.2 involving the *IL1RAPL1* gene (MIM#300206), which was inherited from his unaffected mother and is thought to be non-contributory. A forty-gene childhood-onset epilepsy panel, which includes among others the neuronal ceroid lipofuscinosis genes, *MECP2* (MIM#300005), and *POLG* (MIM#174763), was negative.

Whole exome sequencing, including mitochondrial sequencing, was performed. As an aside, he carries two likely tolerated/benign missense variants in *ALDH5A1* (MIM#610045), which is the causative gene for the autosomal recessive condition succinic semialdehyde dehydrogenase (SSADH) deficiency (MIM#271980). However, the diagnosis of SSADH deficiency can be ruled out because he lacks the ubiquitous gamma hydroxybutyric aciduria on repeated urine organic acid analyses and has normal levels of free and total gamma-aminobutyric acid (GABA) in cerebrospinal fluid. Ultimately, the proband was found to have a likely causative *de novo* heterozygous variant of unknown clinical significance in the *DNM1L* gene (MIM#603850), which encodes DRP1. The novel heterozygous missense change [c.1207C>T (p.R403C)] has

not been reported previously in diseased or healthy individuals and is predicted to be not tolerated and damaging by SIFT and Polyphen-2, respectively.

Functional characterization of R403C in mouse embryonic fibroblasts reveals a dominant negative mechanism and impaired mitochondrial fission

To determine whether the R403C mutation affects DRP1 function, we examined the effect of *Drp1*^{R403C} in mouse embryonic fibroblasts (MEFs), where both wild-type and *Drp1* mutant cells are available. In wild-type MEFs under basal conditions, mitochondria exist as a population of short and/or fragmented tubules (Figure 3.2B, C). In contrast, *Drp1*-null cells, due to unopposed fusion, have highly elongated and interconnected mitochondria (Figure 3.2A, C). Expression of wild-type *Drp1* in these mutant cells restores fission, resulting in shorter mitochondrial tubules, whereas expression of *Drp1*^{A395D} fails to rescue fission (Figure 3.2A, C). Expression of *Drp1*^{R403C} only partially rescues fission in *Drp1*-null cells, resulting in an intermediate phenotype. The R403C mutation therefore impairs DRP1 function in MEFs, but not as severely as the A395D mutation.

Because the R403C mutation was found to be heterozygous in the patients, we sought to determine whether *Drp1*^{R403C} has a dominant-negative effect that can interfere with the function of wild-type DRP1 within the same cell. We expressed the mutant in wild-type MEFs containing endogenous DRP1. Indeed, we find that expression of *Drp1*^{R403C} interferes with fission activity, resulting in mitochondrial elongation compared to control cells or cells expressing wild-type *Drp1* (Figure 3.2B, C). Consistent with the

above results, we also find that expression of *Drp1*^{A395D} has an even more severe dominant-negative effect, resulting in a higher proportion of cells with elongated mitochondria.

R403C reduces DRP1 recruitment to mitochondria and self-assembly

We wondered whether recruitment of DRP1 to mitochondria might be affected by the R403C mutation. To test this idea, we expressed wild-type *Drp1*, *Drp1*^{A395D}, and *Drp1*^{R403C} in *Drp1*-null cells and examined their co-localization with mitochondria (Figure 3.3A). For immunostaining of DRP1, we treated the cells with digitonin to remove cytosolic DRP1 before immunostaining. This treatment fragments mitochondria, but allows clear visualization of DRP1 puncta on mitochondria without interference from cytosolic DRP1 signals. For reference, we examined DRP1 localization in a cell line devoid of a major receptor, MFF, and found that DRP1 co-localization with mitochondria is much reduced compared to wild-type MEFs. In *Drp1*-null cells, we find that expressed wild-type DRP1 co-localizes with mitochondria, whereas expressed DRP1^{R403C} and DRP1^{A395D} show reduced signals, indicating loss of recruitment (Figure 3.3A).

To examine whether expression of the mutants disrupts localization of endogenous Drp1, we expressed *Drp1*^{A395D} and *Drp1*^{R403C} in wild-type cells (Figure 3.3B). We find that both mutants reduce the amount of DRP1 co-localizing with mitochondria, suggesting that the mutants dominantly interfere with recruitment of endogenous DRP1 to mitochondria.

In previous work, we showed that DRP1 recruitment by the major receptor MFF is dependent on the ability of DRP1 to assemble.[12] We therefore tested whether DRP1 assembly is affected by the R403C mutation in a yeast two-hybrid interaction assay (Figure 3.4A). Wild-type DRP1 interacts with wild-type DRP1, as indicated by growth of AD-DRP1 against BD-DRP1, whereas DRP1^{A395D} fails to interact with wild-type DRP1 (Figure 3.4A), indicating loss of higher order oligomer formation between the two. DRP1^{R403C} weakly interacts with wild-type DRP1, suggesting that the R403C mutation affects DRP1 oligomerization but not to the extent of the A395D mutation (Figure 3.4A). Both A395 and R403 reside in a region of DRP1 thought to be important for mediating the dimer-to-dimer interactions required for assembly into oligomeric rings[17] (Figure 3.4B). In dynamin, the homologous residue of DRP1 R403 is R399, which has been demonstrated to be critical for higher order oligomerization.[18] The crystal structure of the dynamin tetramer shows that the R399 residue from one dimer forms polar interactions with glutamate residues on adjacent dimers, helping to link one dimer to the next to form tetramers[19] (Figure 3.4C).

DISCUSSION

Our results indicate that the R403C mutation is a dominant-negative allele that is defective in oligomerization, recruitment to mitochondria, and mitochondrial fission activity. Each of these deficits is also present, and more severe, in the lethal A395D mutation, discovered in an individual who presented with abnormal brain development, encephalopathy, and lactic acidosis.[15] The milder clinical phenotype of the R403C mutation is consistent with its milder defects in DRP1 function, compared to the original A395D mutation.

Interestingly, the higher order oligomerization of DRP1 dimers appears to be critical for recruitment by MFF, the major DRP1 receptor on the mitochondrial surface.[12] In a screen for DRP1 mutants that fail to bind MFF, it was found that mutations impairing DRP1 self-assembly secondarily reduce binding to MFF, whereas binding to the alternative receptors MID49 and MID51 is less affected. Consistent with these findings, the R403C mutant shows reduced self-assembly and impaired recruitment to the mitochondrial surface. Because all the reported heterozygous *DNM1L* mutations[15,16] localize to the stalk domain and appear to act as dominant-negative alleles, the impaired DRP1 self-assembly mechanism shown here may be a major pathogenic mode affecting DRP1 function. Self-assembly is critical for DRP1 function, because it enhances GTP hydrolysis activity and facilitates DRP1 recruitment via MFF. Importantly, the A395D and R403C mutations impair higher order assembly but allow dimer formation. Therefore, they act as dominant-negative alleles, allowing heterozygous mutations to greatly impact neuronal function.

We found the R403C mutation in two unrelated individuals with strikingly similar clinical features. Both had been developing essentially normally for 4-5 years before presenting with sudden-onset refractory status epilepticus after distinct minor metabolic insults. Both subsequently had a devastating course with refractory epilepsy, myoclonus, brain atrophy on MRI, and regression, resulting in profound global developmental delay. The predicted damaging nature of the change, which is corroborated by the functional studies herein, as well as the strikingly similar phenotypes observed, make this the likely cause of the probands' clinical findings. Of the individuals reported to have *DNM1L*-related mitochondrial fission defects, all except for one sibship have had heterozygous *de novo* missense mutations impacting the middle domain of DRP1, and both the R403C (reported here) and A395D[15] mutations exhibit a common dominant-negative mutation mechanism, with the A395D mutation exhibiting a more severe cellular and clinical phenotype compared to R403C.

The previously reported individuals with *DNM1L*-associated mitochondrial fission defects had more severe phenotypes than the two probands reported here with regard to age of onset and severity. Our report therefore expands the phenotypic spectrum of this group of disorders. The patient with the A395D mutation[15] presented in the first days of life with neonatal encephalopathy and died at 37 days of age after attaining no developmental milestones.[15] The patient with the G362D mutation[16] presented at 6 months of age with global developmental delay and went on to develop refractory epilepsy with repeated bouts of status epilepticus. Finally, the sibship containing

compound heterozygous truncating mutations, which would predict little to no DRP1 function, died at 5 days and 3 weeks of life (Yoon et al., 2014, Neuromuscular disorders, abstract). In contrast, the two unrelated probands reported here had periods of essentially normal development until 4-5 years of age when they presented with sudden-onset status epilepticus and subsequent developmental regression and encephalopathy. In all cases, the developmental delay was ultimately profound. The previously reported individuals were not reported to exhibit developmental regression, unlike the probands reported here.

Furthermore, all three living probands have experienced one or more bouts of refractory status epilepticus; however, only two of the three individuals (those reported here) were thought to exhibit similar findings on brain MRI, including diffuse cerebral atrophy involving the hippocampi and non-specific thalamic hyperintensities. Notably, proband 2 was on steroids during his course, which could have contributed to the cerebral atrophy, but the same was not the case for proband 1, supporting the idea that atrophy is part of the disease process rather than being iatrogenic.

Importantly, with respect to laboratory work up, the initially reported A395D mutation exhibited persistently elevated lactate and alanine levels in blood and CSF, and elevated plasma very long chain fatty acids due to the defects in mitochondrial and peroxisomal fission.[15] However, none of the three living probands exhibited these laboratory findings on routine biochemical screening tests, suggesting a less severe defect. Therefore, routine biochemical screening tests will not necessarily identify individuals with these disorders.

Because of this and the extremely rare nature of these conditions, whole exome sequencing is currently the most efficient and effective way to diagnose these conditions.

Another provocative similarity between the two cases reported here, particularly with respect to presentation of more classic mitochondrial disorders, is that there is often a preceding illness or other metabolic insult prior to initial presentation and/or prior to episodes of developmental regression or worsening of seizures. Interestingly, each individual reported here experienced a minor metabolic insult prior to initial presentation. Proband one received a DTaP booster a few weeks prior to his presentation, and proband two had a viral illness the week prior to his presentation. These remain interesting correlations at this point, and there is no way to prove causality. Intriguingly however, a similar correlation exists in three individuals with mitochondrial fission defects resulting from homozygous truncating mutations in STAT2, a novel regulator of DRP1.[20] All three presented shortly after receiving the measles, mumps, rubella (MMR) vaccine with febrile illness, and one of them progressed to having opsoclonus-myoclonus, refractory epilepsy, spasticity, and cortical vision impairment.[20]

Finally, it is worth noting that several members of the dynamin family of large GTPases,[10,11] of which Drp1 is a member, have now been implicated in a range of neurologic disorders. Recently, mutations in *dynamin 1* (*DNM1),* a GTPase involved in synaptic vesicle recycling and endocytosis, have been found in seven individuals with epileptic encephalopathy.[21,22] Mutations in *dynamin2* (*DNM2*), also involved in endocytosis, are responsible for some forms of Charcot-Marie-Tooth,[23] centronuclear

myopathy,[24] and a lethal congenital syndrome.[25] Mutations in *atlastin-1* (*ATL1*), involved in homotypic fusion of the endoplasmic reticulum, have been implicated in some forms of spastic paraplegia[26] and hereditary sensory neuropathy.[27] Furthermore, mutations in the dynamin family genes *MFN2* and *OPA1*, involved in mitochondrial fusion, also cause neurological defects in humans.[28,29] The latter observation, along with the *DNM1L* mutation reported here, suggests that defects in either mitochondrial fusion or fission can cause neurological disease. Indeed, more common late-onset neurodegenerative conditions, like Alzheimer's disease, Parkinson's disease, Huntington's disease, and amyotrophic lateral sclerosis (ALS), have been shown to exhibit abnormal mitochondrial dynamics.[29] These observations further support mitochondrial fission and fusion defects as a pathological mechanism causing significant neurocognitive compromise, and thus morbidity and mortality, for individuals of all ages with both rare and common diseases, and sets the stage for the design of novel therapeutic strategies aimed at restoring the disrupted balance of mitochondrial dynamics.

ACKNOWLEDGEMENTS

We first and foremost thank the patients and their families for permission to publish this work. We thank Zhiyv Niu, PhD, FACMG, for connecting the authors. We thank Vera Joanna Burton, MD, PhD, and Thangamadhan Bosemani, MBBS, for assistance with obtaining MR images. This work was supported by NIH grant GM110039.

WEB RESOURCES

The URLs for data presented herein are as follows:

NHLBI Exome Sequencing Project (ESP) Exome Variant Server,

http://evs.gs.washington.edu/EVS/

OMIM, http://www.omim.org/.

PolyPhen-2, http://genetics.bwh.harvard.edu/pph2/

SIFT, http://sift.jcvi.org/

FIGURE LEGENDS

Figure 3.1. Magnetic resonance imaging of brains from probands 1 and 2.

(A) Axial diffusion-weighted magnetic resonance image with white arrow showing curvilinear intensity in the left thalamus in proband 1. (B,C) Coronal magnetic resonance images obtained from proband 1 at (B) initial presentation and (C) one month following resolution of status epilepticus show progressive atrophy of the brain, most marked in the hippocampi. (D) Axial T2 FLAIR magnetic resonance image with white arrow showing hyperintensity in the right central thalamus in proband 2, which was faintly hyperintense on diffusion-weighted imaging as well. (E,F) Coronal magnetic resonance images obtained from proband 2 at (E) initial presentation and (F) one year following resolution of status epilepticus show progressive atrophy of the brain, particularly involving the right posterior putamen and bilateral hippocampi (left greater than right).

Figure 3.2. Mutants R403C and A395D have dominant-negative effects on mitochondrial fission.

(A) Fission activity upon expression in *Drp1*-null MEFs. *Drp1*-null MEFs expressing wild-type *Drp1*, $Drp1^{A395D}$, and $Drp1^{R403C}$ were fixed and immunostained against the outer membrane protein TOM20 to visualize mitochondrial morphology. (B) Same as (A) except that wildtype MEFs were used. (E) Quantitation of mitochondrial morphology. Cells were scored into three categories of mitochondrial profiles: short, long tubular, or elongated and/or collapsed mitochondrial tubules. Quantitation was done in triplicate, with 100 cells scored per experiment. Error bars, SEM.

Figure 3.3. Recruitment to mitochondria is impaired in the A395D and R403C mutants. (A) Analysis of *Drp1* alleles in *Drp1*-null MEFs. Cells expressing the indicated alleles were briefly permeabilized with digitonin to clear cytosolic DRP1 before fixation. This resulted in mitochondrial fragmentation, but DRP1 puncta remained on mitochondria for visualization by immunostaining with an antibody against DRP1 (DRP1, green). Mitochondria were visualized by immunostaining against TOM20 (Mito, red). The DRP1 signal, mitochondrial signal, and merged signals are shown. Inset squares are magnifications of the boxed region in the main image. In the first column, *Mff*-null MEFs are shown as a reference for defective DRP1 recruitment to mitochondria. (B) Same as (A), except that wildtype MEFs are used.

Figure 3.4. Assembly defect of DRP1 mutants

(A) DRP1 oligomerization assessed by the yeast two-hybrid assay. DRP1 and DRP1 mutants expressed from the pGAD vector as GAL4 activation domain (AD) fusion proteins were tested against DRP1 expressed from the pGBDU vector as a GAL4 DNA-binding domain (BD) fusion proteins. Growth on adenine-deficient plates indicates an interaction. (B) Ribbon diagram of DRP1 (PDB file: 4BEJ) depicting the location of the R403 and A395 residues. Circled is the region (Interface 3) predicted to mediate dimer-to-dimer interactions during DRP1 oligomerization. (C) Ribbon diagram of the dynamin tetramer (PBD file: 5A3F). The violet and green dynamin monomers compose the dimer on the left, and the gray and blue monomers compose the dimer on the right. The inset depicts interface 3 of the dimer:dimer interaction, with the green monomer of the left

dimer removed for clarity. The dynamin residues depicted are labeled on the left, next to the corresponding residues on DRP1.

FIGURES

Figure 3.1

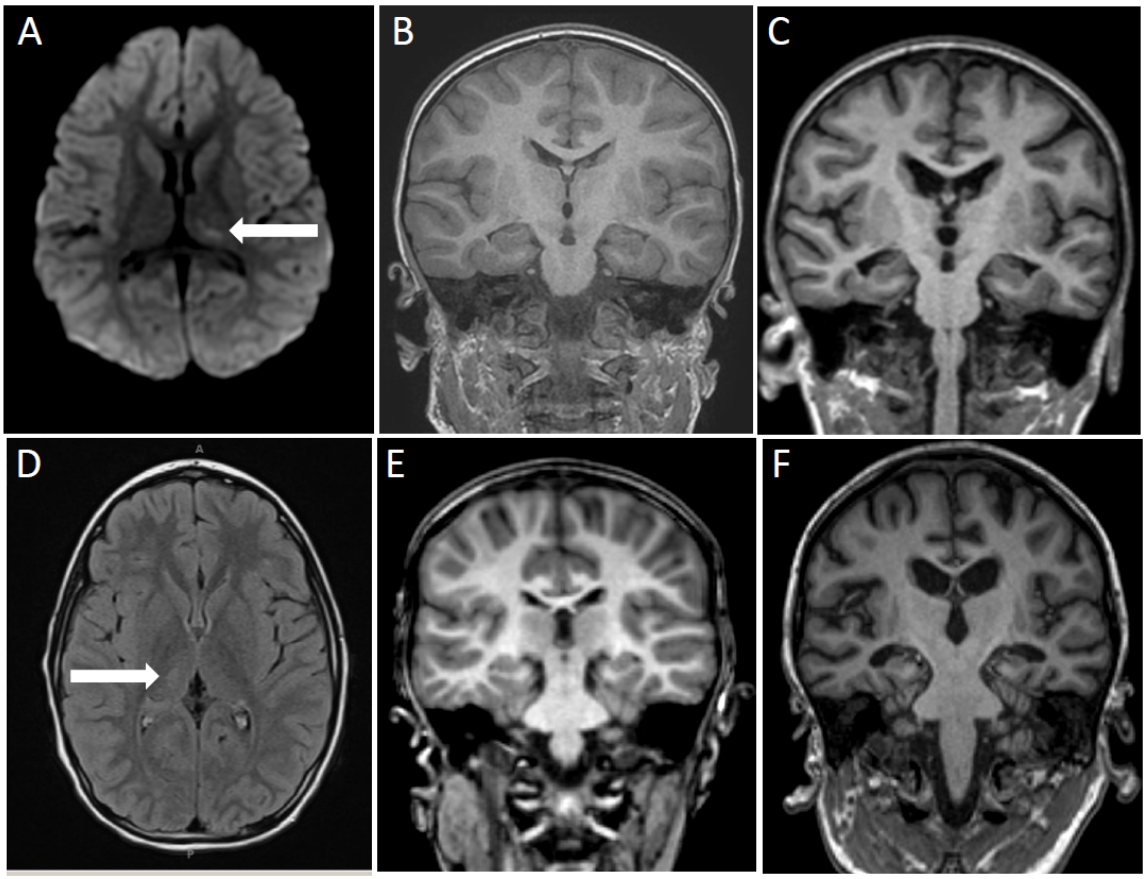

Figure 3.2

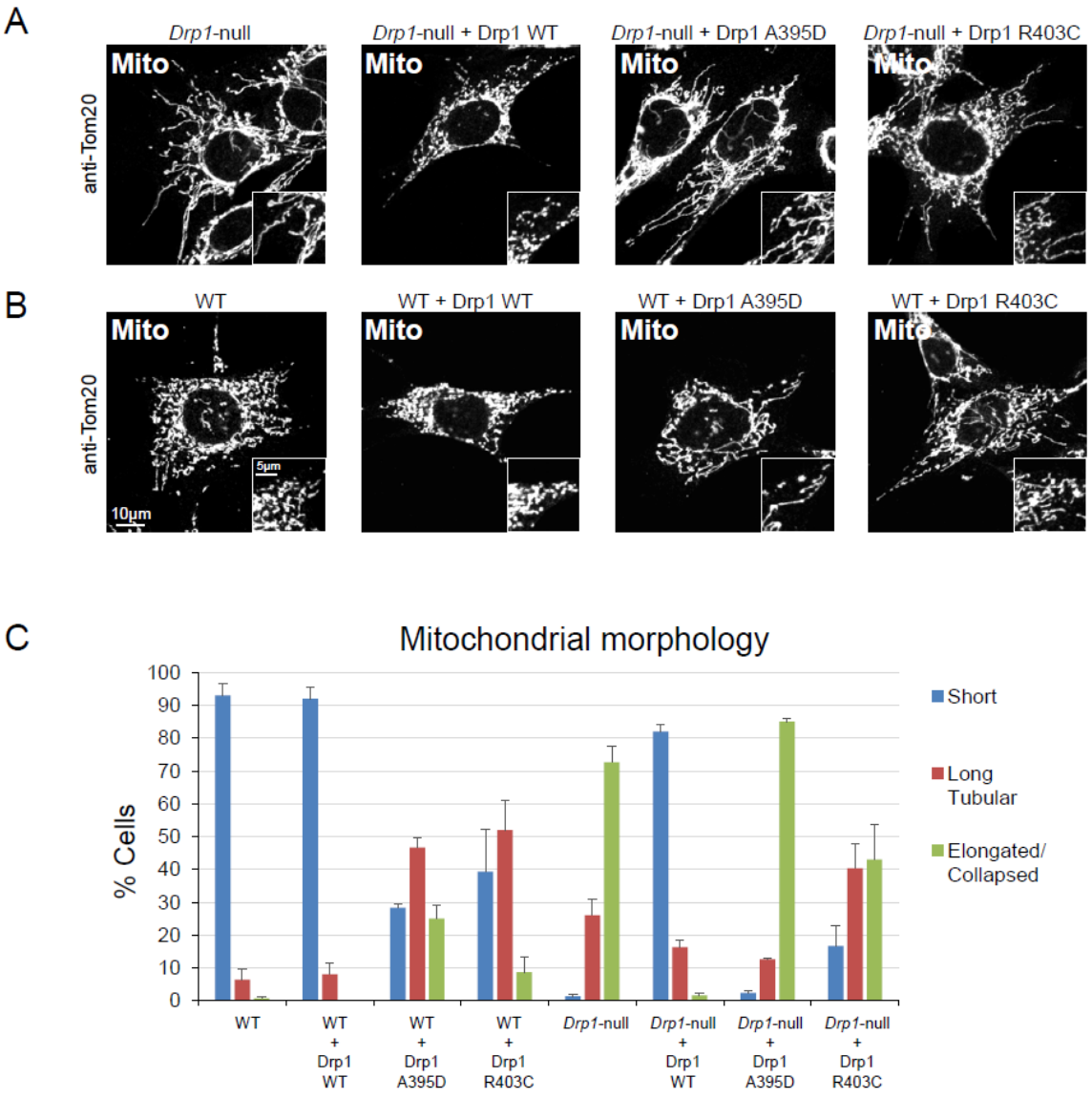
A
Drp1-null
Drp1-null + Drp1 WT
Drp1-null + Drp1 A395D
Drp1-null + Drp1 R403C
anti-Tom20
Mito
B
WT
WT + Drp1 WT
WT + Drp1 A395D
WT + Drp1 R403C
anti-Tom20
Mito
5μm
10μm
C
Mitochondrial morphology
% Cells
100
90
80
70
60
50
40
30
20
10
0
WT
WT + Drp1 WT
WT + Drp1 A395D
WT + Drp1 R403C
Drp1-null
Drp1-null + Drp1 WT
Drp1-null + Drp1 A395D
Drp1-null + Drp1 R403C
Short
Long Tubular
Elongated/ Collapsed

Figure 3.3

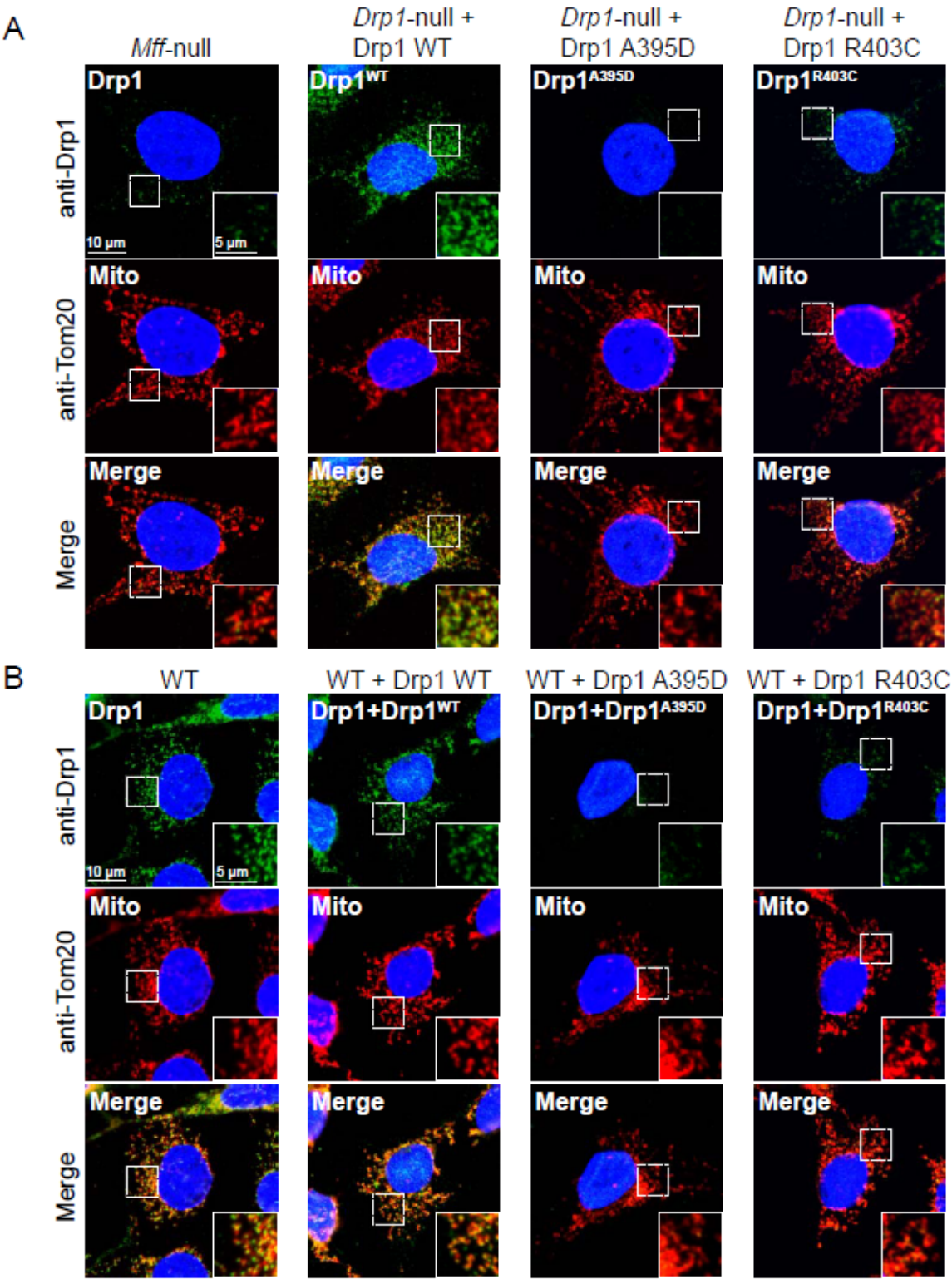
A
Mff-null
Drp1-null + Drp1 WT
Drp1-null + Drp1 A395D
Drp1-null + Drp1 R403C
anti-Drp1
anti-Tom20
Merge
Drp1
Drp1WT
Drp1A395D
Drp1R403C
Mito
Merge
10 μm
5 μm
B
WT
WT + Drp1 WT
WT + Drp1 A395D
WT + Drp1 R403C
Drp1+Drp1WT
Drp1+Drp1A395D
Drp1+Drp1R403C

Figure 3.4

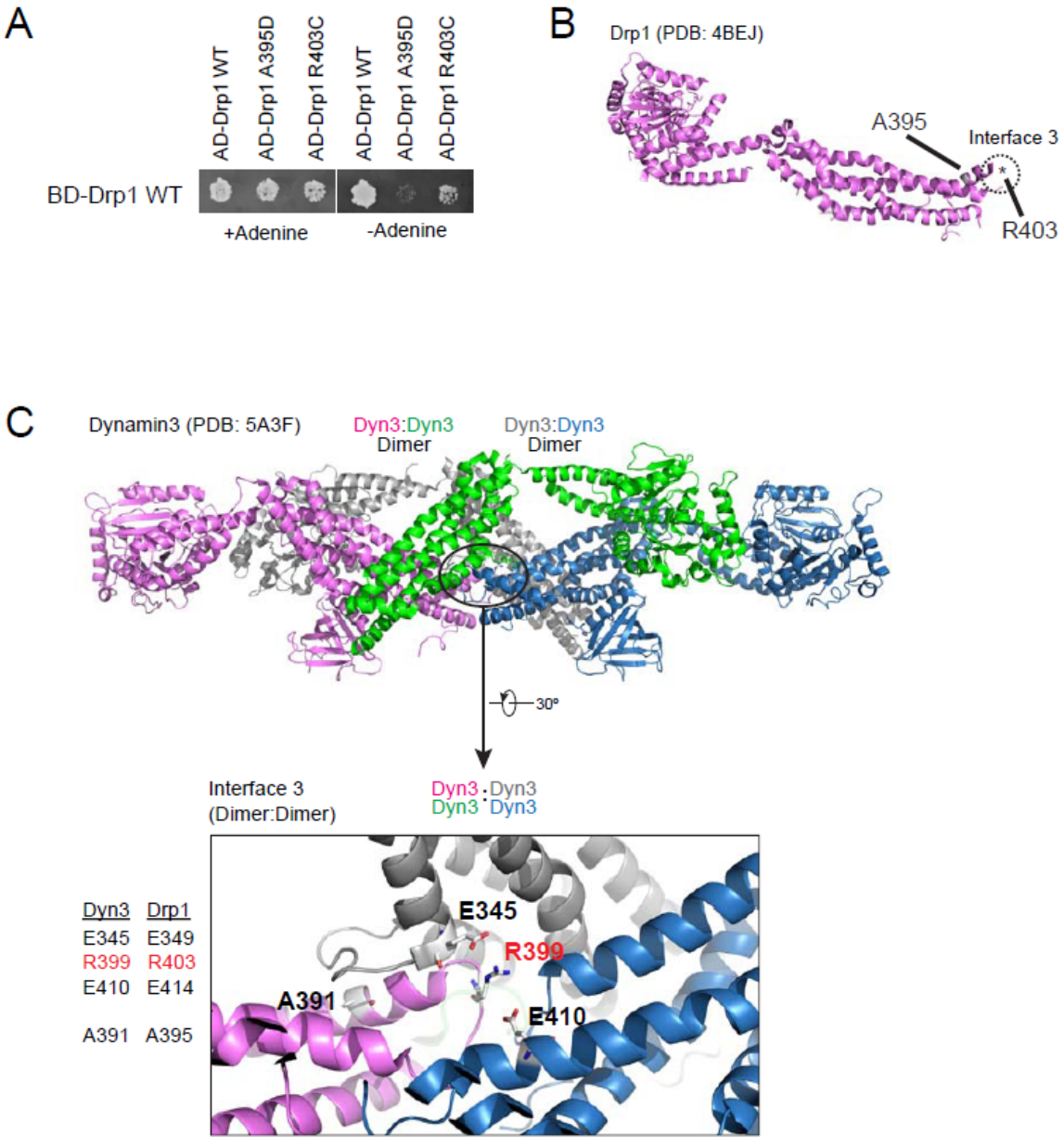
A
AD-Drp1 WT
AD-Drp1 A395D
AD-Drp1 R403C
AD-Drp1 WT
AD-Drp1 A395D
AD-Drp1 R403C
BD-Drp1 WT
+Adenine
-Adenine
B
Drp1 (PDB: 4BEJ)
A395
Interface 3
R403
C
Dynamin3 (PDB: 5A3F)
Dyn3:Dyn3
Dimer
Dyn3:Dyn3
Dimer
30°
Interface 3
(Dimer:Dimer)
Dyn3 : Dyn3
Dyn3 : Dyn3
Dyn3 Drp1
E345 E349
R399 R403
E410 E414
A391 A395
E345
R399
A391
E410

REFERENCES

1. Lightowlers, R.N., Taylor, R.W., and Turnbull, D.M. (2015). Mutations causing mitochondrial disease: What is new and what challenges remain? Science (New York, NY) 349, 1494-1499.

2. Chan, D.C. (2007). Mitochondrial dynamics in disease. N Engl J Med 356, 1707-1709.

3. Smirnova, E., Griparic, L., Shurland, D.L., and van der Bliek, A.M. (2001). Dynamin-related protein Drp1 is required for mitochondrial division in mammalian cells. Molecular biology of the cell 12, 2245-2256.

4. Chan, D.C. (2012). Fusion and fission: interlinked processes critical for mitochondrial health. Annual review of genetics 46, 265-287.

5. Loson, O.C., Song, Z., Chen, H., and Chan, D.C. (2013). Fis1, Mff, MiD49, and MiD51 mediate Drp1 recruitment in mitochondrial fission. Molecular biology of the cell 24, 659-667.

6. Otera, H., Wang, C., Cleland, M.M., Setoguchi, K., Yokota, S., Youle, R.J., and Mihara, K. (2010). Mff is an essential factor for mitochondrial recruitment of Drp1 during mitochondrial fission in mammalian cells. The Journal of cell biology 191, 1141-1158.

7. Ingerman, E., Perkins, E.M., Marino, M., Mears, J.A., McCaffery, J.M., Hinshaw, J.E., and Nunnari, J. (2005). Dnm1 forms spirals that are structurally tailored to fit mitochondria. The Journal of cell biology 170, 1021-1027.

8. Mears, J.A., Lackner, L.L., Fang, S., Ingerman, E., Nunnari, J., and Hinshaw, J.E. (2011). Conformational changes in Dnm1 support a contractile mechanism for mitochondrial fission. Nature structural & molecular biology 18, 20-26.

9. Koch, A., Thiemann, M., Grabenbauer, M., Yoon, Y., McNiven, M.A., and Schrader, M. (2003). Dynamin-like protein 1 is involved in peroxisomal fission. The Journal of biological chemistry 278, 8597-8605.

10. Ferguson, S.M., and De Camilli, P. (2012). Dynamin, a membrane-remodelling GTPase. Nature reviews Molecular cell biology 13, 75-88.

11. Schmid, S.L., and Frolov, V.A. (2011). Dynamin: functional design of a membrane fission catalyst. Annual review of cell and developmental biology 27, 79-105.

12. Liu, R., and Chan, D.C. (2015). The mitochondrial fission receptor Mff selectively recruits oligomerized Drp1. Molecular biology of the cell.

13. Wakabayashi, J., Zhang, Z., Wakabayashi, N., Tamura, Y., Fukaya, M., Kensler, T.W., Iijima, M., and Sesaki, H. (2009). The dynamin-related GTPase Drp1 is required for embryonic and brain development in mice. The Journal of cell biology 186, 805-816.

14. Ishihara, N., Nomura, M., Jofuku, A., Kato, H., Suzuki, S.O., Masuda, K., Otera, H., Nakanishi, Y., Nonaka, I., Goto, Y., et al. (2009). Mitochondrial fission factor Drp1 is essential for embryonic development and synapse formation in mice. Nat Cell Biol 11, 958-966.

15. Waterham, H.R., Koster, J., van Roermund, C.W., Mooyer, P.A., Wanders, R.J., and Leonard, J.V. (2007). A lethal defect of mitochondrial and peroxisomal fission. N Engl J Med 356, 1736-1741.

16. Vanstone, J.R., Smith, A.M., McBride, S., Naas, T., Holcik, M., Antoun, G., Harper, M.E., Michaud, J., Sell, E., Chakraborty, P., et al. (2015). DNM1L-related mitochondrial fission defect presenting as refractory epilepsy. European journal of human genetics : EJHG.

17. Frohlich, C., Grabiger, S., Schwefel, D., Faelber, K., Rosenbaum, E., Mears, J., Rocks, O., and Daumke, O. (2013). Structural insights into oligomerization and mitochondrial remodelling of dynamin 1-like protein. The EMBO journal 32, 1280-1292.

18. Ramachandran, R., Surka, M., Chappie, J.S., Fowler, D.M., Foss, T.R., Song, B.D., and Schmid, S.L. (2007). The dynamin middle domain is critical for tetramerization and higher-order self-assembly. The EMBO journal 26, 559-566.

19. Reubold, T.F., Faelber, K., Plattner, N., Posor, Y., Ketel, K., Curth, U., Schlegel, J., Anand, R., Manstein, D.J., Noe, F., et al. (2015). Crystal structure of the dynamin tetramer. Nature 525, 404-408.

20. Shahni, R., Cale, C.M., Anderson, G., Osellame, L.D., Hambleton, S., Jacques, T.S., Wedatilake, Y., Taanman, J.W., Chan, E., Qasim, W., et al. (2015). Signal transducer and activator of transcription 2 deficiency is a novel disorder of mitochondrial fission. Brain : a journal of neurology 138, 2834-2846.

21. Euro, E.-R.E.S.C., Epilepsy Phenome/Genome, P., and Epi, K.C. (2014). De novo mutations in synaptic transmission genes including DNM1 cause epileptic encephalopathies. American journal of human genetics 95, 360-370.

22. Nakashima, M., Kouga, T., Lourenco, C.M., Shiina, M., Goto, T., Tsurusaki, Y., Miyatake, S., Miyake, N., Saitsu, H., Ogata, K., et al. (2015). De novo DNM1 mutations in two cases of epileptic encephalopathy. Epilepsia.

23. Zuchner, S., Noureddine, M., Kennerson, M., Verhoeven, K., Claeys, K., De Jonghe, P., Merory, J., Oliveira, S.A., Speer, M.C., Stenger, J.E., et al. (2005). Mutations in the pleckstrin homology domain of dynamin 2 cause dominant intermediate Charcot-Marie-Tooth disease. Nature genetics 37, 289-294.

24. Bitoun, M., Bevilacqua, J.A., Prudhon, B., Maugenre, S., Taratuto, A.L., Monges, S., Lubieniecki, F., Cances, C., Uro-Coste, E., Mayer, M., et al. (2007). Dynamin 2 mutations cause sporadic centronuclear myopathy with neonatal onset. Annals of neurology 62, 666-670.

25. Koutsopoulos, O.S., Kretz, C., Weller, C.M., Roux, A., Mojzisova, H., Bohm, J., Koch, C., Toussaint, A., Heckel, E., Stemkens, D., et al. (2013). Dynamin 2 homozygous mutation in humans with a lethal congenital syndrome. European journal of human genetics : EJHG 21, 637-642.

26. Zhao, X., Alvarado, D., Rainier, S., Lemons, R., Hedera, P., Weber, C.H., Tukel, T., Apak, M., Heiman-Patterson, T., Ming, L., et al. (2001). Mutations in a newly identified GTPase gene cause autosomal dominant hereditary spastic paraplegia. Nature genetics 29, 326-331.

27. Guelly, C., Zhu, P.P., Leonardis, L., Papic, L., Zidar, J., Schabhuttl, M., Strohmaier, H., Weis, J., Strom, T.M., Baets, J., et al. (2011). Targeted high-throughput sequencing identifies mutations in atlastin-1 as a cause of hereditary sensory neuropathy type I. American journal of human genetics 88, 99-105.

28. Carelli, V., and Chan, D.C. (2014). Mitochondrial DNA: impacting central and peripheral nervous systems. Neuron 84, 1126-1142.

29. Reddy, P.H., Reddy, T.P., Manczak, M., Calkins, M.J., Shirendeb, U., and Mao, P. (2011). Dynamin-related protein 1 and mitochondrial fragmentation in neurodegenerative diseases. Brain research reviews 67, 103-118.

Chapter 4

Discussion

My work can be distilled into the following findings:

1. The N-terminal Mff motif and the Drp1 stalk domain form the core Drp1-Mff interaction unit.
2. The Drp1 Insert B domain inhibits the interaction between Mff and Drp1.
3. Drp1 mutants that disrupt self-assembly also disrupt stable binding to Mff, but not necessarily MiD51 or MiD49.
4. Drp1 mutants that disrupt self-assembly are implicated in causing human disease

From these findings and the supporting data, we propose a model in which the primary function of Mff is to recruit fission-competent species of Drp1 to mitochondria for productive assembly into oligomeric complexes, promoting mitochondrial fission. The requirement for Drp1 oligomerization in maintaining a stable Drp1-Mff interaction (Figure 4.1) acts as a functional test and filtering mechanism to selectively recruit active species of Drp1. We imagine that the purpose of this can be to facilitate efficient Drp1 oligomerization or assembly following signals to induce fission (Chan *et al.*, 2011). By ensuring that only oligomerization-competent Drp1 can stably occupy Mff foci, a block to ring assembly caused by accumulation of inactive Drp1 species is prevented, allowing timely mitochondrial fission to occur.

The MiD proteins do not seem to follow the same rules, as we observe they are not as strongly affected by the Drp1 oligomerization mutants we tested. This suggests a non-redundant role for MiD in Drp1 recruitment, and future studies aimed at uncovering the rules for their Drp1 recruitment mechanism will be informative (Otera *et al.*, 2016). Though each species has been shown to be capable of recruiting Drp1 and mediating fission independently, it is tempting to speculate how the MiDs and Mff might cooperate to regulate mitochondrial morphology (Koirala *et al.*, 2013; Palmer *et al.*, 2013; Elgass *et al.*, 2015; Otera *et al.*, 2016). It has been suggested that MiD51 binding to Drp1 is more stable than that of Mff (Palmer *et al.*, 2013). In Chapter 2 we propose that the MiDs might play a role in recruiting inactive species of Drp1 (Liu and Chan, 2015). If this is true, then this would have the effect of providing a local Drp1 reservoir that could be accessed by Mff following Drp1 activation by a cellular signal. As discussed in Chapter 1, loss of MiD51 results in a reduction of mitochondrial fission, whereas overexpression of MiD51 leads to accumulation of Drp1, and a block of fission. To test whether MiD51 can source Mff receptors with Drp1, we can induce fission in cells overexpressing MiD51, and examine whether fission is triggered in the presence and absence of Mff. If fission is achieved only in the presence of Mff, then this might support a model in which the MiDs recruits inactive species of Drp1 for Mff to later assemble. How this model reconciles with the observation that the MiDs can mediate some level of mitochondrial fission, which suggests that the MiDs can recruit active species as well, will be worth examining.

Several interesting results were not included in Chapter 2 due to lack of supporting evidence. These results might eventually find their way to publication in a

journal, but in case time runs out, I will describe them here with hope that it will inspire additional work into clarifying the Drp1 recruitment model, or at the very least, inject some ideas into the discussion. As can be gleaned from careful examination of the figures, the oligomerization defects of Drp1 Mutant 10 in Chapter 2 are milder than that of Drp1 Mutants 16 and 17. Since the mutant shows loss of binding to Mff, one possible interpretation is that the residues composing the mutant (Y368 and E372) might also represent part of the Drp1 binding interface to Mff, and that its effects on oligomerization are a consequence of their proximity to the relevant loops. If confirmed, this knowledge might be useful in designing co-crystallization strategies for determining the structure of this complex. In addition to the stalk domain screen described in Chapter 2, a similar yeast two-hybrid screen was conducted on the Drp1 GTPase domain. Interestingly, although the Drp1 stalk domain is sufficient to bind Mff, we find that some GTPase mutants disrupt or weaken the Drp1-Mff interaction. Since the Insert B domain inhibits Drp1 binding to Mff, we tested the same mutants in the absence of Insert B, and found that Drp1-Mff is restored. One idea to explore from this finding is a possible interaction between the GTPase domain and Insert B domain, perhaps between adjacent monomers. I find it likely that nucleotide occupancy plays a role in the conformational state of the Insert B domain, and vice versa. Perhaps most interestingly, we also found that mutations in the Switch 1 domain, such as the T59A mutation, disrupt Drp1 binding to MiD51 more strongly than it does to Mff, especially without the Insert B domain. We find this to be significant, because of all the mutants we have examined, it is the only class of mutants that affects binding to MiD51 more so than to Mff or Drp1. The mechanism behind this is unknown, but I suspect it figures prominently in describing how Drp1 recruits MiD51.

Finally, it is becoming clear that mutations affecting Drp1 oligomerization have an impact on human health and disease. In addition to the discovery of the R403A mutation found in human patients discussed in Chapter 3, several other pathogenic stalk domain mutants of Drp1 have been recently described, raising the possibility that this might not be a rare occurrence (Chang *et al.*, 2010; Chao *et al.*, 2016; Fahrner *et al.*, 2016; Sheffer *et al.*, 2016). Studies examining how these oligomerization defects contribute to the development of these neurological disorders will be of upmost importance.

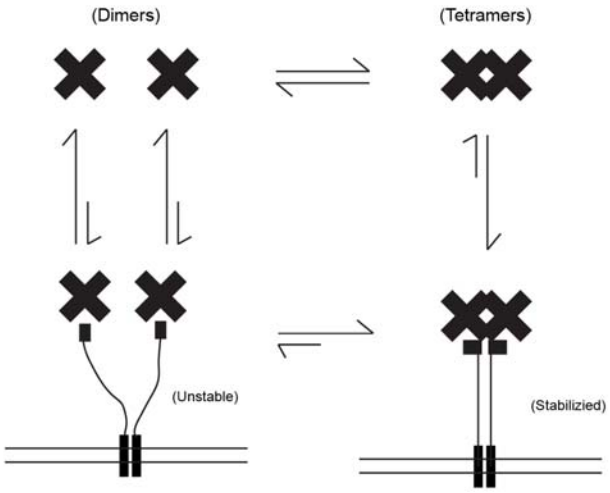

Figure 4.1

Mechanistic model of the Mff-Drp1 interaction. Drp1 (black crosses) exist in equilibrium as soluble dimers and tetramers in the cytosol. Mff (tethered to the outer mitochondrial membrane) can only effectively recruit Drp1 species that are able to oligomerize to form a stable interaction with the Mff dimer.

References

Chan, N.C., Salazar, A.M., Pham, A.H., Sweredoski, M.J., Kolawa, N.J., Graham, R.L.J., Hess, S., and Chan, D.C. (2011). Broad activation of the ubiquitin–proteasome system by Parkin is critical for mitophagy. Human molecular genetics *20*, 1726-1737.

Chang, C.R., Manlandro, C.M., Arnoult, D., Stadler, J., Posey, A.E., Hill, R.B., and Blackstone, C. (2010). A lethal de novo mutation in the middle domain of the dynamin-related GTPase Drp1 impairs higher order assembly and mitochondrial division. The Journal of biological chemistry *285*, 32494-32503.

Chao, Y.H., Robak, L.A., Xia, F., Koenig, M.K., Adesina, A., Bacino, C.A., Scaglia, F., Bellen, H.J., and Wangler, M.F. (2016). Missense variants in the middle domain of DNM1L in cases of infantile encephalopathy alter peroxisomes and mitochondria when assayed in Drosophila. Human molecular genetics *25*, 1846-1856.

Elgass, K.D., Smith, E.A., LeGros, M.A., Larabell, C.A., and Ryan, M.T. (2015). Analysis of ER–mitochondria contacts using correlative fluorescence microscopy and soft X-ray tomography of mammalian cells. Journal of Cell Science *128*, 2795-2804.

Fahrner, J.A., Liu, R., Perry, M.S., Klein, J., and Chan, D.C. (2016). A novel de novo dominant negative mutation in DNM1L impairs mitochondrial fission and presents as childhood epileptic encephalopathy. American journal of medical genetics. Part A *170*, 2002-2011.

Koirala, S., Guo, Q., Kalia, R., Bui, H.T., Eckert, D.M., Frost, A., and Shaw, J.M. (2013). Interchangeable adaptors regulate mitochondrial dynamin assembly for membrane scission. Proceedings of the National Academy of Sciences of the United States of America *110*, E1342-1351.

Liu, R., and Chan, D.C. (2015). The mitochondrial fission receptor Mff selectively recruits oligomerized Drp1. Molecular biology of the cell *26*, 4466-4477.

Otera, H., Miyata, N., Kuge, O., and Mihara, K. (2016). Drp1-dependent mitochondrial fission via MiD49/51 is essential for apoptotic cristae remodeling. The Journal of Cell Biology *212*, 531-544.

Palmer, C.S., Elgass, K.D., Parton, R.G., Osellame, L.D., Stojanovski, D., and Ryan, M.T. (2013). Adaptor proteins MiD49 and MiD51 can act independently of Mff and Fis1 in Drp1 recruitment and are specific for mitochondrial fission. The Journal of biological chemistry *288*, 27584-27593.

Sheffer, R., Douiev, L., Edvardson, S., Shaag, A., Tamimi, K., Soiferman, D., Meiner, V., and Saada, A. (2016). Postnatal microcephaly and pain insensitivity due to a de novo heterozygous DNM1L mutation causing impaired mitochondrial fission and function. American journal of medical genetics. Part A *170*, 1603-1607.